FOR FURTHER TRAN

AD A055820

AD No.

DDC FILE COPY

SECOND INTERIM
TECHNICAL REPORT

ADAPTIVE ANTENNA CONTROL

Peter Monsen
Steen A. Parl

(12) SC

SIGNATRON, Inc.
12 Hartwell Avenue
Lexington, Massachusetts 02173

February 1978

DDC

JUN 29 1978

E

U.S. ARMY
COMMUNICATIONS SYSTEMS AGENCY
Fort Monmouth, New Jersey

MONITORING OFFICE
U.S. ARMY
COMMUNICATIONS R&D COMMAND
Fort Monmouth, NJ

N O T I C E S

DISCLAIMERS

DISPOSITION

REPORT DOCUMENTATION PAGE

1. REPORT NUMBER	2. GOVT ACCESSION NO.	3. RECIPIENT'S CATALOG NUMBER
ECOM 76-8085-2		*Technical*

4. TITLE (and Subtitle)	5. TYPE OF REPORT & PERIOD COVERED
ADAPTIVE ANTENNA CONTROL SYSTEM	Interim Report no. 2, 25 Dec 76 — 25 Sep 71
	6. PERFORMING ORG. REPORT NUMBER
	A212-2

7. AUTHOR(s)	8. CONTRACT OR GRANT NUMBER(s)
PETER MONSEN STEEN PARL	DAAB07-76-C-8085

9. PERFORMING ORGANIZATION NAME AND ADDRESS	10. PROGRAM ELEMENT, PROJECT, TASK AREA & WORK UNIT NUMBERS
Signatron Inc. 12 Hartwell Avenue Lexington, Massachusetts 02173	1X763707D2451702

11. CONTROLLING OFFICE NAME AND ADDRESS	12. REPORT DATE
US Army Communications Systems Agency ATTN: CCM-RD-T Fort Monmouth, NJ 07703	February 1978
	13. NUMBER OF PAGES
	166

14. MONITORING AGENCY NAME & ADDRESS(if different from Controlling Office)	15. SECURITY CLASS. (of this report)
US Army Communications R&D Command Center for Communications Systems ATTN: DRDCO-COM-RM-3 Fort Monmouth, NJ 07703	Unclassified
	15a. DECLASSIFICATION/DOWNGRADING SCHEDULE

16. DISTRIBUTION STATEMENT (of this Report)

Approved for Public Release; Distribution Unlimited.

17. DISTRIBUTION STATEMENT (of the abstract entered in Block 20, if different from Report)

18. SUPPLEMENTARY NOTES

None

19. KEY WORDS (Continue on reverse side if necessary and identify by block number)

Troscatter	Coupling Loss
Communication	Antenna
Angle Diversity	

20. ABSTRACT (Continue on reverse side if necessary and identify by block number)

This interim technical report contains a tropospheric system prediction model which can be used to predict median path loss, aperture to medium coupling loss, and 2σ multipath spread. The prediction model is used to determine design parameters for an angle diversity system. For a dual vertical angle diversity system the optimum beam separation is approximately 1 beamwidth and the antenna take-off angle relative to the horizon is approximately $\frac{1}{2}$

(continued on reverse)

DD $_{1\ JAN\ 73}^{FORM}$ 1473 EDITION OF 1 NOV 65 IS OBSOLETE

UNCLASSIFIED

923760

20. Continued.

beamwidth for C-band systems and ¼ beamwidth for L-band systems. An analysis of long term variability and the decorrelation advantage of angle diversity is presented along with preliminary results.

The prediction model is used to compare 3 specific tropo-scatter system examples with the result that dual space/dual angle diversity is superior in system performance over conventional dual space/dual frequency diversity. The dependence of aperture-to-medium coupling loss on carrier frequency is also investigated. The turbulent scatter theory used in the model analysis suggests that conversion of L-band systems to S-band would result in significant system improvement. Further study of available empirical data is required to validate this result.

ABSTRACT

This interim technical report contains a tropospheric system prediction model which can be used to predict median path loss, aperture to medium coupling loss, and 2σ multipath spread. The prediction model is used to determine design parameters for an angle diversity system. For a dual vertical angle diversity system the optimum beam separation is approximately 1 beamwidth and the antenna take-off angle relative to the horizon is approximately 1/2 beamwidth for C-band systems and 1/4 beamwidth for L-band systems. An analysis of long term variability and the decorrelation advantage of angle diversity is presented along with preliminary results. The prediction model is used to compare 3 specific troposcatter system examples with the result that dual space/dual angle diversity is superior in system performance over conventional dual space/dual frequency diversity. The dependence of aperture-to-medium coupling loss on carrier frequency is also investigated. The turbulent scatter theory used in the model analysis suggests that conversion of L-band systems to S-band would result in significant system improvement. Further study of available empirical data is required to validate this result.

TABLE OF CONTENTS

TABLE OF CONTENTS (Cont'd)

LIST OF ILLUSTRATIONS

LIST OF ILLUSTRATIONS (Cont'd)

LIST OF TABLES

SECTION 1

INTRODUCTION

This report is the second interim technical report under the Adaptive Antenna Control program, Contract No. DAAB07-76-8-85. The Adaptive Antenna Control (AAC) program is under the contract management of the Project Manager for DCS (Army) Communications Systems, Ft. Monmouth, New Jersey. ECOM, Ft. Monmouth, N.J. is responsible for technical direction of the program. SIGNATRON, Inc. of Lexington, Massachusetts with RF Systems, Inc. of Cohassett as a major subcontractor have the responsibility for executing the program tasks.

The AAC program encompasses the investigation of adaptive antenna control techniques to enhance communication on strategic trans-horizon radio paths. For paths dominated by diffraction effects with a small or non existent scatter component, the emphasis is on antenna steering techniques to mitigate beam blockage due to changes in the refractive index gradient. Analysis of the diffraction problem has been included in the first Interim Technical Report [1.1] and a design of a mechanically steered feedhorn with electronic adaptation was presented in the AAC Design Plan [1.2]. The implementation and field test of this system is not part of the existing contract.

For trans-horizon paths dominated by forward scatter reception of communication signals, the failure to successfully illuminate the useful scattering volume results in an aperture to medium coupling loss and neglects an important diversity capability associated with signal angle arrivals from different portions

of the scattering volume. This program includes a comprehensive modeling of this phenomenon, development of a prediction model, analysis of angle diversity capability, design and development of a combiner system for augmentation to 8th order diversity using angle of arrival signals, design and development of a dual vertical feedhorn modification for the C-band RADC test system, and an extensive angle diversity test program to be accomplished on the RADC Youngstown-Verona TRC-132 test link in the fall and winter of 1977. The first Interim Technical Report [1.1] developed much of the theoretical basis for the troposcatter model and the prediction technique. The Design Plan [1.2] contains details of the combiner and feedhorn systems, and the Test Plan [1.3] describes the factory and field tests in detail.

This report continues with the theoretical development of the troposcatter model and prediction technique. Section 2 reviews other approaches to troposcatter modeling and develops the basis for predicting median path loss, 2σ multipath spread, aperture to medium coupling loss, and signal correlation distances at the receiver antenna. Angle diversity systems are considered in Section 3 where the methods of Section 2 are used to derive system design parameters. The variation of hourly median signals is also treated in Section 3 and the approach for determining system availability is outlined. The performance of angle diversity systems with digital signaling is treated in Section 4. A method of computing the average bit error probability for a troposcatter adaptive equalizer in the presence of both implicit and angle diversity is derived for the first time. This method is used in Section 4.2 to compute system performance for some example links.

Some of the major accomplishments and findings developed in this study are

- aperture to medium coupling loss is best considered an integral part of the path loss rather than a separable entity to be calculated by itself,

- a numerical integration technique derived from turbulent scattering theory has been developed to compute the path loss including aperture to medium coupling loss effects,

- an accurate closed form approximation of the above integration technique has been developed for the wide-beam path loss,

- a closed form relationship for aperture to medium coupling loss has been developed. The widebeam path loss and aperature to medium coupling loss equations when used together show good agreement with the numerical integration path loss result,

- vertical angle diversity is superior to horizontal angle diversity for typical narrow beamwidth strategic tropo-scatter systems,

- the optimum squint angle of a duplex dual vertical angle diversity system is approximately one beamwidth. The optimum boresight/horizon angle is about 1/4 beamwidth for L-band systems and 1/2 beamwidth for C-band systems,

- there is a long term advantage for angle diversity over space diversity due to the decorrelation of the scattering volumes in the former. This advantage is reduced by the greater variance of signal strength from the elevated beam. Empirical data from a Bell laboratories study [1.4] indicate that the two effects tend to cancel each other out,

- a method requiring the calculation of a determinant has been developed for the computation of average bit error probability of a troposcatter equalizer in an angle diversity system with multipath dispersion,

- on a system comparison basis, dual space/dual frequency (2S/2F) is generally inferior to dual space/dual angle

(2S/2A). The superiority of 2S/2A results chiefly from
the 3 dB advantage of the second power amplifier exceed-
ing half the squint loss in dB of the elevated beam. The
implication is that the number of frequencies required
for the strategic troposcatter plant could be halved
and overall system performance would be improved,

- the preliminary results on aperture to medium coupling
  loss as a function of frequency suggest that system
  improvement may result if L-band systems are converted
  to S-band.

The major portion of the remaining study effort will con-
centrate on validating the median path loss predictions in
order to provide an accurate absolute median path loss measure
and to verify the coupling loss dependence with frequency. The
results of the field tests will also provide an important em-
pirical guide for path loss prediction and for evaluating the
long term decorrelation advantage of vertical angle diversity.

SECTION 1

REFERENCES

[1.1] P.Monsen, S.Parl, J.N.Pierce,"Adaptive Antenna Control",
Interim Technical Report, ECOM Contract DAAB07-76-C-8085,
December 22, 1976.

[1.2] "Design Plan, Adaptive Antenna Control", ECOM Contract
No. DAAB07-76-C-8085, SIGNATRON, Inc., Feb. 9, 1977.

[1.3] "Test Plan, Adaptive Antenna Control," ECOM Contract No.
DAAB07-76-C-8085, SIGNATRON, Inc., April 29, 1977.

[1.4] P.Monsen, "Performance of an Experimental Angle Diversity
Troposcatter System," IEEE Trans. on Comm., Vol. COM-20,
No.2, April 1972, pp. 242-247.

SECTION 2

TROPOSCATTER PERFORMANCE PREDICTION

2.1 Introduction

In this section we shall describe in detail the background, theoretical as well as historical, for the development of the SIGNATRON troposcatter software package. This discussion will include a theoretical development of the propagation model, analytical performance prediction, and some numerical results. A comparison with the results of other authors will also be presented.

Theory and practical techniques for troposcatter communication started developing around 1950. [Booker and Gordon, 1950.] Two main theories have been proposed, the layer reflection theory [Friis, et. al., 1957] and the turbulent scattering theory. The turbulent scattering theory is based on the theory of turbulence structure developed in 1941 by Kolmogorov and Obukhov. The most complete treatment may be found in Tatarski [1971]. The layer reflection theory received the most attention in the beginning, partly because it predicted the observed linear dependence of the scattering crossection with wavelength. This theory also predicts a dependence on the scattering angle of the form θ^{-5}. In later years, experiments at higher frequencies, and hence narrower antenna beams, have confirmed the validity of the turbulence theory, with a scattering angle dependence of the form $\theta^{-11/3}$ and a wavelength dependence for the scattering crossection of the form $\lambda^{-1/3}$. In practice both phenomena can exist simultaneously with layer reflection being more frequent when wide-beam antennas and/or low frequencies are used. Experimental results [Eklund and Wickerts, 1968] indicate that the wavelength dependence can vary between λ^{-1} to λ^3. The scattering angle dependence has been measured to lie in the range of θ^{-2} to θ^{-6}.

The exponent in the scattering angle is called the refractive index spectrum slope since it also indicates the fall-off of the wave number spectrum of the refractive index, provided the wavelength is in the so-called inertial subrange [Tatarski, 1971, p52].

A third theory that has been proposed is the normal mode theory [Carroll and Ring, 1955]. This technique consists of considering the atmosphere as a waveguide propagating infinitely many modes of the electromagnetic field. Except for diffraction path analysis this method is generally not practical to use.

A number of theoretical and computational models have developed [Rice, et al, 1967; Hartman and Wilkerson, 1959; Booker and Gordon, 1950; Tatarski, 1971; Yeh, 1960]. Further references and a discussion of these models can be found in Larsen (1968) or Panter (1972). Most of these models have been constructed to agree with empirical measurements of a few selected parameters, parttularly the received signal level and its daily or seasonal variations. As a result the majority of the models are not suitable for prediction of a number of other parameters of interest, such as

- coupling loss,
- delay spread,
- receiver correlation distances,
- fade rate,
- angle diversity correlation,
- the dependence on distance,
- elevation angles,
- frequency, and
- standard atmospheric parameters.

The SIGNATRON troposcatter computer program is general in scope and can handle most of the parameter of interest without making unreasonable assumptions about the antenna gain patterns. This greater generality also means that the path has to be specified in a way more consistent with the underlying physics than has typically been done in the past. The ensuing discussion will therefore center on establishing a firm basis for describing the troposcatter model and its associated performance. This includes separate treatments of the

- properties of the troposphere
- path geometry and antenna patterns
- analytical evaluation of the model
- assessment of the effects of the approximations made
- comparison with analytical and empirical results.

The majority of the discussion will be directed to

- small to medium distance path
- microwave frequencies (300 MHz to 20 GHz)
- horizontally stratified atmosphere.

Correction terms for long distance paths are included. Most of the results apply to higher frequencies than listed above, but multiple scattering and large atmospheric absorption will limit the direct application of the model at higher frequencies.

2.2 The Troposphere for Beyond-the-Horizon Propagation

At the frequencies of interest the tropospheric radio propagation is well described by the theory of geometrical optics. We shall thus primarily use the ray-propagation technique and will ignore those almost line-of-sight paths where diffraction is the main mode of communication.

This section is intended partly as a reference for the subsequent sections and partly as an introduction to some of the theories of atmospheric structure employed in tropospheric scatter performance prediction. The topics to be discussed in this section are the standard atmosphere and refractive index variations in Section 2.2.1, layer reflection in Section 2.2.2, refractive index fluctuations in Section 2.2.3 and turbulent scatter in Section 2.2.4.

2.2.1 The Standard Atmosphere

Radio meteorological measurements normally yield pressure, temperature and water vapor content of the atmosphere. From such measurements the refractive index n, or the refractivity $N = (n - 1) \cdot 10^6$, can be determined from an empirical formula. The relation most commonly used is [Smith and Weintraub, 1953],

$$N = (n-1) \ 10^6 = \frac{77.6}{T} \ (p + 4810 \cdot \frac{e}{T}), \tag{2.1}$$

where

p = total pressure in millibars

e = water vapor pressure in millibars

T = temperature in Kelvin degrees.

This formula is designed to be valid in the temperature range $-50°$ C to $+ 40°$ C with an error less than .5% in N up to 30 GHz. An improved equation has been suggested by Thayer (1974) but for most radio application Eq. (2.1) is sufficiently accurate.

Measurements of the refractivity as a function of height above the surface of the earth results in a typical profile, as shown in Fig. 2.1. The refractivity at the surface is of the order of 300, and a nearly linear decrease with height is normally found in the first two or three kilometers. In the standard atmosphere the slope is 40 N-units/km. This line is also shown in Fig. 2.1.

The nearly linear decrease with heights at low altitudes makes it convenient to introduce an "effective earth radius" to account for the ray bending. We have shown previously [Monsen et al, 1976] that modeling the refractive index in the form

$$n(R_o + h) = n(R_o) \left[\frac{R_o}{R_o + h} \right]^\gamma , \quad o \leq h < 2 \text{ km}$$

leads to the exact relationship

$$R_e = \frac{R_o}{1 - \gamma} .$$

In these equations $R_o = 6368$ km is the actual earth radius, h is height above the surface and γ is a parameter determining the slope of the refractivity profile. R_e defines an equivalent earth radius in a transformed coordinate system with preserved distance measure on the surface and with straight line propagation in the atmosphere. For the standard atmosphere γ is

$$\gamma \text{ [standard atmosphere]} = 0.255,$$

corresponding to the earth radius factor K given by

$$K = \frac{R_e}{R_o} \sim \frac{4}{3} \text{ for the standard atmosphere.}$$
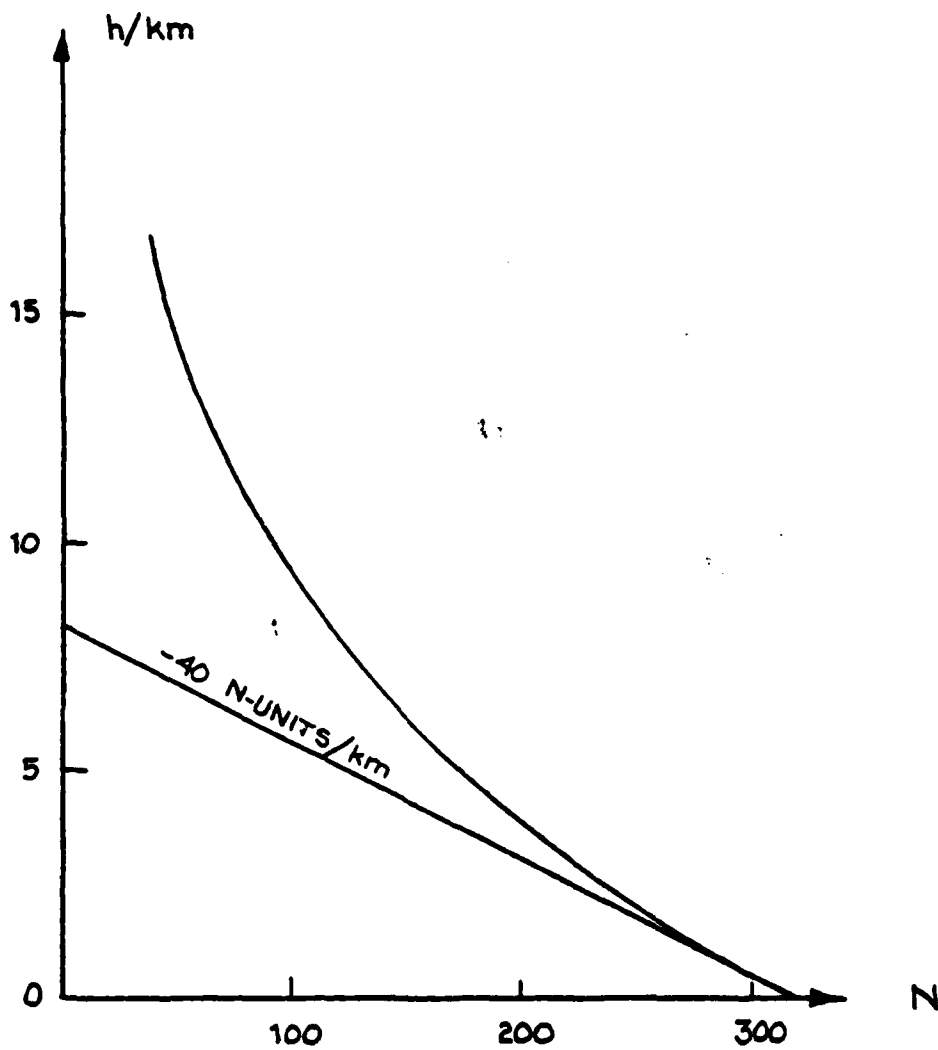
Fig. 2 .1   Typical Refractivity Profile

CCIR even defines a standard refractivity profile of the form

$$N = 289\ e^{-0.136\ h}.$$

In this form N(h) is close to the observed profile, but for most troposcatter applications it is adequate to use the linear approximation valid near the surface. The height of the common volume on a troposcatter path of length d where the antennas are aimed at the horizon is

$$h_c \sim \frac{d^2}{8R_e}$$

$$\sim\ 2\ \text{km if } d = 370\ \text{km (230 mi)}$$

$$\text{and } K = 4/3.$$

For longer paths an equivalent value of K may be found so that the scattering angle is correct. The small altitude errors introduced by this approach can be compensated for in the final analysis.

During conditions of super refraction it can sometimes be possible to have a direct path between transmitter and receiver on a path where troposcatter would normally be the only mode of communication. This can occur when the gradient of refractivity is steeper than -157 N-units/km. In general, variations of surface refractivity and gradient are functions of time-of-year and geographical location. Data have been accummulated over many years to allow a reasonable prediction of these parameters.

2.2.2 Reflection from Atmospheric Layers

The predominantly horizontal stratification of the atmosphere often contains local steep gradients in the transition from one

value of N to another. For electromagnetic waves with a wavelength
large compared to the width of the layer boundary such high
gradient regions look like an abrupt transition and can cause a
substantial reflection of energy. At higher frequencies the
transition appears more gradual and little or no energy is reflected.
At intermediate frequencies layer reflection and turbulent scattering
can exist simultaneously, greatly complicating the analysis of
troposcatter links. In this section we briefly summarize some
results relating to layer reflection or "feuillet" scattering.

Layer reflection and scattering were analyzed by Friis, Crawford
and Hogg (1957). The effective scattering crossection was found
for several types of layer structures. The dependence of the
crossection a_s, on wavelength λ and scattering angle θ, is listed
below (from Rice, et.al., 1967):

Large Layers: $\qquad a_s \propto \lambda^2 \theta^{-6}$ $\qquad\qquad\qquad$ (2.2)

Intermediate Layers: $a_s \propto \lambda^1 \theta^{-4}$ $\qquad\qquad\qquad$ (2.3)

Small Layers: $\qquad a_s \propto \lambda^0 \theta^{-4}$ $\qquad\qquad\qquad$ (2.4)

This may be compared with the mathematical formula listed below,
based on empirical results from radio data [Norton, 1960; Rice
et al, 1967],

$$a_s = \lambda \; \theta^{-5} \cdot \frac{3 \; \sigma_n^2}{L_o^2} \; , \qquad\qquad\qquad (2.5)$$

where σ_n^2 is the variance of the refractive index and L_o is the
outer scale of turbulence (see Section 2.2.3 for further details).
This formula is close to the behavior expected from intermediate
size layers. More recent high frequency data (>1GHz) indicate a some-

what different form of a_s, closer to that predicted by the Kolmogorov-Obukhov turbulence theory described in the next section.

2.2.3 Refractive Index Fluctuations

2.2.3.1 The Covariance Function

Superimposed on the average refractive index variations discussed in Section 2.2.1 is a small, rapidly fluctuating term, attributed to turbulence. Let $n(\underline{r})$ be the refractive index at a point $\underline{r}$, and with

$$n(\underline{r}) = n_o(\underline{r}) + n_1(\underline{r})$$

where $n_o(\underline{r}) = E\{n(\underline{r})\}$ and $n_1(\underline{r})$ is the small, fluctuating component,

$n(\underline{r})$ can be considered as a random field. The covariance function $\varphi_n(\underline{r}, \underline{r}')$ is

$$\varphi_n(\underline{r}, \underline{r}') = E\{n_1(\underline{r}) \, n_1(\underline{r}')\} \; .$$

If φ_n is a function only of $\underline{r} - \underline{r}'$ then the random field of $n(\underline{r})$ is said to be __homogeneous__, and the covariance function is written as $\varphi_n(\underline{r} - \underline{r}')$. If, in addition, φ_n is only a function of $|\underline{r} - \underline{r}'|$, then the random field is said to be __isotropic__ (in addition to homogeneous). The wavenumber spectrum of a homogeneous field is defined as the Fourier transform of the covariance function,

$$\phi_n(\underline{k}) = \phi_n(k_1, k_2, k_3) = \frac{1}{(2\pi)^3} \iiint \varphi_n(\underline{r}) \, e^{i \, \underline{k} \cdot \underline{r}} \, d^3\underline{r}$$

2.2.3.2 The Structure Function

The structure function $D_n(\underline{r}, \underline{r}')$ is defined by

$$D_n(\underline{r}, \underline{r}') = E\left\{[n_1(\underline{r}) - n_1(\underline{r}')]^2\right\}.$$

Where $D_n(\underline{r}, \underline{r}')$ is a function of $\underline{r} - \underline{r}'$ only, the random field $n(\underline{r})$ is said to be _locally homogeneous_. If $D_n(\underline{r}, \underline{r}')$ is a function of $|\underline{r} - \underline{r}'|$ only, then the field is _locally homogeneous and isotropic_. The structure function is occasionally more convenient to use than the covariance function since it allows a simple description of locally homogeneous fields without assuming homogeneity. However, the atmosphere is neither homogeneous nor locally homogeneous in the sense above. At a given point in space it is instead possible to find a small surrounding volume within which the condition for homogeneity is satisfied, and a slightly larger volume within which the condition for local homogeneity is satisfied. In most practical cases the extra generality of the structure function is not very important. In a nearly homogeneous volume the two functions are related by

$$D_n(\underline{r}) = 2\varphi_n(0) - 2\varphi_n(\underline{r}), \tag{2.6}$$

where $\underline{r}$ now represents the difference $\underline{r} - \underline{r}'$.

2.2.3.3 Scales and Structure Constant

In terms of the above defined functions we can define two important scales of the turbulence. The _inner scale_ ℓ_o, of the turbulence is the dimension of a small region near $\underline{r} = o$ where the structure function is well approximated by the first term in its Taylor series. If the turbulence is isotropic this scale is the same in all directions. The _outer scale_, L_o, is the correlation distance of $\varphi_n(\underline{r})$. These scales will be tied to specific formulas later, allowing us to evaluate them numerically. In isotropic turbulence with $\underline{r}$ in the range

$$\ell_o \ll r \ll L_o$$

we can usually write

$$D_n(r) = c_n^2 \, r^q \, .$$ (2.7)

The constant c_n^2 is called the structure constant of the refractive index, and plays a very important role in the study of turbulence. The power, q, has been shown by the theory of Kolmogorov and Obukhov [Tatarski, 1971] to be

$$q = 2/3.$$

2.2.3.4 The von Kármán Spectrum and the Kolmogorov-Obukhov Theory

The above discussion has been relatively general, since no specific covariance has been assumed. In the following we introduce the von Kármán spectrum which has been suggested as a possible approximation to the actual wave number spectra arising in atmospheric turbulence [Tatarski, 1971]. This spectrum has been verified experimentally in certain cases but, as we shall see, it can be necessary to use correcting terms in the inner scale region. The wave number spectrum is (nearly homogeneous and isotropic field assumed):

$$\Phi_n(k) = \frac{\Gamma\left(\frac{m}{2}\right)}{\pi^{3/2}\,\Gamma\left(\frac{m-3}{2}\right)} \frac{\sigma_n^2 \, r_o^3}{\left(1 + k^2 r_o^2\right)^{m/2}} \, , \; m > 3.$$ (2.8)

The corresponding covariance function is

$$\Psi_n(r) = \sigma_n^2 \, 2^{(5-m)/2} \cdot \frac{1}{\Gamma\left(\frac{m-3}{2}\right)} \left(\frac{r}{r_o}\right)^{(m-3)/2} K_{\frac{m-3}{2}}\left(\frac{r}{r_o}\right), \; m > 3$$

(2.9)

2-11

In these expressions σ_n^2 is again the variance of the refractive index, and r_o may be considered equal to the outer scale L_o of turbulence. The exponent m is usually called the refractive index spectrum slope since it indicates the slope of the spectrum when plotted on a logarithmic scale. From the small argument expansion of the Bessel function K_ν, $\nu > 0$, it can be verified that in Eq. (2.9)

$$\sigma_n^2 = \varphi_n(o).$$

Since $\Gamma(o) = \infty$ it is seen from (2.8), (2.9) that spectrum slopes of 3 or smaller may yield negative or infinite power $\varphi(o)$! The main reason for this is that the correct microstructure of the turbulent field has not been taken into account.

If the von Kármán spectrum is used a relation can be found between the variance of the refractive index, and the structure constant. For $r \ll r_o$ it is found that

$$D_n(r) \sim 2 \, \sigma_n^2 \, \frac{\Gamma\left(\frac{5-m}{2}\right)}{\Gamma\left(\frac{-1+m}{2}\right)} \, \frac{1}{\left(2 \, r_o\right)^{m-3}} \, r^{m-3}, \quad 3 < m < 5$$

or

$$c_n^2 = \sigma_n^2 \quad 2 \, \frac{\Gamma\left(\frac{5-m}{2}\right)}{\Gamma\left(\frac{-1+m}{2}\right)} \quad \frac{1}{\left(2r_o\right)^{m-3}} \tag{2.10}$$

For this to be valid it is further required that $m < 5$. In the special case of $m = 11/3$, as predicted by the Kolmogorov-theory (see Tatarski, 1971), we get

$$\frac{r_o^{2/3} \, c_n^2}{\sigma_n^2} \sim 2^{1/3} \quad \frac{\Gamma\left(\frac{2}{3}\right)}{\Gamma\left(\frac{4}{3}\right)} = 0.637 \, . \tag{2.11}$$

If $m \geq 5$ it can be shown that

$$D_n(r) \sim \begin{cases} 4\sigma_n^2 \left[\dfrac{r}{2r_o}\right]^2 \Big/ (m-5) \ , \quad m > 5 \\[20pt] 2\sigma_n^2 \left[\dfrac{r}{2r_o}\right]^2 \left[\ell n\left(\dfrac{r}{2r_o}\right) - 1 - .577\right], m = 5 \ . \end{cases}$$

We have assumed a locally homogeneous and isotropic medium, which is invalid when r is large in Eq. (2.9), or when k is small in Eq. (2.8). In fact, it is usually possible to assume that $k \, r_o \gg 1$ without jeopardizing the validity of Eq. (2.8),

$$\phi_n(k) \simeq \sigma_n^2 \, k^{-m} \, r_o^{3-m} \quad \frac{\Gamma\left(\frac{m}{2}\right)}{\pi^{3/2} \, \Gamma\left(\frac{m-3}{2}\right)}$$

$$= \frac{\Gamma(m-2)}{4\pi^2} \sin\left(\frac{\pi}{2}(m-3)\right) C_n^2 \, k^{-m}, \quad 3 < m < 5. \tag{2.12a}$$

In particular, for m = 11/3 we get

$$\phi_n(k) \simeq 0.033 \, C_n^2 \, k^{-11/3} \tag{2.12b}$$

This is the form in which the spectrum is most often used in turbulence theory.

As noted earlier, if k becomes very large, it is necessary to include the effect of the microstructure of the turbulence (e.g., the inner scale of turbulence). Tatarski (1971) has derived the expression (for m = 11/3)

$$\phi_n(k) = 0.033 \, C_n^2 \, k^{-11/3} \, \exp\left(-\frac{k^2}{k_m^2}\right) \tag{2.13}$$

where

$$k_m = 5.92/\ell_o .$$

The approximate structure function is

$$D_n(r) = \begin{cases} C_n^2 \; \ell_o^{-4/3} \; r^2 & r \ll \ell_o \\ \\ C_n^2 \; r^{2/3} & \ell_o \ll r \ll L_o \end{cases} .$$

ℓ_o is the inner scale of turbulence.

If an exponential factor like the one in Eq. (2.13) is used for other values of m in the general van Karman spectrum then the restriction m > 3 is no longer necessary. However, the variance of the refractive index will be strongly dependent on the inner scale, ℓ_o, when m < 3, while practically independent when m > 3.

2.2.3.5 <u>Theoretical and Empirical Evaluation of the Relevant Parameters</u>

In Section 2.2.1 an empirical formula for the mean refractive index was described. It relied on measurements of pressure, water vapor content, and temperature. A similar formula can be found for the variance σ_n^2 or the structure constant C_n^2. Tatarski (1971) has shown that the following expression can be used for C_n^2 in the Kolmogorov-Obukhov theory,

$$C_n^2 = c \cdot L_o^{4/3} M^2 \tag{2.14}$$

where

$$c \approx 2.8,$$

and

$$M = -\frac{79 \cdot 10^{-6} \cdot p}{T^2} \left(1 + \frac{15500q}{T}\right) \left(\frac{dT}{dz} + \gamma_a - \frac{7800}{1 + \frac{15500q}{T}} \cdot \frac{dq}{dz}\right) .$$

(2.15)

In the above expression,

L_o Outer scale of turbulence (in meters)

p Total pressure in m-bar

T Temperature in degrees Kelvin

$q \simeq 0.62 \, e_o/P$ Specific humidity

e_o Water vapor pressure in m-bar

z Altitude (in meters)

γ_a $.0098^\circ/Km$ (adiabatic temperature gradient).

C_n^2 then has the dimension of $m^{-2/3}$. Sirkis (1971) has used this formula to determine the dependence of M^2 on altitude and humidity for a typical atmosphere. The result is shown in Fig. 2.2. Up to about 2 km little variation with height is found, but C_n^2 can change two orders of magnitude when the humidity changes. Taking the values at the 2 km height and using the values of 20, 50, 100, 150 m for L_o yields the values for C_n^2 listed in Table 2.1.

TABLE 2.1

Typical Values of $10^{15} \cdot C_n^2$ (2 km) (Data by Sirkis, 1971)

L_o/m	Surface Water Vapor Pressure e_o			
	0	5 m-bar	15 m-bar	30 m-bar
20	.68	4.6	38.	106.
50	2.3	15.5	129.	361.
100	5.8	39.0	325.	910.
150	10.0	66.9	558.	1,562.
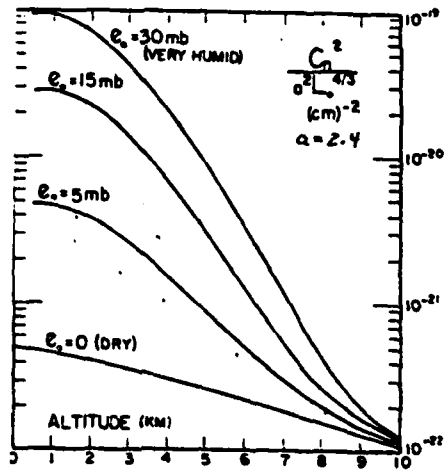
Fig. 2.2 Structure Parameter as Function of Altitude with Sea-Level Water Vapor Pressure as parameter. (From Sirkis, 1971)

In Table 2.2 these numbers for C_n^2 are converted to numbers for σ_n^2 using Eq. (2.11),

$$\sigma_n^2 = 1.57 \, L_o^{2/3} \, C_n^2$$
$$= 4.4 \, L_o^2 \, M^2 \quad .$$

TABLE 2.2

Typical Values of Refractive Index Variance $\sigma_n^2 \cdot 10^{13}$

L_o/m	Surface Water Vapor Pressure			
	0	5 m-bar	15 m-bar	30 m-bar
20	.08	.52	4.4	12.3
50	.5	3.3	27.	77.
100	2.0	13.2	110.	308.
150	4.5	29.7	247.	593.

To get an idea of typical humidity levels we list below the water vapor pressure measured by radiosonde at Albany, NY, November 5, 1976 (morning).

Altitude (m)	Water Vapor Pressure (m-bar)
86	6.02
145	5.80
256	5.08
733	3.35
927	2.56
1197	2.84
1297	1.73
1362	3.48
1456	3.27
1656	3.81
1995	4.31
2977	2.73

Several measurements at Albany and Buffalo of the same time-of-year gave very similar results with surface water vapor in the range of 4-8 m-bar. Lower values can be expected in colder winter months, while considerably higher values are typical in the summer.

Several researchers have made measurements of C_n^2. Radar reflectivity measurements [Kropfli et.al., 1968; Hardy and Katz, 1969] indicated C_n^2 to be in the range

Weak scatter: $C_n^2 \sim 20 \cdot 10^{-15} \; m^{-2/3}$

Medium scatter: $C_n^2 \sim 100 \cdot 10^{-15} \; m^{-2/3}$

Strong scatter: $C_n^2 \sim 6000 \cdot 10^{-15} \; m^{-2/3}$.

The two first numbers match fairly well with the results in Table 2.1 for $L_o \sim 50$ m. The strong scatter returns measured could be due to atmospheric layering. Most (~75%) of the reported measurements lie in the range $0-100 \cdot 10^{-15} \; m^{-/23}$.

Brookner (1970) reported on some measurements of the optical C_n^2 performed by Goldstein, et.al., (1965). A typical measurement of C_n^2 vs time of day is shown in Table 2.3. Brookner (1970) then uses the following values for C_n^2 as typical at optical wavelength

Weak scatter: $C_n^2 \sim .5 \; 10^{-15} \; m^{-2/3}$

Medium scatter: $C_n^2 \sim 50 \; 10^{-15} \; m^{-2/3}$

Strong scatter: $C_n^2 \sim 500 \; 10^{-15} \; m^{-2/3}$.

These somewhat arbitrarily chosen values should be compared with the dry air column in Table 2.1.

TABLE 2.3

C_n^2 vs Time of Day [Goldstein et. al., 1965]

Time	$10^{15} \cdot C_n^2 \ [m^{-2/3}]$
1200	14
1300	140
1400	490
1500	90
1600	20
1700	4
1800	.4
1900	~ 0
2000	.2
2100	1
2200	2
2300	3
2400	6

Approximate relationships for the inner and outer scales of turbulence have also been obtained [Brookner,1970; Fried, 1967],

$$\ell_o \approx 10^{-3} \ h^{1/3} \tag{2.16}$$

$$L_o \approx 2 \ h^{1/2} . \tag{2.17}$$

l_o, L_o and the height h are all in meters. As an example, these relations yield at a 2 km height,

$$l_o \sim 13 \text{ mm}$$

$$L_o \sim 90 \text{ m.}$$

Superimposed on these relationships are variations with time-of-day, season, weather, etc., so they should only be used as a general guide.

The variation of C_n^2 with height has been found empirically to be

$$C_n^2 = C_n^2(h) = C_{no}^2 \, h^{-b} \, \exp(-h/h_o)$$

Fried (1967) used b = 1/3, h_o = 3200 m. In fact, $\sigma_n^2(h)$ was found to be of the form

$$\sigma_n^2(h) \cong 6.7 \cdot 10^{-14} \, \exp(-h/3200 \text{ m}).$$

These results are for optical frequencies, which should correspond to dry air at radio frequencies. A comparison with Fig. 2.2 shows that the expected height dependence is somewhat weaker than indicated by the model of Fried. On the other hand newer data indicates a much stronger height dependence, with b $\sim$ 2/3 and $h_o \sim$ 320 m [see Brookner, 1970, 1971]. Hence the issue of height dependence is not quite resolved, although it appears (see Fig. 2.2) that variations in the first 2-3 km can be ignored, while formulas of the form above can be applied at higher altitudes. Additional data on both the optical and the microwave refractive index variance can be found in Gossard (1977).

From the existing data we can conclude the following typical values (at a height of 1-2 km)

$$C_n^2 \simeq 10^{-15} \ m^{-2/3} \ \text{(dry air)} \ \text{to} \ 10^{-14} \ \text{(maritime air)}$$

$$\sigma_n^2 \simeq 5 \cdot 10^{-14} \ \text{to} \ 10^{-12}, \ \text{depending on humidity;}$$

$5 \cdot 10^{-14}$ will be used to represent winter conditions.

$$L_o \simeq 70 \ m$$

$$\ell_o \simeq 10 \ mm.$$

2.2.4 Results from the Theory of Turbulent Scatter

It is well known that the power received from a small scattering volume can be written

$$P_R = P_T \cdot \frac{G_T}{4\pi R_T^2} \cdot \frac{a_s}{4\pi R_R^2} \cdot \frac{\lambda^2 G_R}{4\pi}, \tag{2.18}$$

where

P_T = Transmitter power

G_T = Gain of transmitting antenna

R_T = Distance from transmitter to scatterer

a_s = Scattering cross-section of the turbulent volume

R_R = Distance from scatterer to receiver

λ = Wavelength

G_R = Gain of receiving antenna.

Eq. (2.18) also serves as a definition of the scattering cross-section (some authors define $a_s/4\pi$ as the scattering cross-section). In section 2.2.2 we describe some general relationship derived for atmospheric layer scattering. Tatarski (1971) has derived the cross-section of turbulent scatter with a given wave number spectrum,

$$a_s = 8\pi^2 \, k^4 \, \Phi_n \left(2k \sin \frac{\theta}{2}\right) \sin^2 \chi \, dV, \quad \ell_o \ll \lambda \ll L_o$$

(2.19)

In this equation,

$k = 2\pi/\lambda$ is the wave number,

$\Phi_n(k)$ is the locally homogeneous and isotropic wave spectrum (e.g., Eq. 2.8)

θ is the scattering angle

$\sin^2 \chi$ accounts for loss due to polarization mismatch (usually negligible).

χ angle between incoming electric field and direction of propagation.

dV is the infinitesimal volume.

Eq. (2.19) is derived under the assumption

$$L_o \ll \sqrt{\lambda R_R} \,, \quad \sqrt{\lambda R_T}$$

but has been verified at much higher frequencies. If a spectrum of the von Kármán type is assumed in the inertial subrange (i.e., $\ell_o \ll \lambda \ll L_o$), it is found

$$a_s = \sigma_n^2 \, 8 \, \sqrt{\pi} \, k^{4-m} \, r_o^{3-m} \, \frac{\Gamma\left(\frac{m}{2}\right)}{\Gamma\left(\frac{m-3}{2}\right)} \, \left(2 \sin \frac{\theta}{2}\right)^{-m} \, dV.$$

Polarization losses have been ignored in this equation. For $m = 11/3$ we get the cross-section prediction by the Kolmogorov-Obukhov theory, while for $m = 5$ we get the semi-empirical formula in Eq. (2.5). The data for Eq. (2.5) are mostly at frequencies below

1 GHz. Newer experiments at higher frequencies indicate that
m = 11/3 provides the better fit to the data (e.g.,Seehars,1971). At
intermediate frequencies a mixture of the different effects may
be described by an equivalent $\dot{m}$ in the range $3 < m \leq 5$. Combining
the above expression for a_s with Eq. (2.18)

$$P_R = P_T G_T G_R \cdot C \iiint\limits_V \frac{1}{R_T^2(\underline{r}) R_R^2(\underline{r})} \left[2 \sin \frac{\theta(\underline{r})}{2} \right]^{-m} d^3\underline{r}, \quad (2.20)$$

where

$$C = \sigma_n^2 \, r_o^{3-m} \, k^{2-m} \cdot \frac{\Gamma\left(\frac{m}{2}\right)}{2\sqrt{\pi}\,\Gamma\left(\frac{m-3}{2}\right)} \quad (2.21)$$

and V is the total scattering volume. Typical values of the at-
mospheric parameters σ_n^2 and $r_o = L_o$ were described in the previous
section. The spectrum slope m is 11/3 for turbulence theory and
5 for the NBS model. Direct measurements of m were performed by
Eklund and Wickerts (1968) by comparing the received power at 1
and 3 GHz at two antennas with the same beamwidth. Average values
of m in the range of 11/3 to 5 were measured, and a significant
correlation with the signal level was observed. This is consistent
with the theory that both turbulence and layer reflection are im-
portant at these frequecies since strong layering both increase m
and the signal level. Eklund and Wickerts concluded that reflection
is dominating at 1 GHz and turbulence at 3 GHz.

Gjessing and McCormick (1974) also report measurement of m in
the range of 2-6 and give an empirical formula for m (Gjessing et.al.,
1969) and an empirical distribution. However, the validity of these
results is apparently limited (Sherwood and Suyemoto,1976) particularly
since a strong frequency dependence of the equivalent measured m
should be expected from the discussion above.

2-23

2.3 Path and Antenna Parameters

In this section we list the parameters that are required to specify the troposcatter path completely, and briefly comment on the significance of some of these parameters. Most of the models developed in the past have used only a subset of them, or have used some of them indirectly through other auxiliary parameters. A few secondary parameters characterizing the path will also be discussed.

2.3.1 Path Geometry

A typical path is shown in Fig. 2.3 with some of the parameters involved. The parameters are

- Frequency f

- Distance d

- Heights h_T, h_R of transmitter and Receiver antennas above mean Sea Level (MSL).

- Horizon elevations above horizontal $(\theta_{TG}, \theta_{RG})$ at transmitter and receiver. These angles can depend on the atmospheric conditions.

- Antenna boresight elevations above horizontal (θ_T, θ_R) at transmitter and receiver.

  Note that $\theta_T - \theta_{TG}$ and $\theta_R - \theta_{RG}$ are then the elevation of the antennas above the horizon. The definition of "boresight" need not be the direction of maximum gain, but may be defined from mechanical consideration (e.g., the normal to a phased array).

- Azimuth pointing angles φ_T, φ_R if horizontal diversity is employed, or beam swinging experiment performed.

2-24
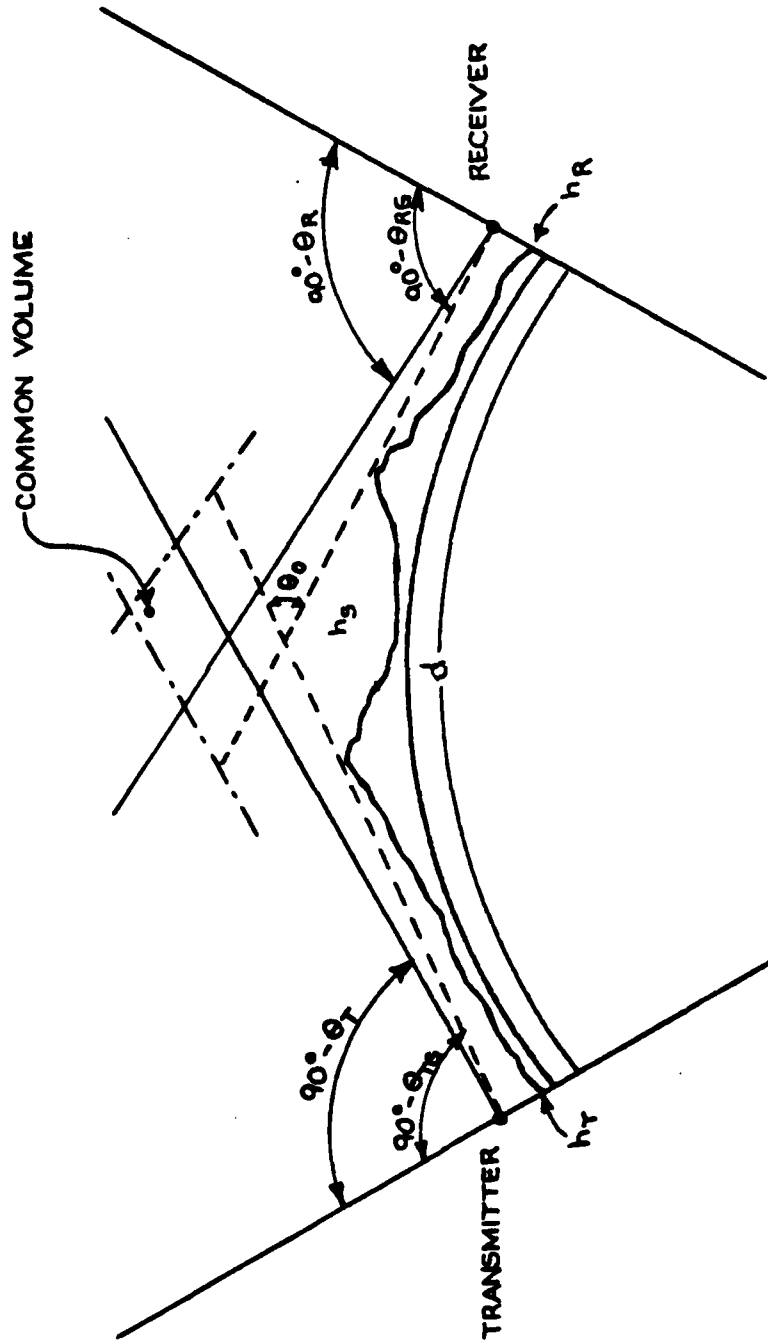
Fig.2.3   Path Geometry

- Gain patterns $G_T(\theta,\varphi)$, $G_R(\theta,\varphi)$ of transmitting and receiving antennas. Determination of the gain patterns requires a number of additional parameters – size and type of antennas, height above ground, ground profile and reflectivity. The patterns should be referenced with respect to the boresight direction. Both amplitude and phase of the voltage gain patterns are required when the cross correlation between two (diversity) pathe is to be calculated.

- Polarization of transmitter and receiver

- Bandwidth

- Power

- Atmospheric parameters K, σ_n^2, wind velocity, attenuation, etc. (See section 2.2)

The performance is particularly sensitive to the antenna elevation angles which are often not adequately specified in actual experiments.

2.3.2 Antenna Parameters

In most theoretical studies it is assumed that the antenna pattern has an ideal rectangular shape. This ideal pattern is extremely convenient for analysis, but the actual pattern is substantially different. An equivalent ideal beam shape may undoubtedly be postulated but a general relation of this to the actual beam shape is not well defined Often the 3 dB beamwidth is arbitrarily chosen to define the equivalent ideal beam. We shall later (section 6) estimate how good such an approximation is for troposcatter purposes. For simplicity the considerations will be limited to the parabolic dish.

The gain pattern of a parabolic dish can easily be evaluated for a uniform illumination by the feedhorn, as well as for some specific non uniform illumination patterns.

2-26

Let

     a = radius of the circular aperture

     A = Area of aperture

     λ = wavelength

     θ = angle off boresight

     r = distance from center of aperture

   $b(r)$ = illumination of aperture; $b(0) = 1$.

The voltage gain pattern is then

$$g(\theta) = \cos\theta \; \frac{1}{A} \iint dA \; e^{j\frac{2\pi x}{\lambda}\sin\theta} \; b(r) \qquad |\theta| < \frac{\pi}{2}$$

where x is the distance from the center along the line at the
intersection of the plane of the aperture and the plane determined
by the incoming ray and the aperture normal. Hence, using the co-
ordinates (r, φ) in the aperture,

$$g(\theta) = \frac{\cos\theta}{\pi a^2} \int_0^a rdr \int_0^{2\pi} d\varphi \; b(r) \; e^{j\frac{2\pi r}{\lambda}\cos\varphi\,\sin\theta}$$

$$= \frac{2\cos\theta}{a^2} \int_0^a dr \; b(r) \cdot r \; J_0\left(\frac{2\pi r}{\lambda}\sin\theta\right) .$$

If the aperture is uniformly illuminated then $b(r) = 1$, and

$$g(\theta) = g_0(\theta) = 2 \; \cos\theta \; J_1\left(\frac{2\pi a}{\lambda}\sin\theta\right) \bigg/ \left(\frac{2\pi a}{\lambda}\sin\theta\right) .$$

If we try a non uniform illumination of the form

$$b(r) = \left(1 - (r/a)^2\right)^{\mu} ,$$

then

$$g(\theta) = g_\mu(\theta) = \cos\theta \; 2^{\mu+1}(\mu+1)! \; \frac{J_{\mu+1}\left(\frac{2\pi a}{\lambda}\sin\theta\right)}{\left(\frac{2\pi a}{\lambda}\sin\theta\right)^{\mu+1}} .$$

2-27

The half power beamwidths are determined by (ignoring the cos θ term)

$$\frac{2\pi a}{\lambda} \sin\left(\frac{B_{3dB}}{2}\right) = \begin{cases} 1.616 & \mu = 0 \\ 1.815 & \mu = \frac{1}{2} \\ 1.994 & \mu = 1 \end{cases}$$

The beamwidth for $\mu = 1$ is approximately 23% larger than for uniform illumination, and this is close to the performance that is obtained with practical dishes. If we define the beamwidth efficiency of the antenna as

$$\text{efficiency} \triangleq \frac{\text{area with uniform illumination giving actual 3 dB width}}{\text{real area of the dish}}$$

we get:

$$\text{efficiency} = \begin{cases} 100\% & \mu = 0 \\ 79\% & \mu = \frac{1}{2} \\ 66\% & \mu = 1 \end{cases} \quad.$$

It can also be useful to know the null-beamwidth of the antenna. If B_{null} is this beamwidth, we have

$$\frac{2\pi a}{\lambda} \sin\left(\frac{B_{null}}{2}\right) = \begin{cases} 3.832 & \mu = 0 \\ 4.493 & \mu = \frac{1}{2} \\ 5.136 & \mu = 1 \end{cases} \quad.$$

The nullwidth with non uniform illumination is much wider than the 3 dB width. Finally the level of the first sidelobe can be found for the general beam pattern above,

$$\text{sidelobe level} = \begin{cases} -17.6 \text{ dB} & \mu = 0 \\ -21.3 \text{ dB} & \mu = \frac{1}{2} \\ -24.6 \text{ dB} & \mu = 1 \end{cases}$$

2-28

For the remote sidelobes the envelope of the asymptotic expansion of the Bessel functions can be used as a bound,

$$G(\theta) = |g(\theta)|^2 \lesssim \cos^2\theta \frac{\left[(\mu+1)!\right]^2}{\pi} \left(\frac{\pi a}{\lambda} \sin\theta\right)^{-2\mu-3} .$$

A nonuniform illumination is often used on purpose to achieve the much better sidelobe properties at a small cost of aperture efficiency. The antenna gain G can be evaluated as follows:

$$4\pi/G = \int_0^{2\pi} d\varphi \int_0^{\pi/2} d\theta \, \sin\theta \, |g_\mu(\theta)|^2$$

$$= 2\pi \int_0^{\pi/2} d\theta \, \cos^2\theta \, \sin\theta \, 4^{1+\mu}(1+\mu)!^2 \frac{J_{1+\mu}^2 (c \sin\theta)}{(c \sin\theta)^{2(\mu+1)}}$$

where

$$c = \frac{2\pi a}{\lambda} \gg 1 .$$

Hence

$$2/G \simeq 4^{1+\mu}\left[(1+\mu)!\right]^2 \frac{1}{c^2} \int_0^c \frac{J_{1+\mu}^2(t)}{t^{2\mu+1}} \, dt$$

or

$$G \simeq \frac{1+2\mu}{(1+\mu)^2} \left[\frac{2\pi a}{\lambda}\right]^2 .$$

A definition of gain efficiency analogous to beamwidth efficiency results in

$$\text{gain efficiency} = \begin{cases} 100\% & \mu = 0 \\ 89\% & \mu = \frac{1}{2} \\ 75\% & \mu = 1 \end{cases} .$$

2.4 The Troposcatter Model with Wide-Beam Antennas: Path Loss Calculation

The path geometry of Section 3 and the tropospheric scatter model of Section 2.4 will be combined to find the performance of some typical, although idealized, troposcatter links. It will be assumed in the following that the earth is smooth and non-reflecting and that the antenna beams are pointed just above the horizon.

2.4.1 Theoretical Development

The integration over the common volume will assume a spectrum of the von Karman type, so that the path loss L_p is given by Eq. (2.20).

$$L_p = -10 \log \left[C \iiint_V \frac{1}{R_R^2(\underline{r}) R_T^2(\underline{r})} \left[2 \sin \frac{\theta(\underline{r})}{2} \right]^{-m} d^3\underline{r} \right]$$

(2.22)

where C is given by Eq. (2.21). The integral will be evaluate by integration over the transmitter and receiver elevation angles θ_T, θ_R and the distance z perpendicular to the great-circle plane. The integration is illustrated in Fig. 2.4 by a view in the great-circle plane, i.e., the z-axis is perpendicular to the paper.

The angles α_R, α_T are defined by

$$\alpha_R = \theta_R + d/2R_e$$

$$\alpha_T = \theta_T + d/2R_e$$

where R_e is the effective earth radius θ_R and θ_T range from the horizon (θ_{TG}, θ_{RG}) and up. The distance d_o is

$$d_o = 2 R_e \sin (d/2R_e),$$
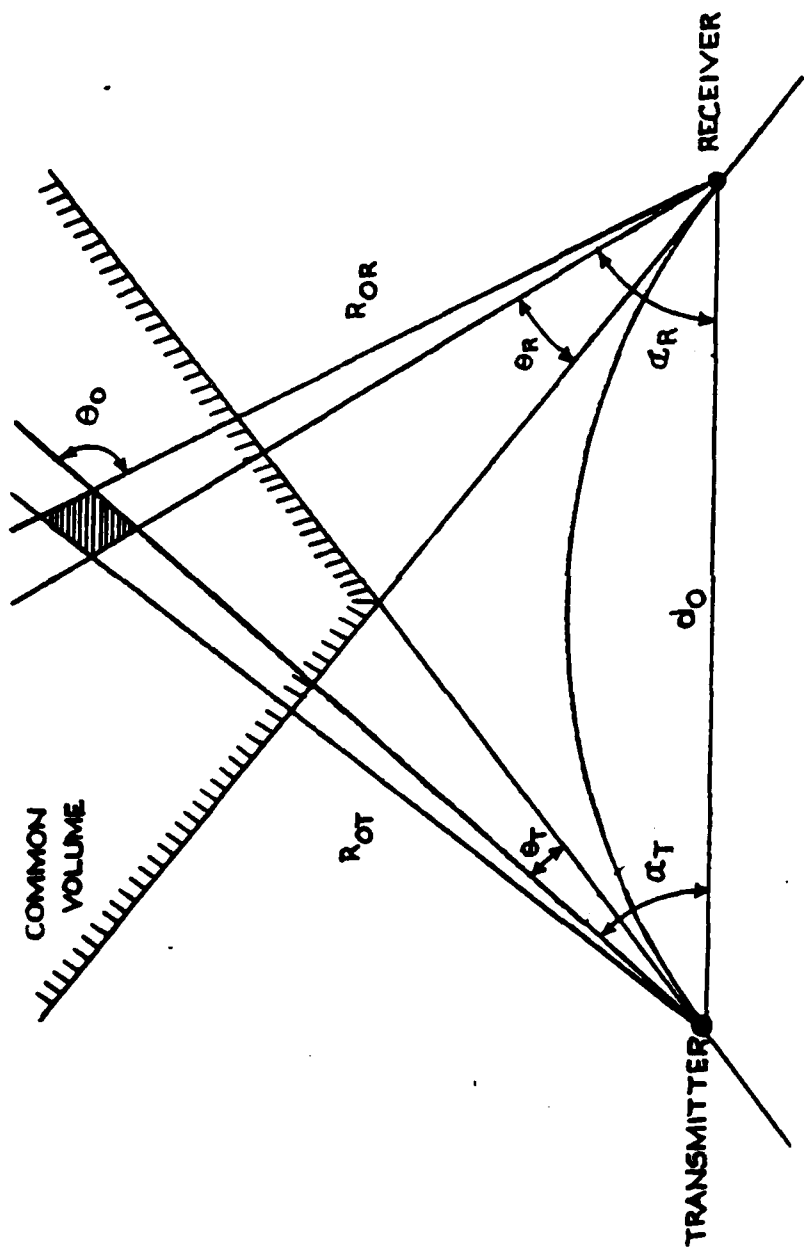
Fig.2.4   The Common Volume Integration

and the scattering angle in the great-circle plane is

$$\theta_o = \alpha_R + \alpha_T \ .$$

The infinitesimal integration volume dV is projected onto the great-circle plane at the distances R_{OT}, R_{OR} from the transmitter and receiver, where

$$R_{OT} = d_o \sin \alpha_R / \sin \theta_o$$

$$R_{OR} = d_o \sin \alpha_T / \sin \theta_o \ .$$

The total distances from the point of integration to the terminals are

$$R_T = \sqrt{R_{OT}^2 + z^2}$$

and

$$R_R = \sqrt{R_{OR}^2 + z^2} \ .$$

The scattering angle θ at the point of integration can be determined by

$$\left(2 \sin \frac{\theta}{2} \right)^2 = \frac{\left(2 \sin \frac{\theta_o}{2} \right)^2 + 2 \left[(1+z_T^2)(1+z_R^2) \right]^{\frac{1}{2}} - 2 + 2 z_T z_R}{\left[(1+z_T^2)(1+z_R^2) \right]^{\frac{1}{2}}}$$

where

$$z_T = z/R_{OT}$$

and

$$z_R = z/R_{OR} \ .$$

It is now assumed that the strong scattering angle dependence allows us to ignore points where $z \gg R_{OR}$ or R_{OT}. This approximation is good if θ is small enough. Hence it is found

2-32

$$\left(2 \sin \frac{\theta}{2}\right)^2 \simeq \left(2 \sin \frac{\theta_O}{2}\right)^2 + \frac{z^2}{R_O^2} \quad ,$$

where the distance R_O is defined by

$$\frac{1}{R_O} = \frac{1}{R_{OT}} + \frac{1}{R_{OR}}$$

The integrand in Eq. (2.22) is first integrated in the z-direction

$$\int_{-\infty}^{\infty} dz \left(2 \sin \frac{\theta}{2}\right)^{-m} \frac{1}{R_T^2 R_R^2} \simeq \frac{1}{R_{OT}^2 R_{OR}^2} \int_{-\infty}^{\infty} dz \left[\left(2 \sin \frac{\theta_O}{2}\right)^2 + \left(\frac{z}{R_O}\right)^2\right]^{-m/2}$$

$$= \frac{R_O}{R_{OT}^2 R_{OR}^2} \left(2 \sin \frac{\theta_O}{2}\right)^{1-m} B\left(\frac{1}{2}, \frac{m-1}{2}\right) \quad .$$

$B(x, y)$ is the beta function,

$$B(x, y) = \frac{\Gamma(x)\Gamma(y)}{\Gamma(x+y)} \quad .$$

The infinitesimal area in the great-circle plane is

$$dA = R_{OT} d_{\alpha T} \cdot R_{OR} d_{\alpha R} / \sin \theta_O \quad .$$

The path loss in Eq. (2.22) now becomes

$$10^{-L_p/10} = C_2 \int_{\alpha_{TO}}^{\pi/2} d\alpha_T \int_{\alpha_{RO}}^{\pi/2} d\alpha_R \left[\left(R_{OT} + R_{OR}\right) \sin \theta_O \left(2 \sin \frac{\theta_O}{2}\right)^{m-1}\right]^{-1}$$

where

$$C_2 = C \ B \left(\frac{1}{2}, \frac{m-1}{2} \right)$$

$$\alpha_{TO} = \alpha_o + \theta_{TG}$$

$$\alpha_{RO} = \alpha_o + \theta_{RG}$$

and

$$\alpha_o = d/2R_e \ .$$

We now involve the small angle assumption,

$$\sin \theta_o \simeq \theta_o$$

$$2 \sin \frac{\theta_o}{2} \simeq \theta_o$$

$$R_{oT} + R_{oR} \simeq d_o \simeq d.$$

L_p is then with good approximation given by

$$10^{-L_p/10} \simeq C_2 \ \frac{1}{d} \int\limits_{\alpha_o + \theta_{TG}}^{\infty} d\alpha_T \int\limits_{\alpha_o + \theta_{RG}}^{\infty} d\alpha_R \ (\alpha_T + \alpha_R)^{-m}$$

$$= \frac{C_2}{d(m-1)(m-2)} \left(2\alpha_o + \theta_{RG} + \theta_{TG} \right)^{2-m}$$

$$= \frac{C \ B\left(\frac{1}{2}, \frac{m-1}{2} \right)}{d(m-1)(m-2)} \left(\frac{d}{R_e} + \theta_{RG} + \theta_{TG} \right)^{2-m} \tag{2.23a}$$

In this equation the factor C contains terms depending on frequency, spectrum slope m, correlation distance r_o, and the refractive index variance. From Eq. (2.21) we have

2-34

$$C = \sigma_n^2 \, r_o^{3-m} \cdot k^{2-m} \, \Gamma\!\left(\frac{m}{2}\right)\!\Big/\!\left(2\sqrt{\pi} \; \Gamma\!\left(\frac{m-3}{2}\right)\right).$$

Assuming for simplicity that $\theta_{RG} = \theta_{TG} = 0$ (no elevated horizons) and introducing the expression for C in terms of the known parameters we get

$$10^{-I_p/10} = \frac{(m-3)}{4\,(m-1)\,(m-2)} \cdot \sigma_n^2 \; r_o^{3-m} \; k^{2-m} \; \theta_{min}^{2-m} \,/d \qquad (2.23b)$$

The approximations made are good when $d \ll R_e$ and $m > 3$. Waterman (1958) has evaluated the integral in Eq. (2.22) exactly for m an even integer and $\theta_{TG} = \theta_{RG} = 0$. For small values of d/R_e his result agrees with Eq. (2.23).

Eq. (2.23) was derived assuming constant values of σ_n^2 and $r_{o_2} = L_o$. The empirical results of Fried (1967) indicates that σ_n^2 and L_o depend on height,

$$\sigma_n^2 = \sigma_{no}^2 \, \exp\,[-h/h_o]$$

$$L_o = L_{oo} \, (h/h_o)^{\frac{1}{2}}$$

where Fried found that

$$h_o = 3200 \text{ m.}$$

$$\sigma_{no}^2 = 6.7 \cdot 10^{-14}$$

$$L_{oo} = 113 \text{ m}$$

The discussion in Section 2.2.3.5 indicates that h_o may be smaller and that σ_{no}^2 can be quite different from the values indicated above. For equal height of the terminals

$$h \simeq R_e \left(\theta_{min}^2 - (\theta_{RG} - \theta_{TG})^2 \right) \left(\theta_{min}^2 - (\theta_{RG} + \theta_{TG})^2 \right) / 8 \theta_{min}^2$$

and L_p can be written directly in terms of usually specified parameter.

2.4.2 Comparison with Other Methods

A number of empirically based methods exist to predict path loss. Unfortunately most of the empirical results were found at frequencies below 1 GHz, where layer reflection is likely to be more dominant than turbulent scatter. This means that these methods often have limited applicability at higher frequencies. One of the most widely used techniques is that developed by NBS (Rice, et. al., 1967). At distances such that $\theta d < 10$ km the predicted path loss with omnidirectional antennas is

$$L_p = 135.8 + 0.34 \frac{\theta d}{1 \text{ km}} + 30 \log \frac{f}{1 \text{ MHz}} + 10 \log \frac{d}{1 \text{ km}} + 30 \log \theta \text{ dB}$$

$$= -74.2 \text{ dB} + 0.34 \cdot 10^{-3} \theta d + 30 \log f + 10 \log d + 30 \log \theta$$

where θ is the scattering angle in radians and all other units are MKS. This has the same form as Eq.(2.23) if m = 5. This is consistent with the fact that the NBS method is mostly based on measurements in the 100-1000 MHz range, where layer reflection is expected to dominate the scatter mechanism. Hence the values of σ_n^2 and r_o found in Section 2.2 for turbulent scatter are not directly applicable, but can be chosen to fit the above equation, which could then be used at low frequencies. We shall restrict the comparison to nearly symmetric links. First, let the term $.34 \cdot 10^{-3} \theta d$ be due to variations of σ_n^2 with height of the form

$$\sigma_n{}^2 = \sigma_{no}{}^2 \exp\lceil -h/h_o\rceil = \exp(-d(\theta+\theta_T+\theta_R)/8h_o).$$

Assuming small elevation angles it is then seen that

$$.34 \cdot 10^{-3} = \frac{10}{2.303}\ \frac{1}{8h_o}\ ,$$

or

$$h_o = 1.6 \text{ km.}$$

This is only two times smaller than the value suggested by Fried for optical system, and compares favorably with other data (Brookner, 1971; Gossard, 1977). By comparison with Eq. (2.23) $\sigma_{no}{}^2/r_o{}^2$ is found,

$$\frac{\sigma_{no}{}^2}{r_o{}^2} = \left.\frac{\sigma_n{}^2}{r_o{}^2}\right|_{h \,\widetilde{\approx}\, o} = 5.8 \cdot 10^{-15}\ m^{-2}$$

This number would also be found in a humid turbulent atmosphere. At higher elevation the dependence of r_o on h is significant. This is reflected in the NBS method by the use of a different formula when $\theta d > 10$. It can be verified from the above numbers that the Fried formula for $\sigma_n{}^2\, r_o{}^{-2/3}$ combined with the rest of Eq. (2.23b) with m = 5 deviates by less than 1 dB from the NBS method in the altitude range 300-3000m.

We can now compare layer-refledtion with turbulent scatter. Fig.2.5 shows the expected path loss as predicted by the NBS formulas; and the path loss is predicted by the turbulent scatter theory with

$$\sigma_n{}^2 = 5 \cdot 10^{-14}\text{(typical for dry air)}$$
$$r_o = 70 \text{ m}$$
$$m = 11/3.$$

It is clear seen how turbulent scatter is dominant at higher frequencies and distances. In the transition region (usually in the band between 1 and 10 GHz) both layer reflection and turbulence can be dominant, depending critically on actual parameters and therefore also both on location and season.   In wet
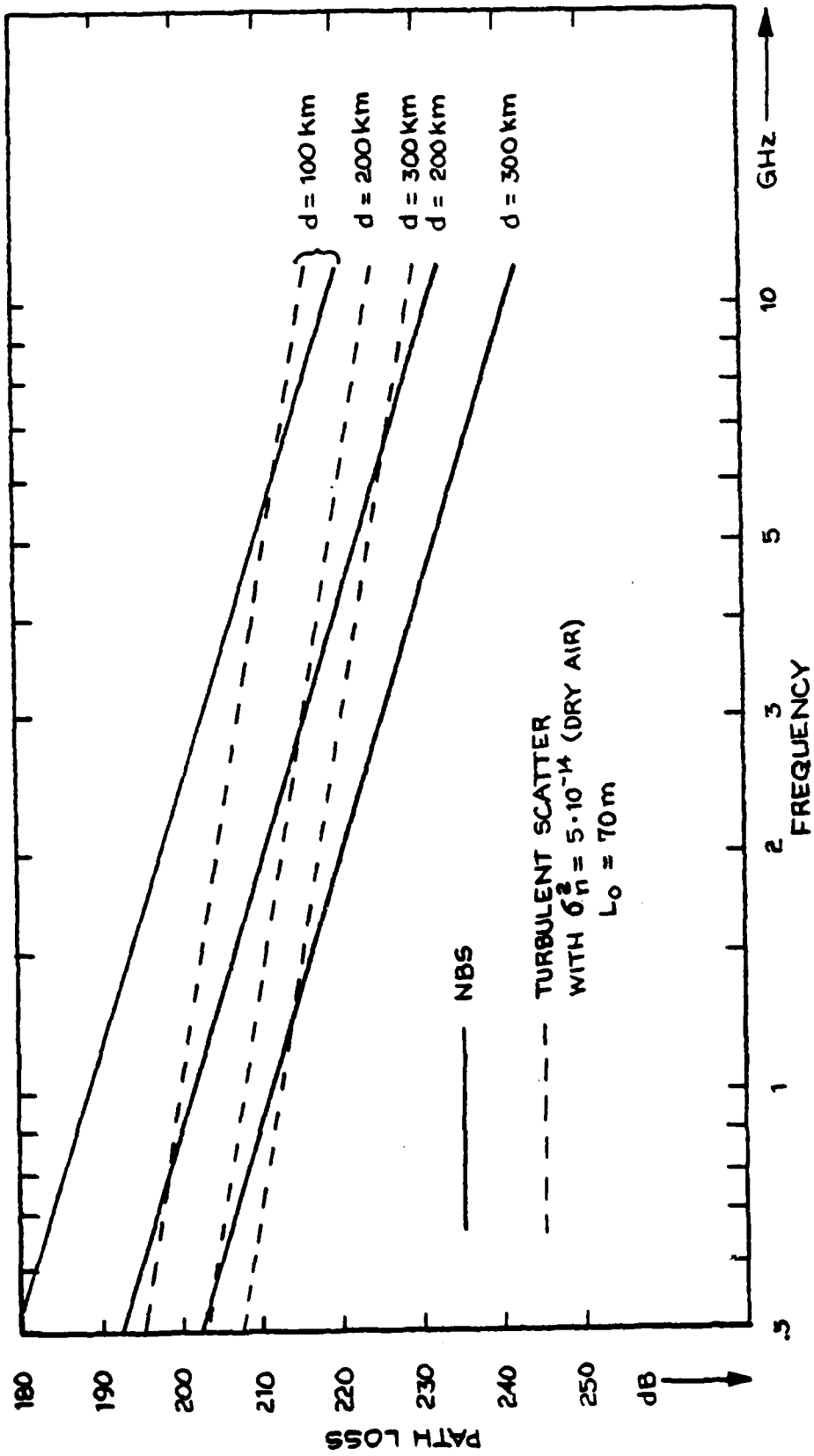
Fig. 2.5   Path Loss Versus Frequency for the NBS Model and the Turbulent Scatter Theory with Typical Parameters.

2-38

air the turbulence signal can be 20 dB stronger. Several methods
other than that of NBS are discussed by Panter (1972). We can
mention the CCIR method (nearly the same as the NBS method), Yeh's
method and the method of Collins Radio.

The method of Yeh predicts the path loss

$$L_p = 30 \log \frac{f}{1 \text{ MHz}} + 20 \log \frac{d}{1 \text{ mi}} + 573 \, d/R_e - 0.2 \, (N_s - 310) + 57$$

where N_s is the surface refractivity. This is shown in Fig. 2.6
for a 5 GHz link, together with some of the other prediction
methods.

The method of Collins is based on an experimental curve at
1 GHz. An excellent approximation to this curve up to 300 mi
yields

$$L_p = 30 \log \frac{f}{1 \text{ GHz}} + 80 \log \frac{d}{1 \text{ mi}} + 34.$$

This curve is also shown in Fig. 2.6 at $f = 5$ GHz. The received
power by Collins method falls off much more rapidly as a function
of distance than does any of the other methods.

We conclude that the turbulent scatter theory agrees well
with other methods in the frequency range of 2-5 GHz, and that
the method of NBS is more accurate at lower frequencies. This
means that lower values of the spectrum slope, and higher values
of the refractivity variance should be used at lower frequencies,
but the model with a von Kármán refractive index spectrum may
still be used.
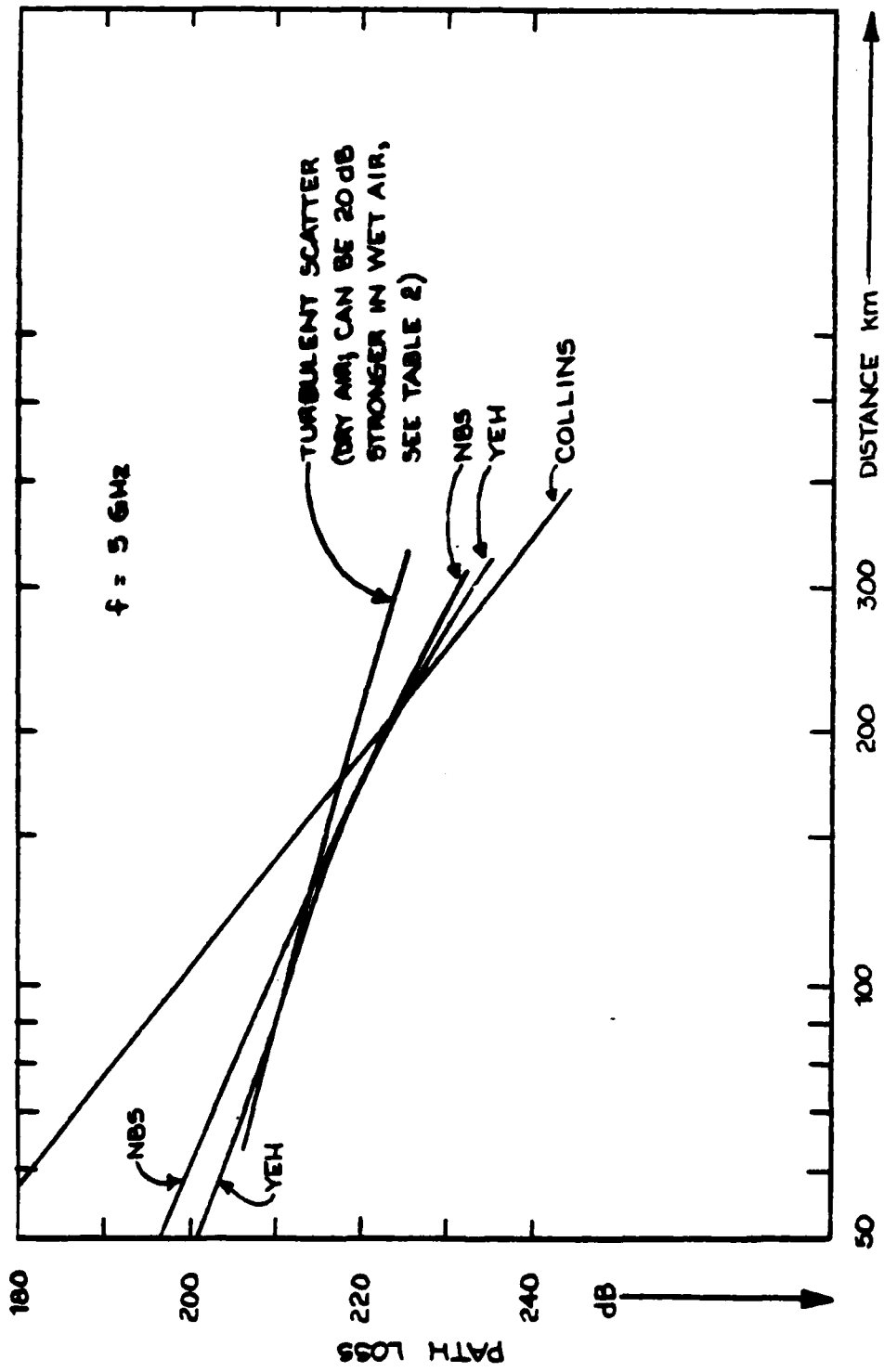
Fig.2.6   Path Loss Versus Distance for Several Prediction Methods

2.4.3 Preliminary Comparison With Empirical Results

Numerous measurement of troposcatter loss have been made in the past, but we shall only chose two examples for comparison here.

The first example is a 210 km European path at 12.3 GHz (Abel, 1971). The parameters of the path and the median received field are listed in Table 2.4.

TABLE 2.4

Parameters of 12.3 GHz Link (Abel, 1971)

Transmitter:	10 W
Distance:	210 km
Frequency:	12.3 GHz
Total Antenna Gain, $G_T + G_R$:	80 dB
Minimum Scatter Angle (K = 4/3):	11 m-rad
Antenna Diameter (Both):	1 m
Median Field Strength, Winter:	16 dB/$\frac{1\mu V}{m}$
Summer:	22 dB/ $\frac{1\mu V}{m}$

The antenna beamwidth (33 m-rad) is large enough to apply the widebeam results of Section 2.4.1. From Table 2.4 the measured path loss is found:

        Path Loss (Winter): 225 dB

        Path Loss (Summer): 219 dB.

The "predicted path loss" is found by inserting the above parameters in Eq. (2.23a), using

$$m = 11/3$$
$$\sigma_n^2 = 5 \cdot 10^{-14} \quad \text{(dry air)}$$

and

$$r_o = 70 \text{ m.}$$

With these parameters the _estimated path loss_ is

Path Loss (calculated) = 220 dB,

which certainly is very close to the measured loss. If a small coupling loss is associated with the path the theoretic loss will probably be closer to the winter measurements where the humidity is low. The stronger signal measured in the summer is due to the higher humidity (σ_n^2 larger, see Table 2.2).

Now consider some recent data on a 4.8 GHz link (Sherwood and Suyemoto, 1976). The parameters and measured pathloss on this link are listed in Table 2.5.

TABLE 2.5

Parameters of 4.78 GHz Link   (Sherwood and Suyemoto, 1976)

Power, P_T:	1000 W
Distance:	86 st. mi.
Frequency:	4.780 GHz
Total Antenna Gain, $G_T + G_R$:	78.2 dB
Antenna Diameters (Both):	8 ft.
Horizon Elevation (Both):	.75°
Median Received Signal Level, Winter:	-96 dBm
Median Received Signal Level, Summer:	-84 dBm

The parameters in Table 2.5 yield the <u>measured</u> <u>path loss</u>

or

$$L_p = P_T + G_T + G_R - RSL,$$

Path Loss (winter): 234 dB

           (summer): 225 dB .

This is now compared with the path loss predicted from Eq. (2.23), using again the parameters

$$m = 11/3$$

$$\sigma_n^2 = 5 \cdot 10^{-14} \quad \text{(dry air)}$$

$$r_o = 70 \text{ m.}$$

Inserting the parameter above and those of Table 2.5 in Eq. (2.23a) results in the <u>estimated path loss:</u>

      Path Loss (calculated) = 222 dB.

This is close to the median measured in the summer. Theoretically, with the assumed parameters, the results should be closer to the winter measurement. However, a small coupling loss is undoubtedly present (5.2 dB according to the CCIR formula) and the uncertainty of the atmospheric data (e.g., height variation of σ_n^2 and r_o) shows that the measurements are again consistent with the turbulent scatter model. In Table 2.6 below the results of the above two comparisons are summarized.

2.5 <u>Spatial Correlation at Receiving Site</u>

The derivations in this section follow the development in section 2.4.1 closely and we will therefore refer to that section for

Table 2.6

Comparison with Empirical Data (Summary)

	Path 1 (Table 2.4)	Path 2 (Table 2.5)
Median measured path loss, winter	225 dB	234 dB
Median meas. path loss, summer	219 dB	222 dB
Path loss calculated using $m=11/3$, $r_O = 70m$, and $\sigma_n^2 = 5 \cdot 10^{-15}$ coupling loss not included	220 dB	222 dB

intermediate results. Horizontal and vertical correlation will be considered separately. The case of a wide beam transmitter is treated first.

2.5.1 Horizontal Correlation, Wide-beam Transmitter

Suppose a second omnidirectional receiver is situated a distance b from the main receiver. Assuming b is small we can still use the integration volume in Fig. 2 .4 for both received power levels as well as for calculating the correlation. The only difference from the integration in Section 2.4.1 is that the integrand is modified by the phase factor.

$$e^{-j \frac{kb}{R_R} z}$$

where z is the distance from the great circle plane in Fig. 2.4. As a reasonable approximation assume that $z \ll R_{oR}$, so that

$$R_R = \left(R_{oR}^2 + z^2 \right)^{\frac{1}{2}} \sim R_{oR} .$$

The correlation, η_H, is now (compare Eq. (2.22)

$$\eta_H(b) = C \iiint_V \frac{1}{R_R^2 R_T^2} e^{-j \frac{kbz}{R_{oR}}} \left(2 \sin \frac{\theta}{2}\right)^{-m} d^3\underline{r} \ .$$

The integration in the z direction (perpendicular to the paper in Fig.2.4 becomes

$$\int_{-\infty}^{\infty} dz \ e^{-j \frac{kb}{R_{oR}}} \left(2 \sin \frac{\theta}{2}\right)^{-m} \frac{1}{R_T^2 R_R^2}$$

$$= \frac{R_o}{R_{oT}^2 R_{oR}^2} \left(2 \sin \frac{\theta_o}{2}\right)^{1-m} \int_{-\infty}^{\infty} e^{-j\beta x} (1+x^2)^{-m/2} dx$$

$$= \frac{R_o}{R_{oT}^2 R_{oR}^2} \left(2 \sin \frac{\theta_o}{2}\right)^{1-m} B\left(\frac{1}{2}, \frac{m-1}{2}\right) F_m(\beta)$$

where

$$\beta = \frac{kb}{R_{oR}} 2 R_o \sin \frac{\theta_o}{2}$$

and

$$F_m(\beta) = \frac{2}{\Gamma\left(\frac{m-1}{2}\right)} \left(\frac{\beta}{2}\right)^{m-1/2} K_{m-1/2}(\beta) \ .$$

We are primarily interested in finding the integral of $\eta_H(b)$ but note that the above formula can also be used to find higher order moments of $\eta_H(b)$. If we write $\beta = b \cdot \alpha$, where

$$\alpha = \frac{kR_o}{R_{oR}} 2 \sin \frac{\theta_o}{2} \ ,$$

we use the well known Fourier relation

$$\int_{-\infty}^{\infty} e^{jaxy} \, dx = \frac{2\pi}{a} \, \delta(y)$$

and get

$$\int_{0}^{\infty} \eta_H(b) \, db = \frac{\pi C}{k} \int_{\alpha_{RO}}^{\pi/2} d\alpha_R \int_{\alpha_{TO}}^{\pi/2} d\alpha_T \frac{1}{R_{oT}} (\sin \alpha_o)^{-1} (2 \sin \theta_o/2)^{-m}$$

$$\simeq \frac{\pi C}{kd} \int_{\alpha_{RO}}^{\infty} d\alpha_R \frac{1}{\alpha_R} \frac{\left(\alpha_R + \alpha_{T_O}\right)^{1-m}}{m-1}$$

$$= \frac{\pi C}{kd} \frac{\theta_{min}^{1-m}}{m-1} \sum_{k=0}^{\infty} \frac{1}{m-1+k} \left(\frac{\alpha_{T_O}}{\alpha_{T_O} + \alpha_{RO}}\right)^K .$$

In this equation,

$$\theta_{min} = \alpha_{TO} + \alpha_{Ro} = R_\ell + \theta_{TG} + \theta_{RG}$$

is the scattering angle. Let us define the function

$$\beta_n(x) = n \sum_{k=0}^{\infty} \frac{1}{n+k} x^k \quad , \quad 0 < x < 1$$

the following bounds on $\beta_n(x)$ are useful

$$\left(1 - x \, e^{-1/n}\right)^{-1} \le \beta_n(x) \le (1-x)^{-1}.$$

The lower bound is often an excellent approximation. Thus we have

$$\int_0^\infty \eta_H(b) \, db = \frac{\pi C}{kd} \frac{\theta_{min}^{1-m}}{(m-1)^2} \beta_{m-1}\left(\frac{\alpha_{TO}}{\alpha_{TO} + \alpha_{RO}}\right)$$

$$= \frac{1}{2} \eta_H(0) \, \lambda \, \frac{m-2}{m-1} \, \theta_{min}^{-1} \frac{\beta_{m-1}(\alpha_{TO}/\theta_{min})}{B\left(\frac{1}{2}, \frac{m-1}{2}\right)}$$

$\eta_H(0)$ is the receiver power calculated in Section 2.4.1. The horizontal correlation distance is defined below.

Definition of Horizontal Correlation Distance:

$$L_H = \int_{-\infty}^\infty \eta_H(b) \, db / \eta_H(0). \tag{2.24}$$

With this definition the result is

$$\frac{L_H \theta_{min}}{\lambda} = \frac{m-2}{m-1} \frac{\beta_{m-1}\left(\alpha_{TO}/\theta_{min}\right)}{B\left(\frac{1}{2}, \frac{m-1}{2}\right)}. \tag{2.25}$$

Note that for a symmetric link ($\theta_{TG} = \theta_{RG}$) $\alpha_{TO}/\theta_{min} = 0.5$ so the right hand side in Eq. (2.25) is then independent of the distance and the elevation angles.

2.5.2 Vertical Correlation

We now determine the spatial correlation in the vertical direction. Suppose the line along which the correlation is taken is tilted a small angle δ from vertical. δ determines how far the combined antenna is pointed above the horizon.

In this case the phase difference between the two received signals is

$$kb \sin (\theta_R - \delta)$$

where again b is the distance between the two receivers. The correlation, $\eta_v(b)$ is

$$\eta_v(b) = C \iiint_V e^{-jkb(\theta_R - \delta)} \frac{1}{R_R^2 R_T^2} \left(2 \sin \frac{\theta}{2}\right)^{-m} d^3 \underline{r} .$$

Integration along the z-axis is just as in Section .4.1, so

$$\eta_v(b) = C_2 \int_{\alpha_{To}}^{\pi/2} d\alpha_T \int_{\alpha_{Ro}}^{\pi/2} d\alpha_R \, e^{-jkB(\alpha_R - \alpha_{Ro} + \theta_{RG} - \delta)} \left[(R_{oT} + R_{oR})\right.$$

$$\left. \sin \theta_o (2 \sin \frac{\theta_o}{2})^{m-1}\right]^{-1}$$

$$\simeq \frac{C_2}{d(m-1)} \int_{\alpha_{Ro}}^{\infty} e^{-jkb(\alpha_R - \alpha_{Ro} + \theta_{RG} - \delta)} \left(\alpha_{To} + \alpha_R\right)^{1-m} d\,\alpha_R .$$

Here C_2 is again the constant

$$C_2 = C \, B\left(\frac{1}{2} , \frac{m-1}{2}\right).$$

$\eta_v(b)$ can be written in terms of the incomplete Gamma function of a complex argument,

$$\eta_v(b) = \frac{C_2}{d(m-1)} (kb)^{m-1} e^{jkb(\alpha_{To} + \alpha_{Ro} - \theta_{RG} + \delta)} e^{-j\pi/2(2-m)}$$
$$\Gamma\left(2-m, jkb(\alpha_{To} + \alpha_{Ro})\right) .$$

2-48

In analogy with the horizontal diversity the correlation distance should be defined in terms of

$$\int_{-\infty}^{\infty} \eta_V(b) \ db/\eta_V(0).$$

However, in this case it is important that the aperture is aiming at the right point over the horizon, so the definition must include an optimization of the angle δ,

Definition of Vertical Correlation Distance:

$$L_V = \max_{\delta} \left| \int_{-\infty}^{\infty} \eta_V(b) \ db/\eta_V(0) \right| \qquad (2.26)$$

It can be verified that the maximum is at $\delta = \theta_{RG}+$ (corresponding to physically aiming the antenna just above horizon) and that

$$\max_{\delta} \int_{-\infty}^{\infty} \eta_V(b) \, db = \frac{C_2}{d(m-1)} \ \frac{2\pi}{K} \ (\alpha_{To} + \alpha_{Ro})^{1-m}$$

so that

$$\frac{L_V \ \wedge \ min}{\lambda} = \frac{L_V}{\lambda} \left(\frac{d}{R_e} + \theta_{RG} + \alpha_{TG} \right) = m-2 \qquad (2.27)$$

Compared to the horizontal case it is seen then L_V is larger than L_H by a factor of 2.6 - 3.4.

2.5.3 Comparison of Horizontal and Vertical Correlation Distance With Results by Gjessing and McCormick (1974)

Gjessing and McCormick (1974) give the following approximate expressions for the correlation distances (also assuming a wide-beam transmitter):

2-49

$$\frac{L_H d}{\lambda R_e} = \frac{0.44}{(4^{1/m} - 1)^{1/2}}$$

$$\frac{L_V d}{\lambda R_e} = \frac{0.44}{2^{1/m} - 1}$$

These formulas clearly assume that the horizon angles are zero. A similar method by Waterman (1958) yields expresions of the same form, but with different parameters. A comparison of these expressions with ours is shown in Table 2.7.

Table 2.7

Comparison of Formulas for Correlation Distance
(Symmetric Link, Smooth Earth)

	Spectrum Slope m:	3	11/3	4	5	6
$\frac{L_H d}{\lambda R_e}$	(Eq. (.25))	0.39	.64	0.65	0.95	1.18
	Gjessing and McCormick	.57	.65	.68	.78	.86
$\frac{L_V d}{\lambda R_e}$	(Eq. (.27))	1.00	1.67	2.00	3.00	4.00
	Gjessing and McCormick	1.69	2.11	2.33	2.96	3.59

It is clearly seen that there is only little difference between the results here and those of Gjessing and McCormick (1974). The experimental verification in their paper therefore also applies to our results. However, our approach is more accurate (asymptotically exact integration), more general (includes elevated

horizon angles), and is based on a definition of the correlation distance which has a direct physical meaning (as discussed in Section 2.6).

2.5.4 Correlation Distances with a Narrow Beam Transmitter

The horizontal correlation function is extremely wide in this case since the receiver only sees scattered power from a thin vertical column in the horizon. So,

$$\eta_H(b) \simeq 1. \tag{2.28}$$

The vertical correlation function is found as in Section 2.5.2, but integrating only in a transmitter beam with the solid angle $\Delta\Omega$

$$\eta_V(b) = C \int_{\alpha_{Ro}} e^{-jkb(\theta_R - \theta_{RG})} \frac{1}{R_{oR}^2 R_{oT}^2} \theta^{-m} R_{oT}^2 \theta^{-m} R_{oT}^2 \Delta\Omega \frac{R_{oR} d\alpha_R}{\theta}$$

$$= \frac{C\Delta\Omega}{d\alpha_T} \int_{\alpha_{Ro}} e^{-jkb(\alpha_R - \alpha_{Ro})} \theta^{-m} d\alpha_R.$$

Hence,

$$\eta_V(0) = \frac{C\Delta\Omega}{d\alpha_T} \frac{\theta_{min}^{1-m}}{m-1}$$

and

$$\int_{-\infty}^{\infty} \eta_V(b) \, db = \frac{C\Delta\Omega}{d\alpha_T} \lambda \; \theta_{min}^{-m}.$$

The vertical correlation distance is then

$$L_v = \int_{-\infty}^{\infty} \eta_v(b) \, db / \eta_v(0) = \frac{\lambda}{\theta_{min}} \quad (m-1). \qquad (2.29)$$

This is almost the same as for a wide-beam transmitter (Eq. (2.24)).

2.6 Coupling Loss - Widebeam Transmitter

Coupling loss may be defined as the power loss incurred by not illuminating the scatterers outside the common volume. Alternatively it can be defined as the loss due to the decorrelation over the receiving aperture. These definitions are equivalent when the transmitter has a wide-beam antenna, while only the first is directly applicable with a narrowbeam transmitting antenna.

Coupling loss is a commonly used parameter since it permits the engineer to express the path loss in terms of the basic path loss with omnidirectional antennas, the antenna gains, and the coupling loss. However, for an actual path, such a division of the path loss is not very useful since it requires the introduction of the atmospheric structure outside the actual antenna beams. Thus, the coupling loss will depend on the presence and strength of inversion layers outside the common volume! Although the definition can be modified to be based on a yearly median, say, this would imply that short term variations in the path loss has to be included in the "basic path loss" which then would loose its interpretation as the loss with omnidirectional antennas.

The logical approach is to calculate the path loss directly by an integration over the common volume, using the formulas discussed in the previous sections. This integration is performed by the SIGNATRON TROPO-path loss computer program.

For historical reasons it is still of some interest to calculate the coupling loss. This coupling loss will, of course, only have direct physical meaning if the atmosphere approaches the model atmosphere assumed. When this is kept in mind coupling loss can be a convenient analytical tool.

In practice a realistic coupling loss is not well defined in the 1-10 GHz range where layer reflection and turbulent scatter may be of equal influence, depending on location, season, time-of-day, etc.

In the following the coupling loss for a turbulent atmosphere is found.

2.6.1 Coupling Loss for an Ideal Narrow Receiving Beam

Consider a narrow receiving beam with unit gain in a small solid angle $\Delta\Omega$, and zero gain outside. It is assumed that all of this angle is pointing over the horizon. If L_{pn} is the path loss with this narrow beam, and L_p is the widebeam path loss formed in Section 2.4.1, the coupling loss L_c (in dB) is

$$L_c = L_p - L_{pn}.$$

L_{pn} is now calculated. The common volume is a section of a cone, but we can still reference to Fig. 2.4 for the integration. L_{pn} is

$$10^{-L_{pn} 10} = C \iiint_{V_n} d \quad \frac{1}{R_R^2 R_T^2} \left(2 \sin \frac{\theta}{2}\right)^{-m} d^3\underline{r}$$

$$= C\Delta\Omega \int_{\alpha_{To}}^{\pi/2} dd_T \quad \frac{1}{R_{oT}} \frac{1}{\sin \theta_o} \left(2 \sin \frac{\theta_o}{2}\right)^{-m}$$

2-53

Assuming that $d \ll R_e$, this becomes

$$10^{-L_{pn}/10} \simeq \frac{C\Delta\Omega}{d \sin \alpha_{Ro}} \; \frac{\left(\alpha_{Ro} + \alpha_{To}\right)^{1-m}}{m-1}$$

$$\simeq \frac{C\Delta\Omega}{d\left(\frac{d}{2R_e} + \theta_{RG}\right)} \; \frac{\left(\frac{d}{R_e} + \theta_{RG} + \theta_{TG}\right)^{1-m}}{m-1}$$

From this, and Eq. (.23a) the <u>coupling loss</u> is

$$L_C = 10 \log \left[\frac{\left(\frac{d}{R_e} + \theta_{RG} + \theta_{TG}\right)\left(\frac{d}{2R_e} + \theta_{RG}\right)}{\Delta\Omega} \cdot \frac{B\left(\frac{1}{2}, \frac{m-1}{2}\right)}{m-2} \right]$$

$$(2 .30)$$

This expression is only valid asymptotically, e.g., for small, solid angles $\Delta\Omega$. If the beam is rectangular with horizontal and vertical beamwidth β_h and β_v, respectively, then

$$\Delta\Omega = \beta_h \cdot \beta_v$$

For a circular antenna with beamwidth β, $\Delta\Omega$ is

$$\Delta\Omega = \pi \, (\beta/2)^2.$$

For a link where $\theta_{TG} \simeq \theta_{RG}$ the coupling loss depends directly on $\theta_{min}/\Delta\Omega$, where θ_{min} is the angular distance (minimum scattering angle).

2.6.2 <u>Coupling Loss of a Uniformly Illuminated Receiving Aperture</u>

The coupling loss can also be determined from the correlation distances calculated in Section 2.5. Suppose $E_o(\underline{r})$ is the field

received at a point $\underline{r}$ in the receiving aperture A_R. Assuming that $E(\underline{r})$ is locally homogeneous, let $\rho(\underline{r} - \underline{r}')$ be the correlation function,

$$\rho(\underline{r} - \underline{r}') = E\left\{ E_0(\underline{r}) \cdot E_0(\underline{r}')\right\} .$$

The received power is then

$$P_R = \iint_{A_R} d\underline{r} \iint_{A_R} dr' \quad \rho(\underline{r} - \underline{r}')$$

Perfect correlation would have yielded the maximum power,

$$P_{R, \, max} = \rho(o) \, A_R^{\,2} .$$

Assume for simplicity that $\rho(o) = 1$. This entails no loss of generality. The coupling loss is therefore

$$10^{-L_c/10} = \frac{1}{A_R^{\,2}} \iiiint d\underline{r} \, d\underline{r}' \, \rho(\underline{r} - \underline{r}')$$

Exact calculation of L_c is not possible unless the complete correlation function $\rho(\underline{r} - \underline{r}')$ is known, but simple approximations often yield nearly the correct result. Consider first a rectangular aperture of dimensions a_H, a_V, so that

$$A_R = a_H \, a_V .$$

The coupling loss can then be written in the form

$$10^{-L_{C'}/10} = \frac{1}{a_H a_V} \int\limits_{-a_H}^{a_H} dx \int\limits_{-a_V}^{a_V} dy \left(1 - \frac{|x|}{a_H}\right)\left(1 - \frac{|y|}{a_V}\right) \rho(x, y)$$

where x and y here are the horizontal and vertical aperture coordinates, respectively. The following approximation is often adequate:

$$\rho(\underline{r} - \underline{r}') = \rho(x - x', y - y')$$

$$\cong \rho_x(x - x') \rho_y(y - y').$$

This yields

$$10^{-L_{C'}/10} \simeq \frac{1}{a_H} \int\limits_{-a_H}^{a_H} \rho_x(x)\left(1 - \frac{|x|}{a_H}\right) d_x \cdot \frac{1}{a_V} \int\limits_{-a_V}^{a_V} \rho_y(y)\left(1 - \frac{|y|}{a_V}\right) dy \qquad (2.31)$$

If only the asymptotic coupling loss is considered, i.e., a_H, a_V large, then

$$10^{-L_C/10} \simeq \frac{L_H}{a_H} \cdot \frac{L_V}{a_V} ,$$

where L_H and L_V are the correlation distances calculated in Section 2.5. Using Eqs. (2.25), (2.27) we get the approximate coupling loss for rectangular aperture:

$$L_c \simeq -10 \log \left[\frac{\lambda^2}{a_H a_V}\left(\frac{d}{R_e} + \theta_{TG} + \theta_{RG}\right)^{-2} \frac{(m-2)^2 \, _{m-1}\left(\alpha_{TO}/\theta_{min}\right)}{(m-1)\, B\left(\frac{1}{2}, \frac{m-1}{2}\right)} \right] \qquad (2.32)$$

If the separability of the horizontal and vertical coordinates is not assumed, the following more accurate result is obtained by integration over the common volume,

$$10^{-L_c/10} = \frac{1}{a_H a_V} \int_{-\infty}^{\infty} d_x \int_{-\infty}^{\infty} d_y \; \rho(x, y)$$

$$= \frac{1}{a_H a_V} \frac{\lambda^2}{\alpha_{Ro}\theta_{min}} \frac{m-2}{B\left(\frac{1}{2}, \frac{m-1}{2}\right)}$$

or

$$L_c = 10 \log \left[\frac{a_H a_V}{\lambda^2} \left(\frac{d}{R_e} + \theta_{RG} + \theta_{TG}\right)\left(\frac{d}{2R_e} + \theta_{RG}\right) \frac{B\left(\frac{1}{2}, \frac{m-1}{2}\right)}{m-2} \right]$$

$$(2.33)$$

This is the same as Eq. (2.30) if the solid beam angle of the equivalent ideal beam is

$$\Delta\Omega = \frac{\lambda^2}{A} \qquad (2.34)$$

where A is the aperture area. This relation assumes equal gain for both the aperture and the ideal beam.

A comparison of Eqs. (2.32) and (2.33) shows that the separability assumed in Eq. (2.32) leads to slightly different values for L_c. However, for a link where $\theta_{RG} = \theta_{TG}$ the difference in coupling loss is only

$$\Delta L_c = 10 \log \left(\frac{1}{2} \frac{m-2}{m-1} \, \theta_{m-1}(\frac{1}{2}) \right)$$

which is in the range -4.1 dB to 0 dB.

Let us next consider a circular aperture with diameter D. For the purpose of determining the asymptotic coupling loss it is easy to see that only the area of the aperture is significant (this assumes that $\rho(\underline{r})$ decreases sufficiently in all directions). Then <u>coupling loss for circular aperture</u>:

$$L_c = 10 \log \left[\frac{\pi D^2}{4\lambda^2} \left(\frac{d}{R_e} + \theta_{TG} + \theta_{RG} \right) \left(\frac{d}{2R_e} + \theta_{RG} \right) \frac{B\left(\frac{1}{2}, \frac{m-1}{2} \right)}{m-2} \right] \qquad (2.35)$$

The beamwidth of the equivalent ideal circular beam is simply

$$\beta = \frac{4}{\pi} \frac{\lambda}{D} = 1.27 \frac{\lambda}{D} \ .$$

For a uniformly illuminated aperture this is found to correspond to the 4.8 dB beamwidth, using the results of Section 2.3.2.

2.6.3 Comparison With Other Results

For a link with zero horizon elevation angles, Gjessing and McCormick (1974) suggest the formula

$$\frac{R_e^2 \lambda^2}{A d^2} (L_c) = 5 \, (2^{1/m} - 1)(4^{1/m} - 1)^{\frac{1}{2}}.$$

$\Big((L_c) \text{ not in dB} \Big)$. Waterman (1958) derives a similar expression:

$$\frac{R_e^2}{d^2} \beta^2 (L_c) = (5^{1/m} - 1)(5^{2/m} - 1)^{\frac{1}{2}} \, ,$$

where β is the beamwidth. From the discussion of Section 2.3.2 and the results of the previous section, a reasonable expression

2-58

for R is

$$R \simeq \frac{\lambda}{D} \, .$$

The above mentioned results are compared with ours in Table 2.8.

TABLE 2.8

Comparison of Formulas for Coupling Loss

Spectrum Slope m:		3	11/3	4	5	6
$\dfrac{\lambda^2 (L_c)}{A \theta_{min}^2}$	Eq. (.35)	1	.0.47	0.39	0.22	0.15
	Gjessing and McCormick	1	0.71	0.61	0.42	0.31
	Waterman	0.98	0.65	0.55	0.36	0.26

The essential difference between these expressions is a slightly stronger dependence on m in our result. Also the ad hoc methods of Gjessing and McCormick, and Waterman, seem to over-estimate the coupling loss by up to 3 dB.

The coupling loss formula in Eq. (2.35) can also be compared with experimental data. Consider the path used by Crawford, et.al., (1953). The parameters for this path are listed below:

Frequency f:	4.1 GHz
Transmitting Dish:	10 ft
Receiving Dish, D:	60 ft
Angular Distance θ_{min}:	0.9° (k = 4/3)
Coupling Loss (relative to 8 ft. Dish) Measured as:	11 dB.

In setting these parameters into Eq. (2.35), using m = 11/3, yields:

Calculated asymptotic coupling loss: 7.6 dB.

The difference is due to the fact that the asymptote has not yet been reached (see Fig. 2.7 for the typical behavior of the coupling loss), and that the transmitting beam is not exactly omnidirectional. In Section 2.7 we shall attempt to find how the actual coupling loss approaches the asymptotic results.

2.7   Coupling Loss for Narrow-Beam Antennas at Both Sites

In the previous section a widebeam transmitter was assumed. On most practical paths the coupling loss is associated with narrowing of both transmitting and receiving beams. In this section the case of extremely narrow beams of comparable size are considered.

2.7.1   Coupling Loss for Ideal Narrow Beams

The loss is dependent on the relative horizontal beamwidths of the two beams. Let the beamwidths of two rectangular beams be

$$\theta_{T,V} = \text{vertical beamwidth at transmitter,}$$

$$\beta_{T,H} = \text{horizontal beamwidth at transmitter,}$$

$$\beta_{R,V} = \text{vertical beamwidth at receiver,}$$

$$\beta_{R,H} = \text{horizontal beamwidth at receiver.}$$

Assume that the receiving beam is the narrowest horizontally,

$$\beta_{R,H} R_{oR} < \beta_{T,H} R_{oT}$$

If this is not the case, the subscripts T and R should be inter-
changed in the remaining expressions in this section.

Since the integration (see Fig. 2.4) is now over a very
small volume, it is simple to write down the path loss L_p. Using
Eq. (2.22) we get

$$10^{-L_p/10} = C \frac{1}{R_R^2 R_T^2} \theta_{min}^{-m} \cdot \frac{R_R^{\alpha}R_{,H} \cdot R_R^{\alpha}R_{,V} \cdot R_T^{\beta}T_{,V}}{\theta_{min}}$$

$$= \frac{C}{d} \alpha_{R,V} \beta_{R,H} \alpha_{T,V} \theta_{min}^{-m} \alpha_{Ro}^{-1}$$

Combining this with Eq. (2.23a) yields the coupling loss

$$L_c = 10 \log \left[\frac{\theta_{min}^2 \cdot \alpha_{RO}}{\theta_{R,V} \beta_{R,H} \alpha_{T,V}} \cdot \frac{B\left(\frac{1}{2}, \frac{m-1}{2}\right)}{(m-1)(m-2)} \right] \qquad (2.36)$$

where

$$\theta_{min} = \frac{d}{R_e} + \theta_{TG} + \theta_{RG}$$

and

$$\alpha_{Ro} = \frac{d}{2R_e} + \theta_{RG} .$$

Loosely speaking, the coupling loss depends on $(\theta/\beta)^3$ for two
equal narrow beams, and on $(\theta/\beta)^2$ for only one narrow beam
(Eq. 2.30). Viewed as a function of frequency, the coupling
loss has a slope of 9 dB/octave for two narrow beams and 6 dB/
octave for one narrow beam.

Following the general principles of the preceding section,
the coupling loss can also be expressed in the form

$$L_c = 10 \log \left[\frac{A_T \, a_{R,V}}{\lambda^3} \theta_{min}^2 \, \alpha_{Ro} \frac{B\left(\frac{1}{2}, \frac{m-1}{2}\right)}{(m-1)(m-2)} \right] \qquad (2.37a)$$

$$a_{T,H} \big/ a_{R,H} < R_{oT} \big/ R_{oR} \qquad (2.37b)$$

where

A_T = Area of transmitting aperture

$a_{R,V}$ = Vertical dimension of receiving aperture

$a_{T,H} a_{R,H}$ = Horizontal dimensions of transmitting and receiving apertures, respectively.

When inequality in Eq. (2.37b) is reversed, the role of the transmitter and receiver should also be reversed in Eq. (2.37a).

2.7.2 Coupling Loss With Intermediate Values of Vertical Beamwidths.

So far we have only considered the asymptotic case of very narrow beams. Here this assumption is relaxed in the vertical direction, while the horizontal beamwidth will be assumed either very large or very small. The ideal beamshape will be used, i.e., the beam pattern is

$$G(\theta) = \begin{cases} 1 & |\theta| < \beta/2 \\ 0 & |\theta| > \beta/2 \end{cases}$$

where β is the beamwidth.

If the beam is wide horizontally, then the path loss is (from Section 2.4.1)

$$10^{-Lp/10} = \frac{CB\left(\frac{1}{2}, \frac{m-1}{2}\right)}{d} \int_{\alpha_{Ro}}^{\alpha_{Ro}+\beta_{RV}} d\alpha_R \int_{\alpha_{To}}^{\alpha_{To}+\beta_{TV}} d\alpha_T \, (\alpha_R + \alpha_T)^{-m}$$

$$= \frac{CB\left(\frac{1}{2}, \frac{m-1}{2}\right)}{d(m-1)(m-2)} \ \theta_{min}^{2-m} \ F\left(\frac{\beta_{TV}}{\theta_{min}}, \frac{\beta_{RV}}{\theta_{min}}\right),$$

where

$$F(x_1, x_2) = \left(1 - (1+x_1)^{2-m} - (1+x_2)^{2-m} + (1+x_1+x_2)^{2-m}\right)$$

The coupling loss is simply

$$L_c = -10 \ \log \ F(\beta_{TV}/\theta_{min}, \ \theta_{RV}/\theta_{min}) \qquad (2.38)$$

For wide vertical beams this reduces to Eq. (2.23a), while for narrow vertical beams we can use

$$F(x_1, x_2) \simeq (m-1)(m-2) \ x_1 \ x_2.$$

If we instead assume that one of the beams, the receiving one say, is narrow horizontally, then we have

$$10^{-Lp/10} = \frac{C\beta_{RH}}{d} \int_{\alpha_{Ro}}^{\alpha_{Ro}+\beta_{RV}} d\alpha_R \int_{\alpha_{To}}^{\alpha_{To}+\beta_{TV}} \frac{1}{\alpha_R} \ \left(\alpha_R + \alpha_T\right)^{-m}$$

$$= \frac{C\beta_{RH}}{d(m-1)} \int_{\alpha_{Ro}}^{\alpha_{Ro}+\beta_{RV}} d\alpha_R \ \frac{1}{\alpha_R} \ \left[\left(\alpha_R + \alpha_{To}\right)^{1-m} - \left(\alpha_R + \alpha_{To} + \beta_{TV}\right)^{1-m}\right]$$

$$= \frac{C\beta_{RH}}{d(m-1)^2} \left\{ \theta_{min}^{1-m} \beta_{m-1}\left(\frac{\alpha_{TO}}{\theta_{min}}\right) - \left(\theta_{min}+\beta_{RV}\right)^{1-m} \beta_{m-1}\left(\frac{\alpha_{TO}}{\theta_{min}+\beta_{RV}}\right)\right.$$

$$- \left(\theta_{min}+\beta_{TV}\right)^{1-m} \beta_{m-1}\left(\frac{\alpha_{TO}+\beta_{TV}}{\theta_{min}+\beta_{TV}}\right)$$

$$\left. + \left(\theta_{min}+\beta_{TV}+\beta_{RV}\right)^{1-m} \beta_{m-1}\left(\frac{\alpha_{TO}+\beta_{TV}}{\theta_{min}+\beta_{TV}+\beta_{RV}}\right)\right\}.$$

The function $\beta_{m-1}(x)$ was defined in Section 2.4, and is a special case of the hypergeometric function,

$$\beta_{\nu}(x) = F(\nu, 1; \nu+1; x).$$

The above expression for the path loss may be easier to interpret if written as an infinite sum,

$$10^{-L_p/10} = \sum_{k=0}^{\infty} \frac{C\beta_{RH}}{d(m-1)(m-1+k)} \left[\alpha_{TO}^k \theta_{min}^{1-k-m} - \alpha_{TO}^k \left(\theta_{min}+\beta_{RV}\right)^{1-k-m}\right.$$

$$\left. - \left(\alpha_{TO}+\beta_{TV}\right)^k \left(\theta_{min}+\beta_{TV}\right)^{1-k-m} + \left(\alpha_{TO}+\beta_{TV}\right)^k\left(\theta_{min}+\beta_{TV}+\beta_{RV}\right)^{1-k-m}\right]$$

The coupling loss is then

$$L_C = -10 \log \frac{\beta_{RH}(m-2)}{\theta_{min}B\left(\frac{1}{2},\frac{m-1}{2}\right)} \cdot \sum_{k=0}^{\infty} \frac{1}{m-1+k} \left(\frac{\alpha_{TO}}{\theta_{min}}\right)^k \qquad \times$$

2-64

$$\times \left\{ 1 - \left(1+X_{RV}\right)^{1-m-k} - \left(1+X_{TV} \cdot \frac{\theta_{min}}{\alpha_{To}}\right)^{k} \left(1+X_{TV}\right)^{1-m-k} \right.$$

$$\left. + \left(1+X_{TV} \cdot \frac{\theta_{min}}{\alpha_{To}}\right)^{k} \left(1+X_{TV}+X_{RV}\right)^{1-m-k} \right\} \qquad (2.39)$$

where

$$X_{TV} = \beta_{TV}/\theta_{min}$$

$$X_{RV} = \beta_{RV}/\theta_{min} .$$

This is shown in Fig. 2.7 for a particular link, together with the asymptote, Eq. (2.36) and the curve for a wide horizontal beam, Eq. (2.38). Combining the curves for Eqs. (2.38) and (2.39) yields an excellent approximation to the coupling loss when this is less than 5-7 dB. When the coupling loss is higher Eq. (2.39) is sufficiently accurate by itself.

Although Eq. (2.39) is not difficult to evaluate numerically it may be worthwhile to note that the following approximation may be used at values of the coupling loss larger than approximately 10 dB,

$$L_{C} \sim -10 \log \frac{\beta_{RH}}{\alpha_{Ro} B\left(\frac{1}{2}, \frac{m-1}{2}\right)} \; F\left(X_{TV}, \; X_{RV}\right) ,$$

where $F(\cdot , \cdot)$, X_{TV} and X_{RV} were defined above. Numerical calculations indicate that the error is less than 1 dB.
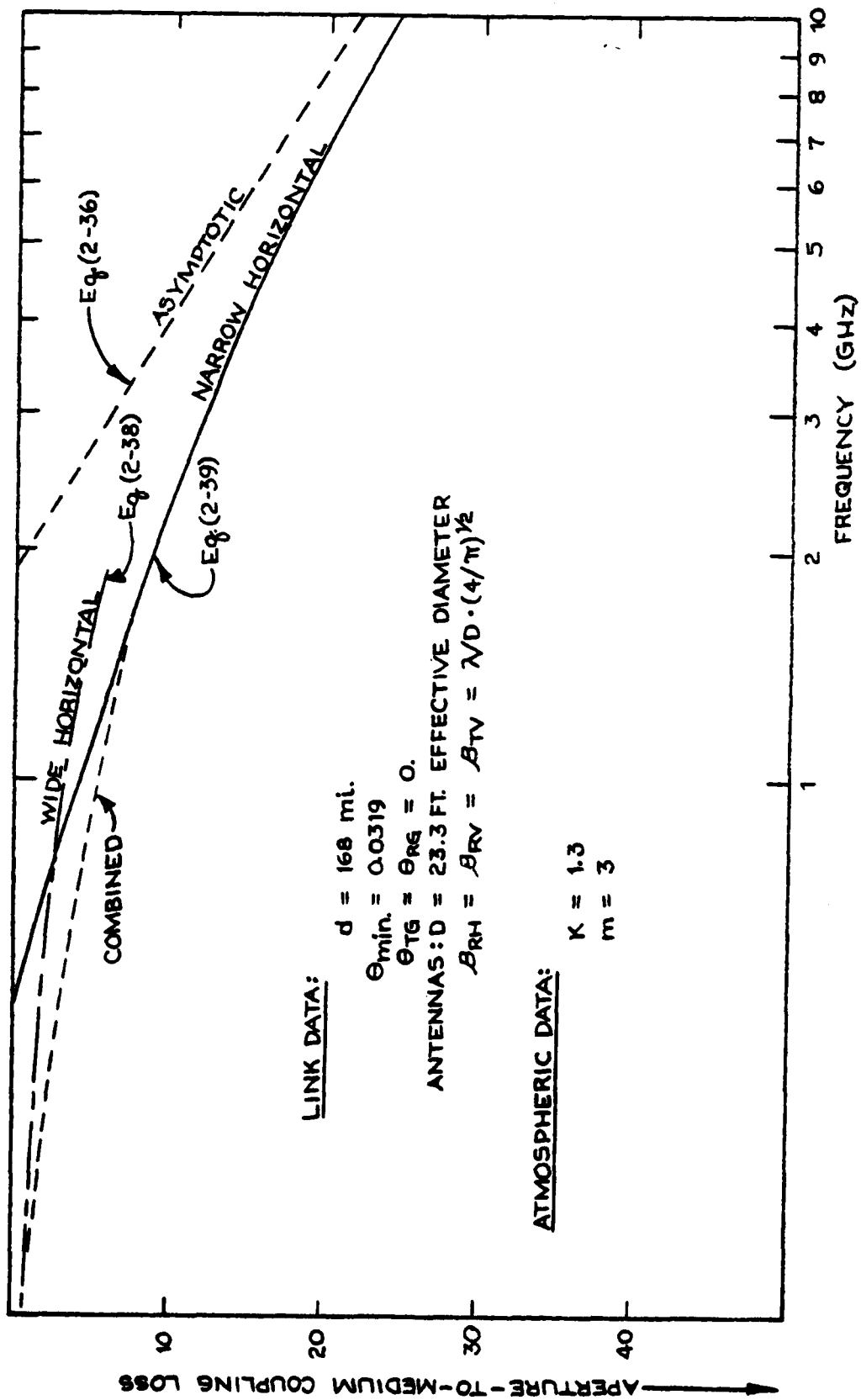
Fig.2.7   Coupling Loss as Function of Frequency for Typical Path

The derivation of Eq. (2.39) assumes that one beam is narrow horizontally in comparison to the other beam. It has been verified numerically for symmetric links where the two beams are equals. In the important case of nonsymmetric links with equal horizontal beamwidths (assumed narrow as in Eq.(2.33)) the following approximation and lower bound is easily found:*

$$L_c \geq - 10 \log \frac{2(m-2)}{mB\left(\frac{1}{2}, \frac{m-1}{2}\right)} \frac{\beta_H}{\theta_{min}} F_{m-1}\left(X_{TV}, X_{RV}\right)$$

$$+ 10 \log \left(1 + \frac{1}{\theta_{min}} \left| \frac{2(h_R - h_T)}{d} + \theta_{RG} - \theta_{TG} \right| \right) \quad (2.40)$$

where

$$F_{m-1}\left(X_T, X_R\right) = 1 - \left(1 + X_T\right)^{1-m} - \left(1 + X_R\right)^{1-m} + \left(1 + X_T + X_R\right)^{1-m}$$

and

$h_R - h_T$ = difference in elevation of receiver and transmitter

$\theta_{RG} - \theta_{TG}$ = difference in elevation angles of receiving and transmitting antennas.

This formula reduces to Eq. (2.36) in the asymptotic case of very narrow beams.

2.8 Conclusions

The preceding analysis leads us to the following conclusions:

- The concept of coupling loss should not be used as a universal answer to the question of antenna gain loss

---

* The Beta function $B\left(\frac{1}{2}, \frac{m-1}{2}\right) = 1.68$ for $m = 11/3$

on a troposcatter channel. The total path loss is a more fundamental parameter since it only depends on the atmosphere inside the common volume.

- Coupling loss should only be used in connection with a specific model of the atmosphere. Hence, it makes little sense to compare the coupling loss for different atmospheric models. In particular, the coupling loss we have calculated for $m = 11/3$ cannot be compared to that of NBS ($m = 5$) nor to that of CCIR.

- The pathloss can be calculated directly from the atmospheric parameters of

    effective earth radius

    variance of refractive index

    outer scale of turbulence.

  This provides a direct physical background for finding the long term distribution of the received power level, and opens the way for more accurate prediction of the performance of specific links.

- The turbulent scatter theory is accurate at higher frequencies (> 1 GHz) while layer reflection can be dominant at lower frequencies. The simultaneous existence of the two scatter modes can complicate accurate link prediction at all times, but turbulent scatter represents worst case and should therefore always be used for link design.

- For best results, the pathloss should be calculated by numerical integration over the common volume, using the actual antenna patterns.

- Highly accurate formulas have been derived for the pathloss for the turbulent scatter model. The pathloss is expressed in terms of the basic pathloss (Eq. 2.23a) with omnidirectional antennas, and the coupling loss (Eqs. 2.38, 2.39, 2.40). The accuracy of the coupling loss will be verified below, along with a summary of the relevant formulas.

- The computer program and the formulas derived yield results for the pathloss which are very close to those predicted by the NBS method when a spectrum slope $m = 5$ is used.

The relevant formulas and parameters needed are listed below:

The Scatter Model:

Von Karman Spectrum with the spectrum slope parameter m,

$$3 < m.$$

The resulting scattering cross-section is described in Section 2.2.4.

The Basic Pathloss L_{bp} (Omnidirectional antennas):

$$L_{bp} = - 10 \log_{10} \left[\frac{(m-3)}{4(m-1)(m-2)} \sigma_n^2 r_o^{3-m} k^{2-m} \frac{1}{d} \left(\frac{d}{R_e} + \theta_{RG} + \theta_{TG} \right)^{2-m} \right]$$

where

m = spectrum slope (11/3 for turbulent scatter)

σ_n^2 = variance of the refractive index. The median value for optical wavelengths [Fried, 1967] can be used to represent dry turbulent air conditions (winter), implying

$$= 6.7 \cdot 10^{-14} \exp(-h/3.2 \text{ km}).$$ h is the height of the scattering point. This is only to be considered as a typical example since considerable variation with climate and location exists (Gossard, 1977)

r_o = correlation distance of the refractive index fluctuations. For turbulence this may be equated to the outer scale of turbulence L_o. With the results of Fried (1967) this yields

$$= L_o = 2(h/1m)^{\frac{1}{2}}.$$

k $= 2\pi/\lambda = 2\pi f/c$

  = wavenumber of the link frequency.

d = path distance.

R_e = effective earth radius

θ_{RG} = horizon elevation relative to horizontal at receiver.

θ_{TG} = horizon elevation relative to horizontal at transmitter.

The Coupling Loss

Several formulas have been derived for the coupling loss. One represents the coupling loss, L_{CWH}, with a wide horizontal beam, and the others the coupling loss, L_{CNH}, with a narrow horizontal beam.

The formulas assume that the antenna beams have been approximated by ideal rectangular beams. The validity of this approximation was carefully analyzed for the asymptotic case (large coupling loss). The results (Eqs. 2.38 - 2.40) are

$$L_{CWH} = -10 \log \left[1 - \left(1 + \frac{\theta_{TV}}{\theta_{min}} \right)^{2-m} - \left(1 + \frac{\theta_{RV}}{\theta_{min}} \right)^{2-m} \right.$$

$$\left. + \left(1 + \frac{\theta_{RV} + \theta_{TV}}{\theta_{min}} \right)^{2-m} \right]$$

2-70

where

θ_{min} = minimum scatter angle

= angular distance.

β_{RV} = vertical beamwidth at the receiver

$\simeq \lambda/D_R$ in radians.

β_{TV} = vertical beamwidth at the transmitter

$\simeq \lambda/D_T$ in radians.

For L_{CNH} two results were obtained. If one beam is narrower than
then

$$L_{CNH} = - 10 \log \frac{m-2}{B\left(\frac{1}{2}, \frac{m-1}{2}\right)} \cdot \frac{\beta_{RH}}{\theta_{min}} \cdot S,$$

where

$B(x,y)$ is the Beta function,

$$S = \sum_{k=o}^{\infty} \frac{1}{m-1+k} \left(\frac{\alpha_{To}}{\theta_{min}}\right)^k \left[1 - \left(1 + \frac{\beta_{RV}}{\theta_{min}}\right)^{1-m-k} \right.$$

$$- \left(1 + \frac{\beta_{TV}}{\alpha_{To}}\right)^k \left(1 + \frac{\beta_{TV}}{\theta_{min}}\right)^{1-m-k}$$

$$\left. + \left(1 + \frac{\beta_{TV}}{\alpha_{To}}\right)^k \left(1 + \frac{\beta_{TV}+\beta_{RV}}{\theta_{min}}\right)^{1-m-k} \right] ,$$

and where we have, in addition to the parameters defined above,

β_{RH} = horizontal beamwidth at the receiver, assumed
narrower than at the transmitter,

$\alpha_{To} = \frac{d}{2R_e} + \theta_{TG}$ (terminals at equal height)

If the horizontal beamwidth of the two antennas are identical ($\beta_{RH} = \beta_{TH} = \beta_H$) then the loss L_{CNH} is bounded by, and approximately equal to for very narrow beams,

$$L_{CNH} \gtrsim - 10 \log \left[\frac{2(m-2)}{mB\left(\frac{1}{2}, \frac{m-1}{2}\right)} \frac{\beta_H}{\theta_{min}} \right.$$

$$\left. \cdot \left\{ 1 - \left(1 + \frac{\beta_{RV}}{\theta_{min}}\right)^{1-m} - \left(1 + \frac{\beta_{TV}}{\theta_{min}}\right)^{1-m} + \left(1 + \frac{\beta_{TV} + \beta_{RV}}{\theta_{min}}\right)^{1-m} \right\} \right]$$

$$+ 10 \log\left(1 + |\alpha_{To} - \alpha_{Ro}|/\theta_{min}\right) \qquad (2.40a)$$

where

$$\alpha_{Ro} - \alpha_{To} = \frac{2(h_R - h_T)}{d} + (\theta_{RG} - \theta_{TG})$$

and $h_R - h_T$ is the height difference of the antennas.

To test the accuracy of these analytical formulas they have been compared to the results of a direct integration in Fig. 2.8. The stipled curve in Fig. 2.8 has been found by combining L_{CNH} from Eq. 2.39 and L_{CWH} by the expression

$$L_{CC} \overset{\Delta}{=} 7 \log \left[10^{L_{CNH}/7} + 10^{L_{CWH}/7} \right] .$$

The form of this equation was chosen arbitrarily to get a smooth transition between the results for a narrow and a wide horizontal beam. The number 7 was chosen to fit the results of the numerical integration. Perfect agreement is then found for coupling losses larger than 5 dB. For smaller coupling losses the numerical integration routine becomes inaccurate due to the large common

2-72

volume so it appears likely that the expression for L_{CC} is accurate even in this range.

The formula (2.40) for equal size antennas can be adapted to work over the entire range of beamwidths by using the following expression

$$L_C = - 10 \log F_{m-1}\left(\frac{\beta_{TV}}{\theta_{min}} , \frac{\beta_{RV}}{\theta_{min}}\right)$$

$$+ 10 \log\left(1 + \frac{mB\left(\frac{1}{2}, \frac{m-1}{2}\right)}{2(m-2)} \frac{\theta_{min}}{\beta_H}\right)$$

$$+ 10 \log\left(1 + |\alpha_{To} - \alpha_{Ro}|/\theta_{min}\right) \tag{2.41}$$

This formula is asymptotically correct and is an excellent approximation for intermediate size antennas, as evidenced by the points calculated in Fig. 2.8.
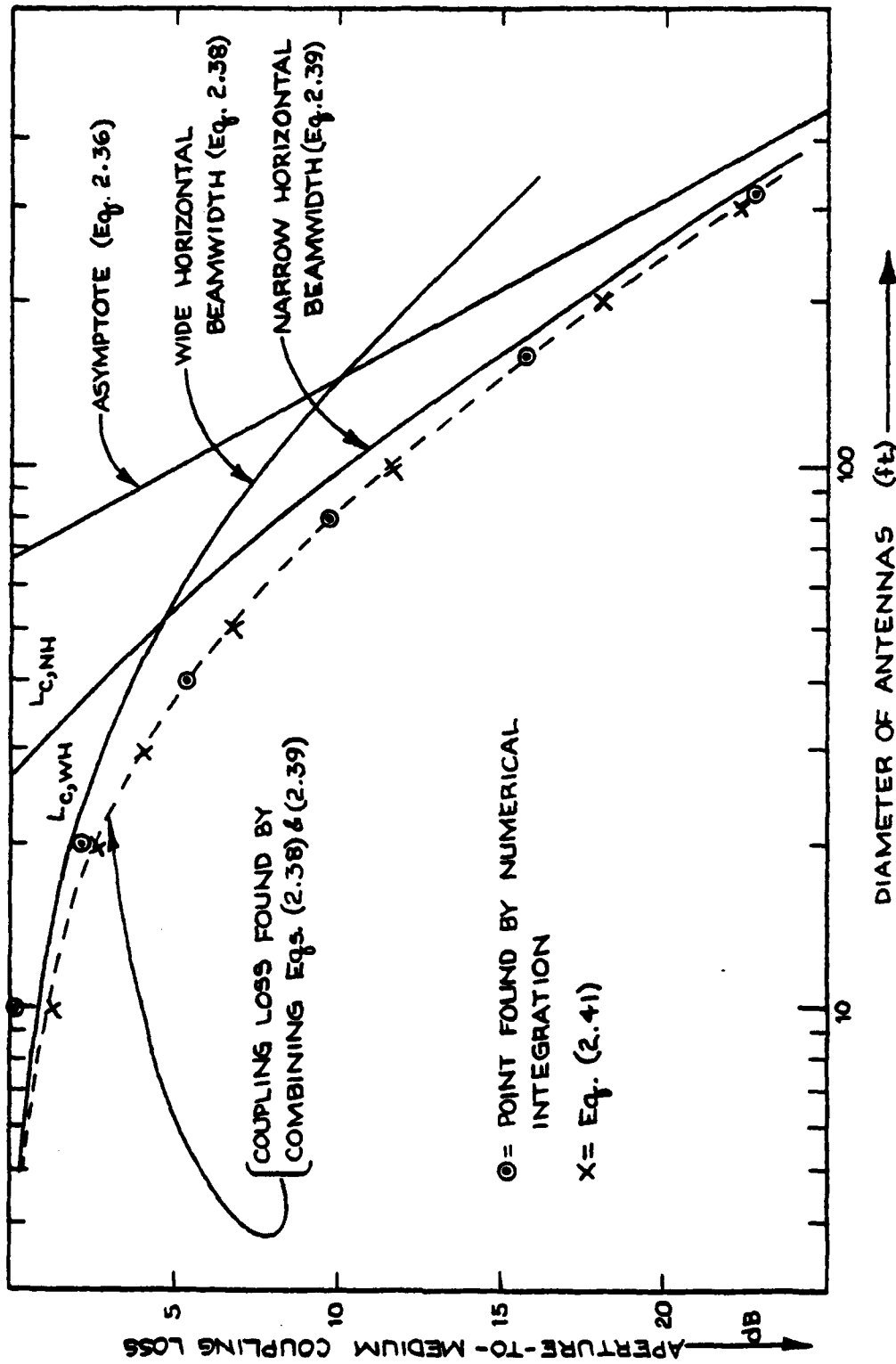
Fig. 2.8 Comparison of Derived Coupling Loss Formulas with Numerical Integration Results for A Symmetric Link (100 mi., 1 GHz, smooth earth, turbulent scatter)

2-7ʌ

Section 2
REFERENCES

Abel, N. (1971), "Observations on a 12 GHz Scatter Link over a 210 km Path". Tropospheric Wavepropagation, Pt. II, AGARD Conf. Proc. No.70, Feb. 1971.

Battesti, J. and L. Boithas (1971), "Propagation par Les Hetero-geneités de l'Atmosphere et Prevision des Affeiblissements", Tropospheric Wavepropagation, Pt. II, AGARD Conf. Proc. No.70, Feb. 1971.

Booker, H.G., and J.T. deBettencourt (1955), "Theory of Radio Trans-mission by Tropospheric Scatter using very Narrow Beams", Proc. IRE, Vol. 43, No. 3, pp. 281-290.

Booker, H.G., and W.E. Gordon (1950), "A Theory of Radio Scattering in the Troposphere", Proc. IRE, Vol. 38, pp. 401-402.

Brookner, E. (1970), "Atmospheric Propagation and Communication Channel Model for Laser Wavelengths", IEEE Trans. Comm. Techn., Vol. COM-18, No. 4, pp. 396-416.

Brookner, E. (1971), "Improved Model for Structure Constant Varia-tion with Altitude", Appl. Optics, Vol. 10, No. 8, pp. 1960-1963.

Carroll, T.J. and R.M. Ring (1955), "Propagation of Short Waves in a Normally Stratified Atmosphere", Proc. IRE. Vol. 43, p. 1384.

Crawford, A.B., D.C. Hogg and W.H. Kummer (1959), "Studies in Tropo-spheric Propagation Beyond the Horizon", Bell System Tech. J., Vol. 38, No. 5, pp. 1067-1178.

Eklund, F. and S. Wickerts (1968), "Wavelength Dependence of Micro-wave Propagation Far Beyond the Radio Horizon", Radio Science, Vol. 3, No. 11, pp. 1066-1074.

Friis, H.T., A.B. Crawford and D.C. Hogg (1957), "A Reflection Theory for Propagation Beyond the Horizon", Bell System Tech. J., Vol. 36, p. 627.

Fried, D.L. (1967), "Optical Heterodyne Detection of an Atmospherically Distorted Wave Front", Proc. IEEE, Vol. 55, No. 1, pp. 57-67.

Gjessing, D.T., A. Kjelaas and J. Nordø (1969), "Spectral Measurements and Atmospheric Stability", J. Atmosph. Sci., Vol. 26, pp. 426-468.

Gjessing, D.T. and K.S. McCormick (1974), "On the Prediction of the Characteristic Parameters of Long Distance Tropospheric Communication Links", IEEE Trans. Comm., Vol. COM-22, pp. 1325-1331.

Goldstein, I., P. Miles and A. Chabot (1965), "Heterodyne Measurements of Light Propagation through Atmospheric Turbulence", Proc. IEEE, Vol. 53, pp. 1172-1180.

Gossard, E.E. (1977), "Refractive Index Variance anu its Height Distribution in Different Air Masses", Radio Sci., Vol.12, No. 1, pp. 89-105.

Hardy, K.R., and I. Katz (1969), "Probing the Clear Atmosphere with High Power, High Resolution Radars", Proc. IEEE, Vol.53, pp. 468-480.

Hartman, W.J. and R.E. Wilkerson (1959), "Path Antenna Gain in an Exponential Atmosphere", J. Res. N.B.S., Vol. 63D, No. 3, pp. 273-286.

Kropfli, R.A., I. Katz, T.G. Konrad and E.B. Dobson (1968), "Simultaneous Radar Reflectivity Measurements and Refractive Index Spectra in the Clear Atmosphere", Radio Sci., Vol. 3, pp.991-994.

Larsen, R.E., "A Comparison of Some Troposcatter Prediction Methods", IEE London Tropospheric Wave Propagation Conf., 1968.

Monsen, P., S. Parl and J.N.Pierce (1976), Adaptive Antenna Control, 1st Interim Technical Report, SIGNATRON, Inc., Lexington, MA., Dec. 1976.

Panter, P.F., Communication Systems Design: Line-of-Sight and Tropo-Scatter Systems , McGraw Hill Book Co., New York 1972.

Rice. P.L., A.G. Longley, K.A. Norton and A.P. Barsis (1965, Rev. 1967), "Transmission Loss Predictions for Troposcatter Communications Circuits", N.B.S. Techn., Note 101.

Seehars, H.D. (1971), Observations with Synchronously-Offset Beams on a 77 km path at 1.8 and 44 cm', Tropospheric Radio Wave Propagation, Pt. II, AGARD Conf. Proc. No. 70.

Sherwood, A. and L. Suyemoto (1976), "Multipath Measurements Over Troposcatter Paths", MTP-170, the Mitre Corp.

Sirkis, M.D. (1971),"Contribution of Water Vapor to Index of Refraction Structure Parameter at Microwave Frequencies", IEEE Trans.Ant. Prop. AP-19, July 1971, pp.572-574.

Smith, E.K. and S. Weintraub (1953), "The Constants in the Equation for Atmospheric Refractive Index at Radio Frequencies", Proc. IRE, Vol. 41, pp. 1035-1037.

Staras, H. (1957), "Antenna-to-Medium Coupling Loss", IRE Trans. Ant. Prop., Vol. AP-5, pp.228-231.

Tatarski,V.I.: The Effects of the Turbulent Atmosphere on Wave Propagation, Israel Program for Scientific Translation, Jerusalem, 1971.

Thayer,G.D. (1974), "An Improved Equation for the Refractive Index of Air", Radio Sci., Vol. 9, No. 10, pp. 803-807.

Waterman, A.T.,Jr. (1958), "Some Generalized Scattering Relationships in Transhorizon Propagation", Proc. IRE, Vol. 46, pp. 1842-1848.

Yeh, L.P., "Experimental Aperture-to-Medium Coupling Loss", Proc. IRE, Vol. 50, No. 2, p. 205, Feb. 1962.

SECTION 3

ANGLE DIVERSITY PERFORMANCE

In this section, the troposcatter model for performance pre-
diction is used to design angle diversity systems. A qualitative
approach is followed to provide general guidelines for angle
diversity implementation and three specific examples are used to
provide a quantitative base. The three examples are the C-band
RADC troposcatter test system, an operational DCS L-band tropo-
scatter system, and an operational NATO L-band troposcatter sys-
tem. The parameters of these links are summarized in the follow-
ing table. This section also presents the long term variability
model to be used with the troposcatter model for prediction of
link availability. The question of a long term decorrelation
advantage of angle diversity vs. space diversity is also discussed.

3.1 Angle Diversity Design

The short term ($\sim$ seconds) fading characteristics of tropo-
scatter signal reception are mitigated by the provision of redun-
dant, i.e., diversity, channels and an associated combining scheme
to utilize the stronger received signals and eliminate the weaker
ones. One method of realizing additional diversity channels is
to use multiple feedhorns at the focal point of a parabolic re-
flector to realize multiple angle of arrival signals. This method
is normally only employed at the receiver since the production of
multiple transmit beams requires either additional power amplifiers
or a reduction in power with power splitters. Thus, conventional
angle diversity has one transmit beam and two or more angle of ar-
rival receive beams.

3-1

Table 3.1

Path Parameters

Name	RADC Test Link	S.Tepesi Yamanlar	Oslo Kristiansand
Path Distance(mi.)	168.3	172.	205.
Transmitter Height(ft.)	340.	2893.	823.
Receiver Height(ft.)	460.	3176.	1109.
Transmitter Antenna(ft.)	28.	60.	65.6
Receiver Antenna(ft.)	28.	60.	65.6
Transmitter Boresight/Horizontal ∢ (°)	1.27	0.320	0.46
Boresight/Horizon ∢ (°)	0.27	0.320	0.3
Receiver Boresight/Horizontal ∢ (°)	0.77	0.110	0.02
Boresight/Horizon ∢ (°)	0.27	0.320	0.3
Squint Angle (°)	0.54	1.30	1.2
Frequency (GHz)	4.5	0.87	0.9

One of the first questions a system designer may ask concerns the relative advantages of beams spread either *vertically or horizontally*. Since the diversity advantage stems from the lack of correlation between the two received diversity signals, the correlation fall-off as a function of squint angle in the vertical and horizontal directions is the determining factor in assessing the performance difference. The power loss fall-off as a function of squint angle is of the same order for the two directions and therefore is not significant in the selection process. The correlation fall-off as a function of squint angle can be related to the correlation distance in the plane of the receive antenna. The correlation distance r_c may be defined in terms of two point antennas, one located on the great circle path and one at a distance r_c, where the received processes on the two point antennas have a normalized correlation coefficient of $1/e$. Clearly if the correlation distance is much greater than the troposcatter system parabolic reflector then the correlation between squinted beams will be very high whereas if the correlation distance is small compared to the parabolic reflector the squinted beam correlation will be small. The correlation distance is defined in terms of a vector $\underline{u}$ in the plane of the parabolic reflector as

$$\varphi(\underline{u}) = \overline{E(\underline{r})\ E^*(\underline{r} + \underline{u})}$$

where $E(\underline{r})$ is the received electric field at a distance $\underline{r}$ from the center of the scattering volume. The results of 2.4.1 and 2.5.1 establish that the above spatial correlation function is related to the scattering volume "size" through a three dimensional Fourier integral

$$\varphi(\underline{u}) = C \iiint V(\underline{r}') \ e^{jk\frac{\underline{u}\cdot\underline{r}'}{r}} \ d^3r' \ .$$

3-3

The integration is over the scattering volume defined by $V(\underline{r}')$ which is determined by the antenna gain patterns and the refractive index spectrum fall-off as a function of scattering angle. The constant k is equal to $2\pi f_o/c$ where f_o the carrier frequency and c is the speed of light. Now Fourier variables in one domain are inversely related to Fourier variables in the other domain, e.g., a short time pulse corresponds to a wide frequency band. Thus the correlation distance in a particular direction at the receiver is inversely related to the common volume size in that same direction. In Fig. 3.1 we examine the common volume dimensions in the vertical (side view) and horizontal (top view) directions. For angle diversity systems, the transmit beamwidth Ω is typically smaller than the minimum scattering angle θ_o in order to minimize the loss associated with the squinted beam. The common volume "size" in the horizontal direction is then limited by the transmit beamwidth and is on the order of $\gamma_H r \doteq \Omega r$. In the vertical direction, the common volume "size" is not limited by the beamwidth as much as the refractive index spectrum fall-off which has a dependence of $\theta^{-11/3}$ where θ is the scattering angle. Since $\theta > \theta_o > \Omega$ the vertical common volume size $\gamma_V r$ is larger than the horizontal common volume size $\gamma_H r$. The area of useful scattering energy returned to the receiver is figuratively shown in Fig. 3.1 as a shaded area. Since $\gamma_V > \gamma_H$ it follows that the vertical correlation distance will be less than the horizontal correlation distance for narrow beamwidth antennas. Thus the vertical angle diversity system will result in a lower correlation between squinted beams than a horizontal angle diversity system.

It turns out that as the transmit beamwidth is increased such that $\Omega \gg \theta_o$, the situation reverses and γ_V becomes smaller

Υ_H

r

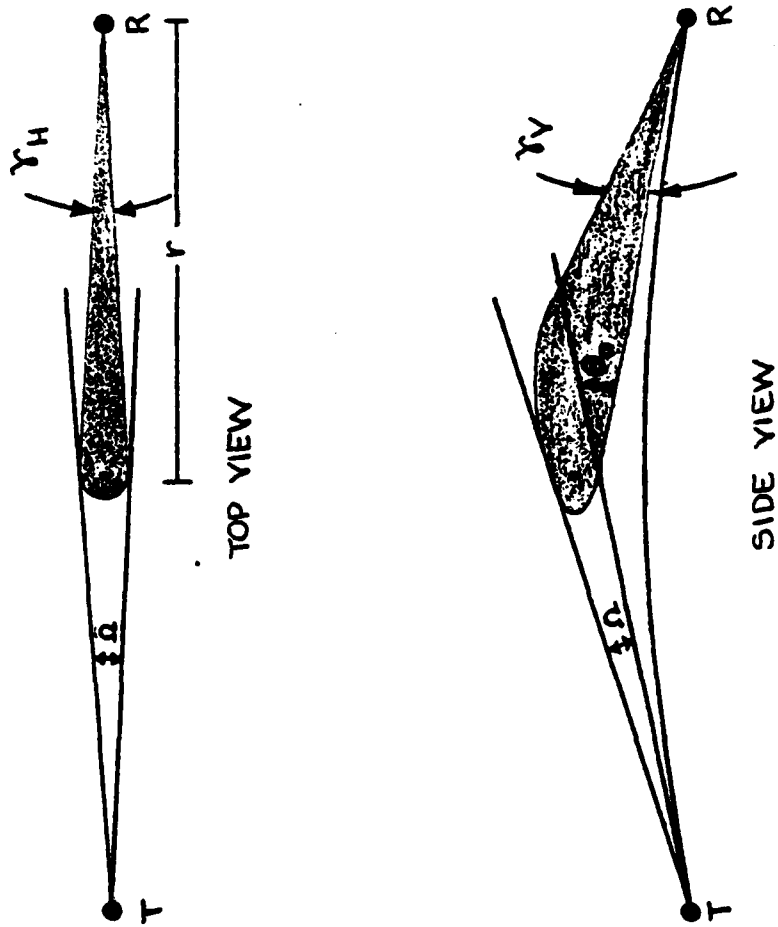TOP VIEW

Υ_V

SIDE VIEW

Fig. 3.1 Troposcatter Path Structure

than γ_H with the result of a smaller horizontal correlation distance than vertical. This result is consistent with "fat" transmitter beam measurements and analysis [3.1] of correlation distances in the vertical and horizontal planes. However, in any practical application, the transmit beams must be narrow in order to provide the required antenna gain for successful operation.

This qualitative discussion of correlation distances is supported by a quantitative evaluation of the horizontal and vertical correlation distances in Section 2.5.4.

Because the vertical correlation distance is smaller than the horizontal correlation distance for practical systems, the angle diversity design should utilize a vertical squinted beam as the first additional angle of arrival signal. Since a dual feedhorn vertical angle diversity (VAD) system increases the conventional quadruple diversity system to an eight order system, the use of more angle of arrival signals is not advantageous both because of system complexity and the diminishing return from additional diversity. Thus we fix the system design as a dual feedhorn VAD system and turn our attention to the choice of vertical squint angle and antenna boresight/horizon angle.

The angle between the centerlines of the antenna patterns of the two feedhorns in a dual VAD system is defined as the squint angle. When the squint angle is appreciably more than a beamwidth, the correlation between the received angle diversity signals is small but the relative signal loss of the elevated beam may be excessive due to the increased scattering angle. Decreasing the squint angle reduces this loss but increases the correlation between diversity signals. The diversity combining loss due to

signal correlation alone can be expressed for flat fading channels
at large signal-to-noise ratios as

$$L = -5 \ LOG(1-\rho^2) \qquad\qquad (3.3)$$

where ρ is the normalized correlation coefficient between two com-
plex Gaussian processes. This function is plotted in Fig. 3.2.
The optimum squint angle for the three example systems has been
computed by using this relation in conjunction with the calcula-
tion of the correlation coefficient and squint loss as a function
of squint angle. This calculation used the turbulent scatter model
and common volume integration technique described in Section 2.
The results are shown in Figs. 3.3 - 3.5.

In computing the diversity combining loss DCL, the squint
loss S_L results in an effective loss of $S_L/2$ because performance
at large signal-to-noise ratio SNR is determined by the geometric
mean of the diversity branch SNR values or equivalently by the
mean of the SNR values in dB.

In these examples and all others computed, the optimum squint
angle was determined to be approximately 1 beamwidth. Also note
that the optimum is relatively broad such that the dB loss is small
if the squint angle should be larger than one beamwidth. Since
feedhorn design is more difficult with smaller squint angle re-
quirement, this result has important practical implications. The
feedhorn design for the RADC test link resulted in the measured
squint angles given in Table 3.2. Vertical polarization is used
for signal reception in the RADC tests. The additional loss for
this link resulting from a squint angle larger than 1 beamwidth
can be determined from Fig. 3.3 to vary between 0.1 and 0.4 dB.
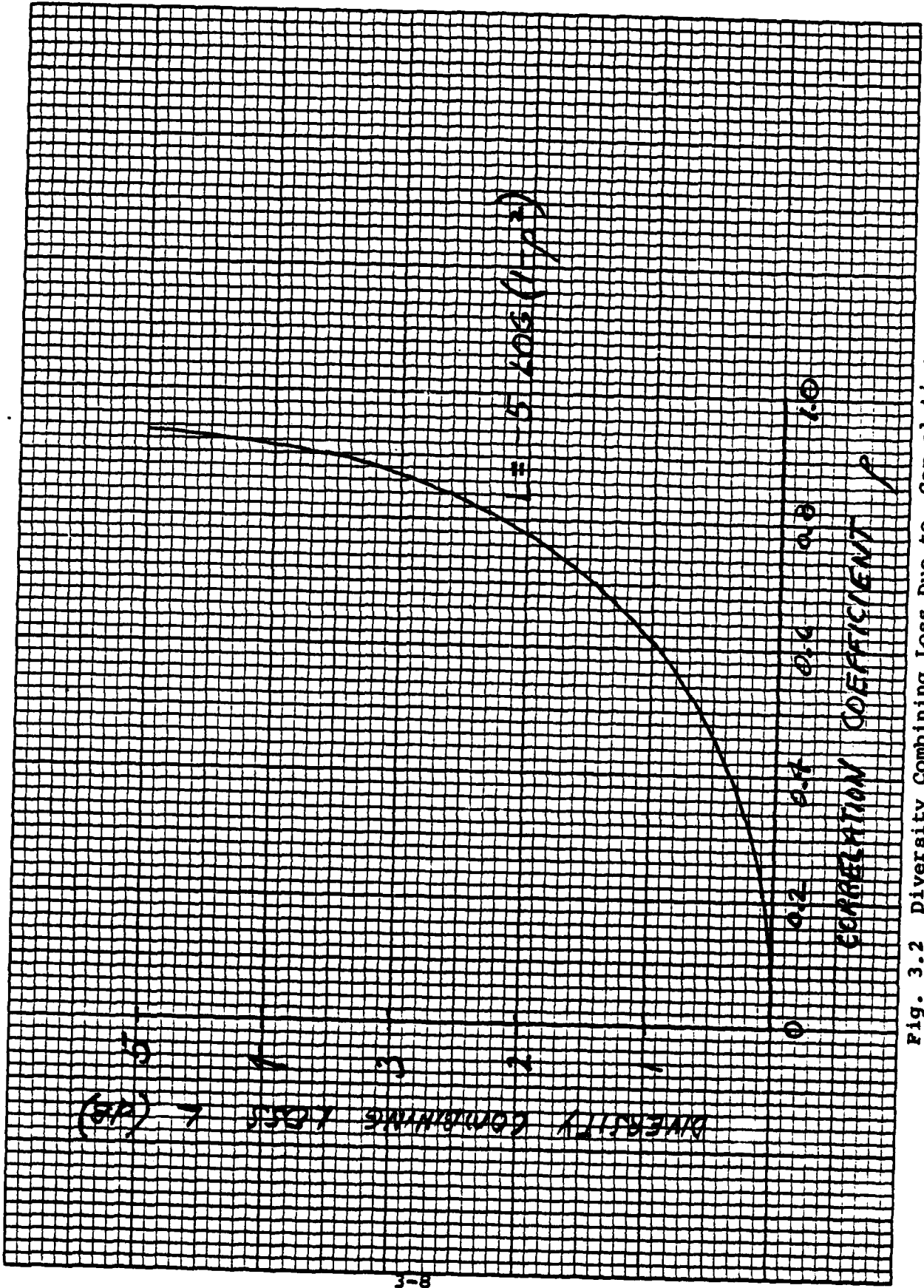
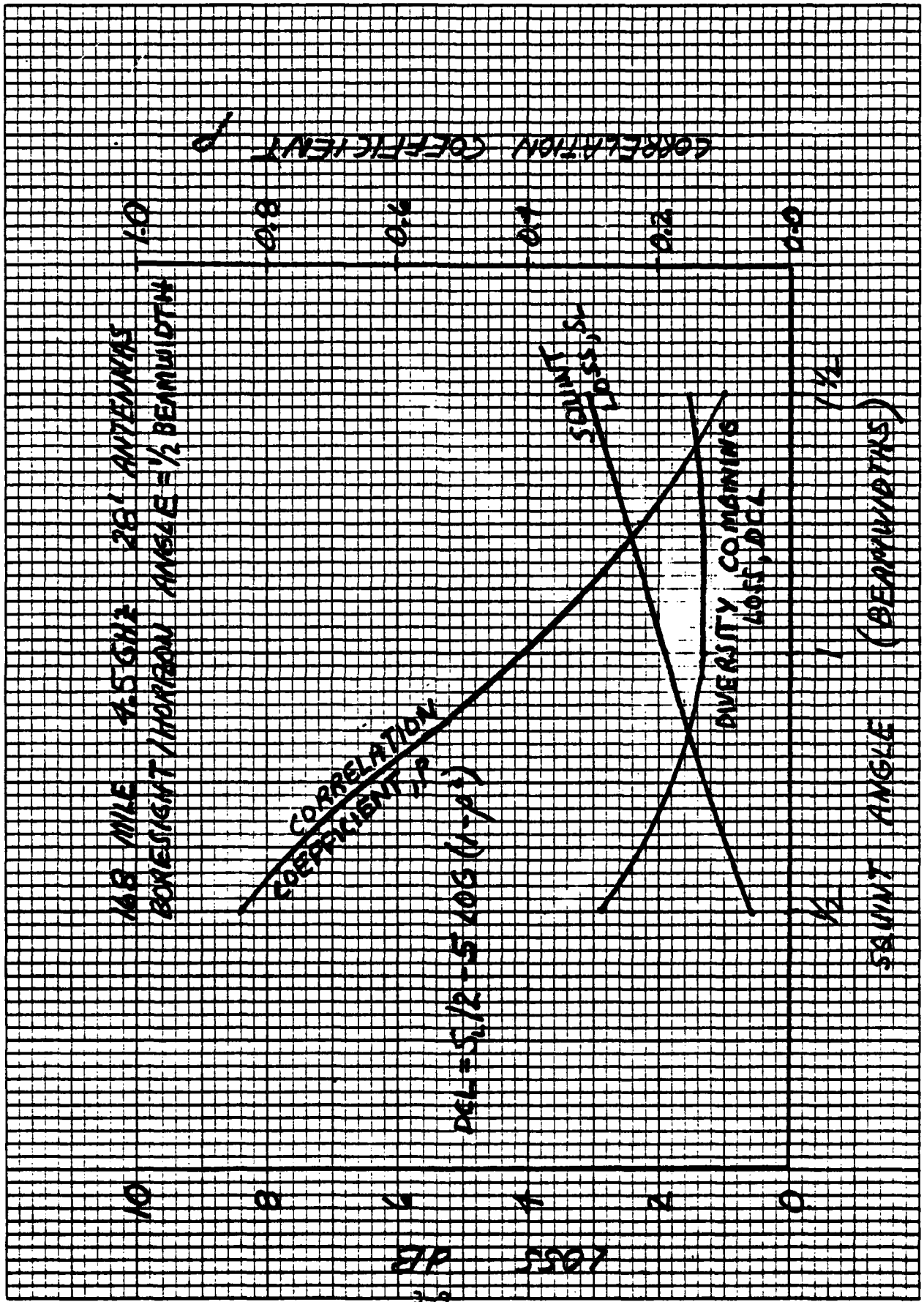Fig. 3.2 Diversity Combining Loss Due to Cor.elation

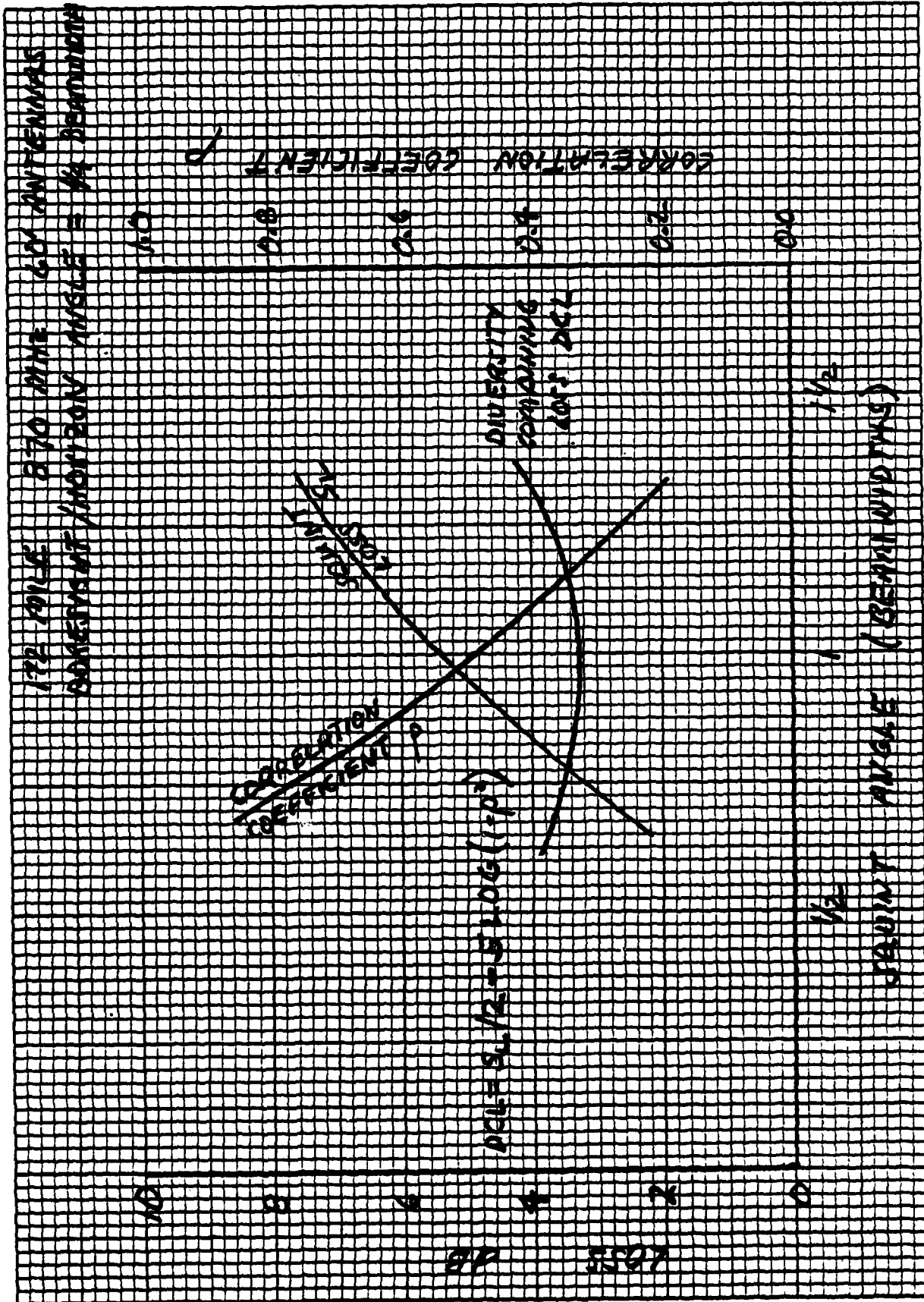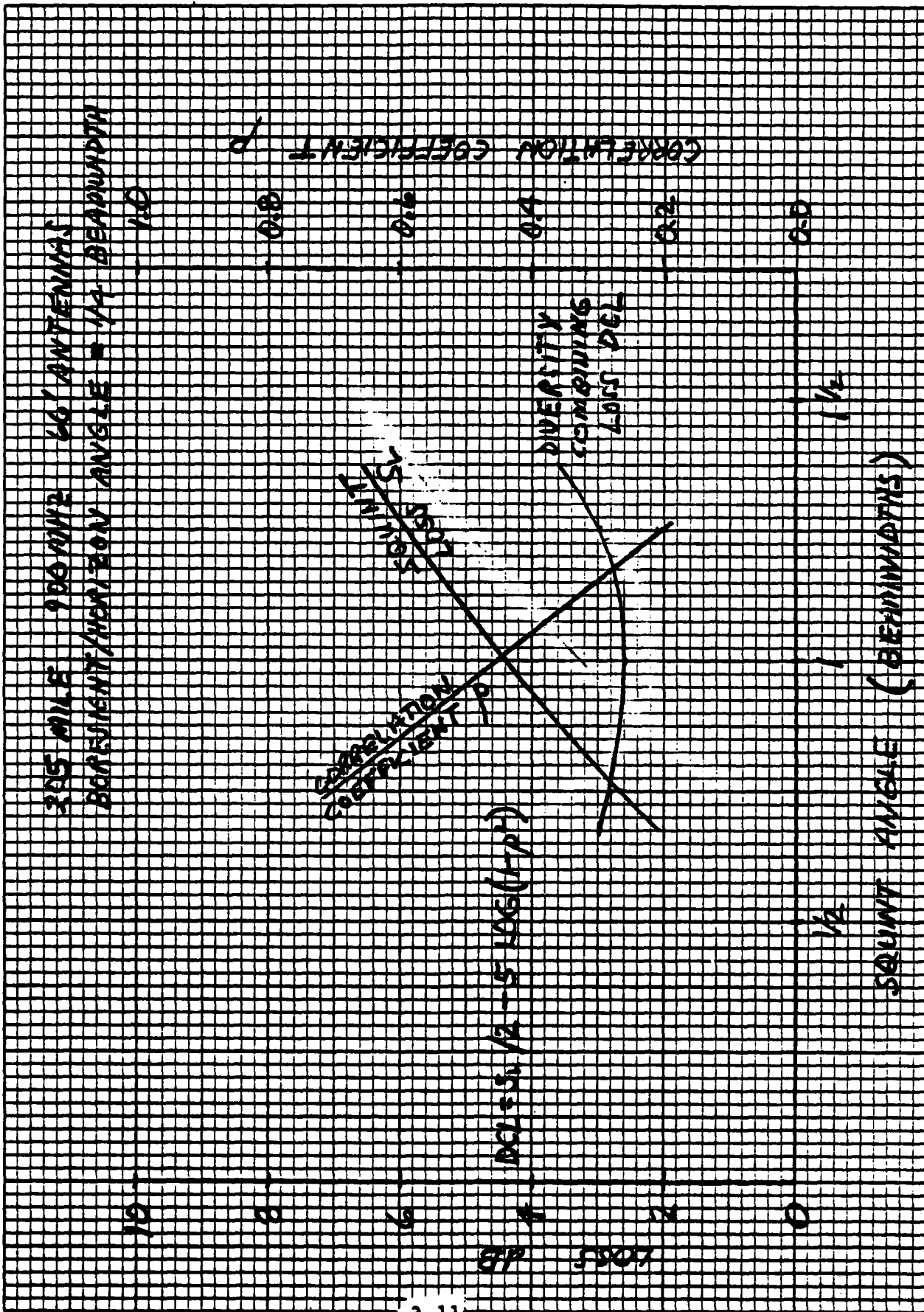Fig. 3.3 Optimum Squint Angles, RADC Test Link

Fig. 3.4 Optimum Squint Angle, S.Tepesi ~ Yamanlar

46 0782

3-10

Fig. 3.5 Optimum Squint Angle, Oslo-Kristiansand

Table 3.2
Test Link Parameters

	Right Antenna		Left Antenna	
	H Pol.	V Pol.	H. Pol.	V Pol.
Squint Angle	0.65°	0.73°	0.55°	0.68°
Half-Power Beamwidth	0.55°	0.53°	0.50°	0.50°

The next question to be addressed is the choice of antenna pointing angle, i.e., the angle between the main beam antenna pattern centerline (boresight) and the horizon. As this angle is decreased, the relative loss of the elevated beam is reduced but more of the main beam pattern is blocked by the ground such that an optimum pointing angle exists. Since operational angle diversity system are utilized in both directions, the boresight/ horizon angles at transmitter and receiver are constrained to be equal in the optimization search. Using the optimum squint angle of one beamwidth, the main beam loss for a conventional system was determined as a function of antenna pointing angle and in addition the diversity combining loss due to squint loss and correlation was computed from the model of Section 2. The sum of these losses establishes the optimum pointing angles for the three example systems. The results are shown in Figs. 3.6 - 3.8. In these and other examples the optimum boresight/horizon angle for the transmit and receiver antennas was found to fall between 1/4 and 1/2 beamwidth elevation above the local horizon. This result was only slightly influenced by the frequency of operation since lower frequency systems use larger antennas. It is also worth noting

3-12

168 MILE 4.5 GHz 28' ANTENNAS

SQUINT ANGLE = 1 BEAMWIDTH

TOTAL LOSS

MAIN BEAM LOSS

DIVERSITY COMBINING LOSS

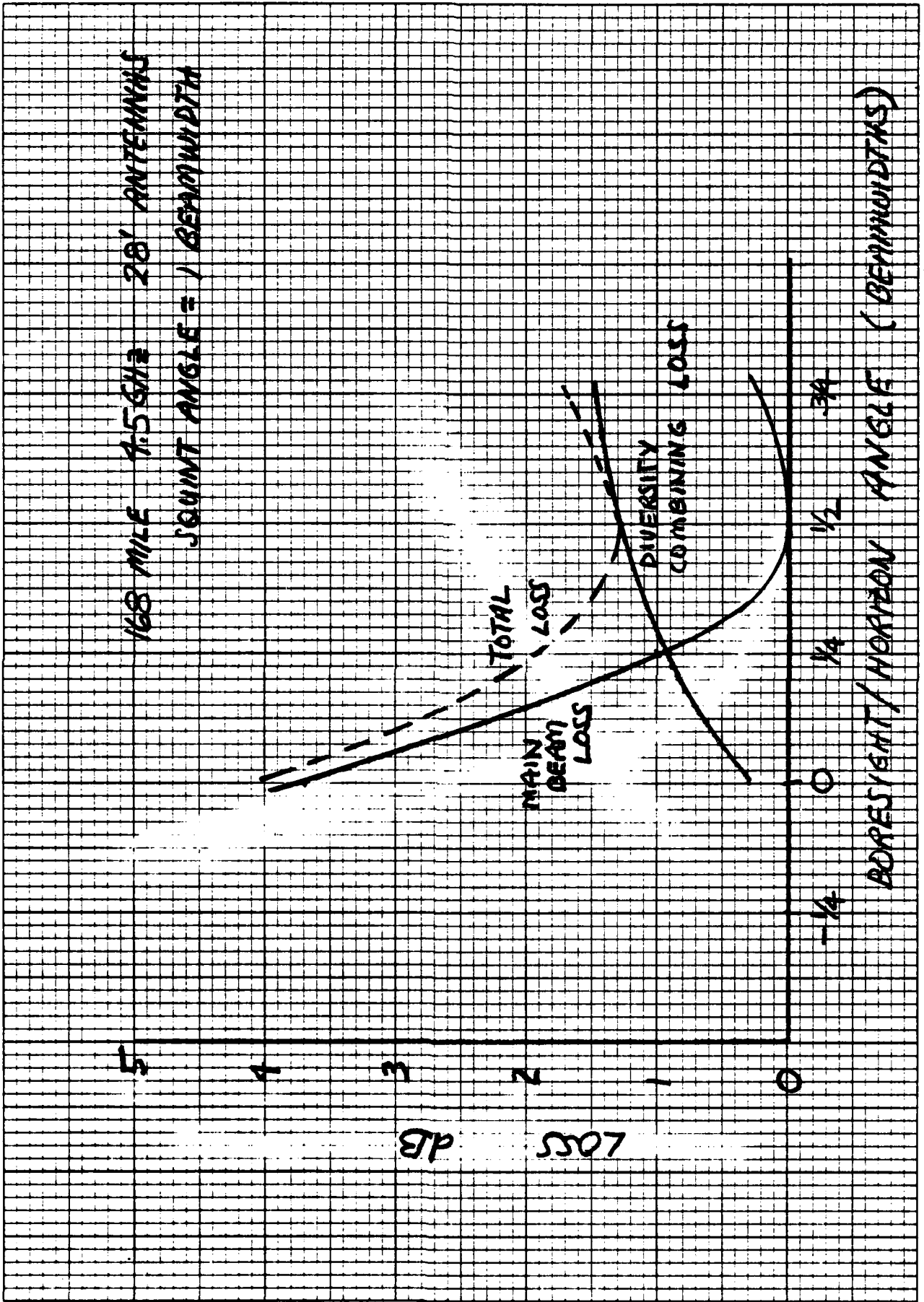BORESIGHT/HORIZON ANGLE (BEAMWIDTHS)

LOSS dB

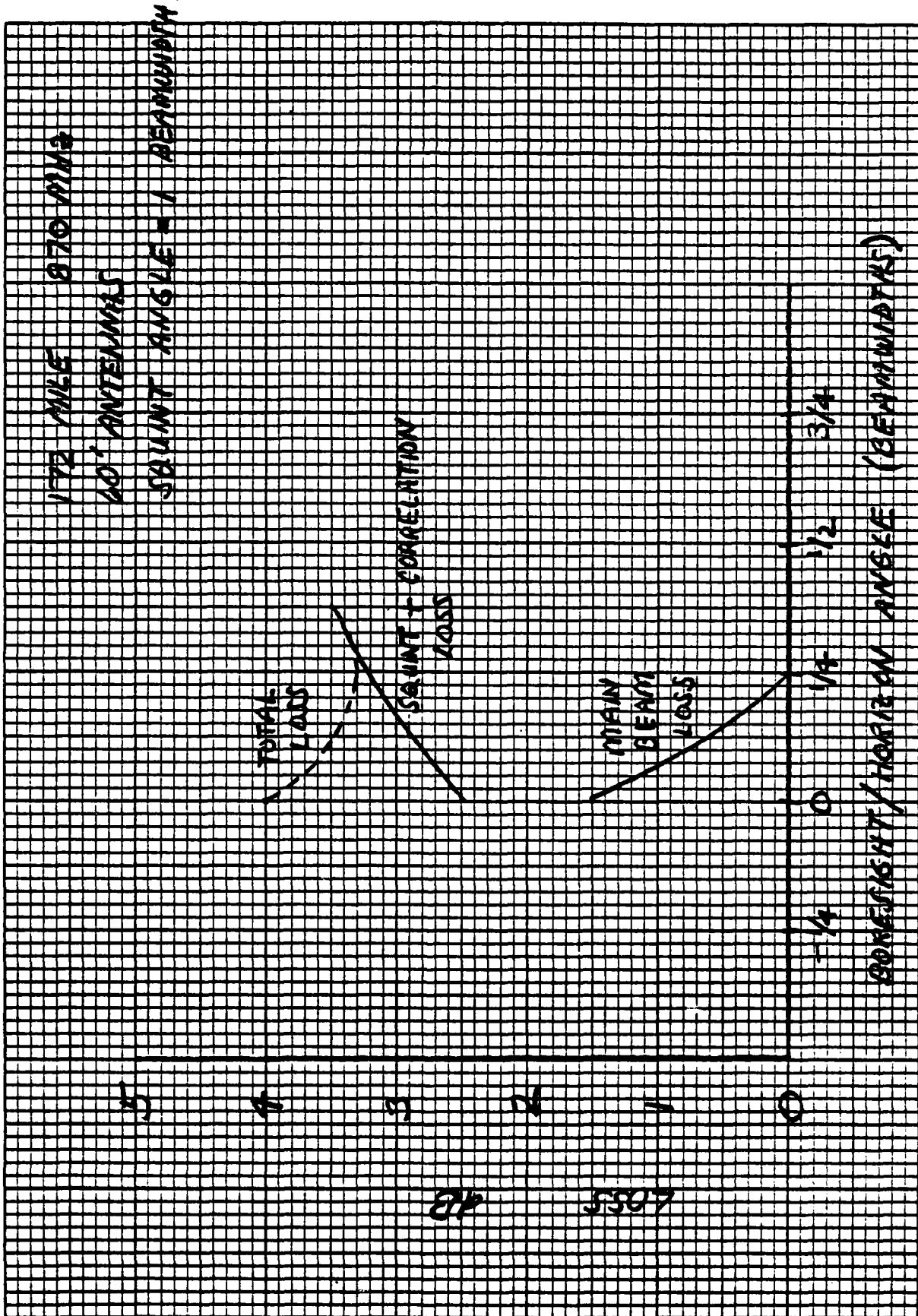Fig. 3.6   Antenna Pointing Angle Optimization, RADC Test Link

46 0782

Fig. 3.7 Antenna Pointing Angle Optimization, S.Tepesi-Yamanlar
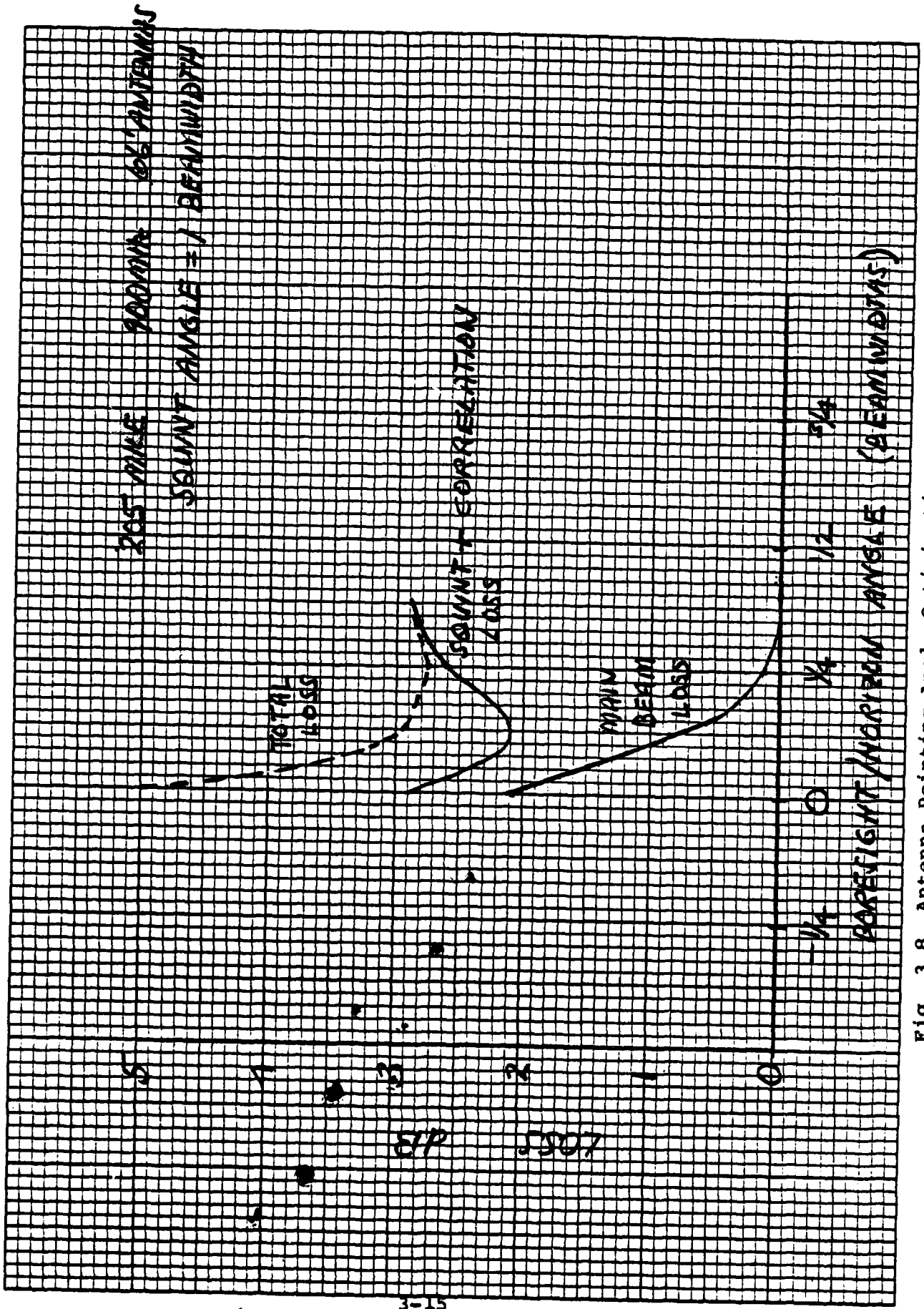
Fig. 3.8 Antenna Pointing Angle Optimization, Oslo-Kristiansand

that the optimum pointing angle for conventional systems would be about 1/2 beamwidth (main beam loss curves) but that little loss is incurred if the antennas are not realigned for an angle diversity application.

A final consideration in choice of antenna pointing angle is the effect of increased multipath in both beams due to larger pointing angles. Because digital modems can utilize the multipath to increase the effective diversity order if the multipath spread is not too large, it is advantageous to choose a somewhat larger pointing angle if the nominal multipath spread is small compared to the data symbol interval. However, for L-band systems the multipath spread, particularly in the elevated beam, may exceed the multipath capabilities of the digital modem. In this situation degraded performance due to intersymbol interference results.

The results from the numerical integration of the common volume using a turbulent scattering hypothesis are shown in Figs. 3.9 - 3.11 for the example systems. The 2σ multipath spread of the product beam refers to the cross channel multipath profile defined in [3.2]. The C-band test link has small multipath spread* for data rates of interest and because of the small dB loss associated with larger pointing angles, the optimum pointing angle for a digital VAD system is probably very close to the optimum pointing angle for a conventional 2S/2F analog troposcatter system, i.e., approximately 1/2 beamwidth. For the L-band

------

* Measured results from C-band systems tend to be larger [3.3] due to the inclusion of the terminal equipment filter characteristics and measurement noise.

46 0782

148 MHz   4.5 GHz   28' ANTENNAS

SQUINT ANGLE = 1 BEAMWIDTH

ELEVATED BEAM

PRODUCT BEAM

MAIN BEAM

MULTIPATH SPREAD (NS)

400

300

200

100

1/4   0   1/4   1/2   3/4
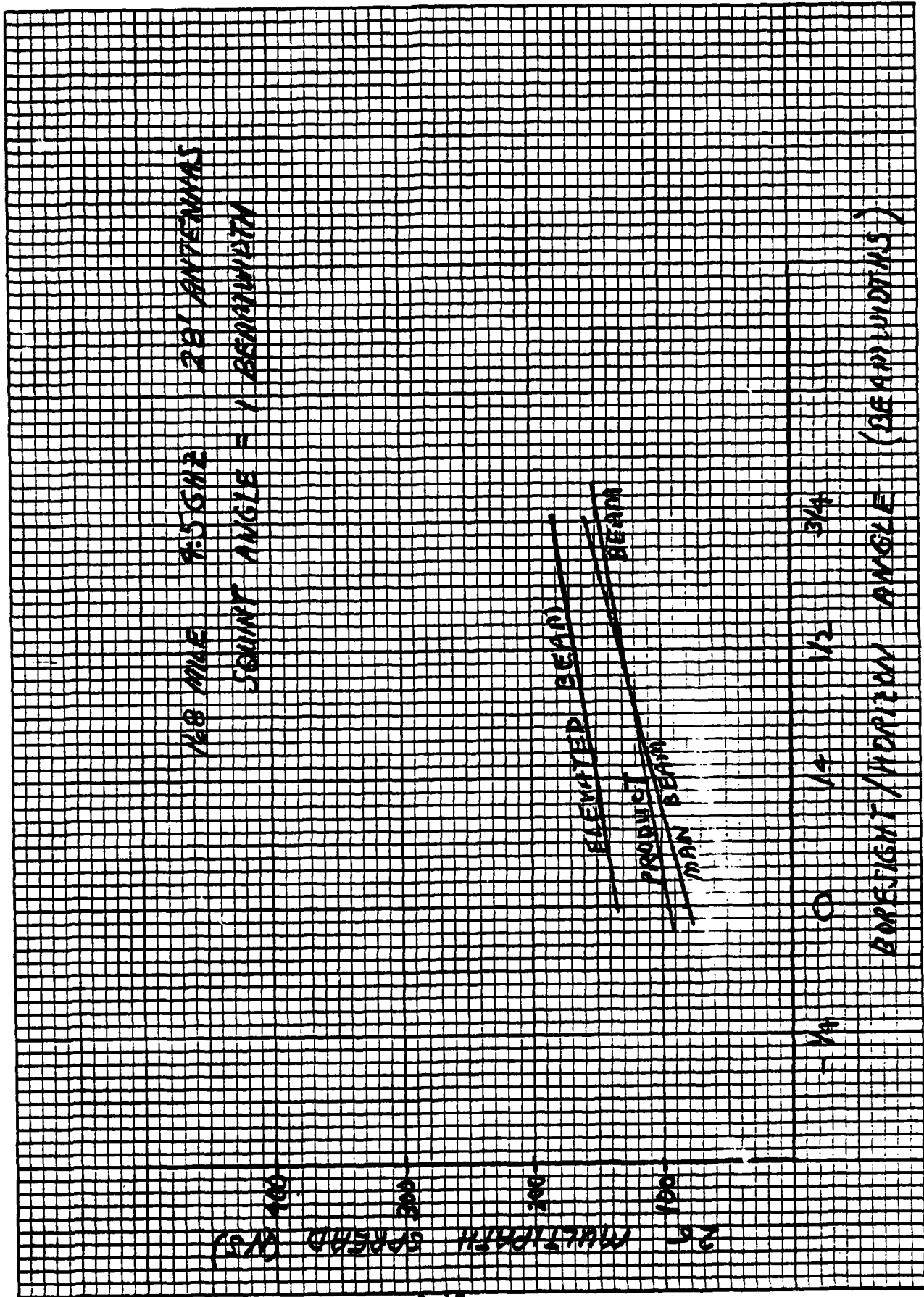
BORESIGHT (VERTICAL) ANGLE (BEAMWIDTHS)
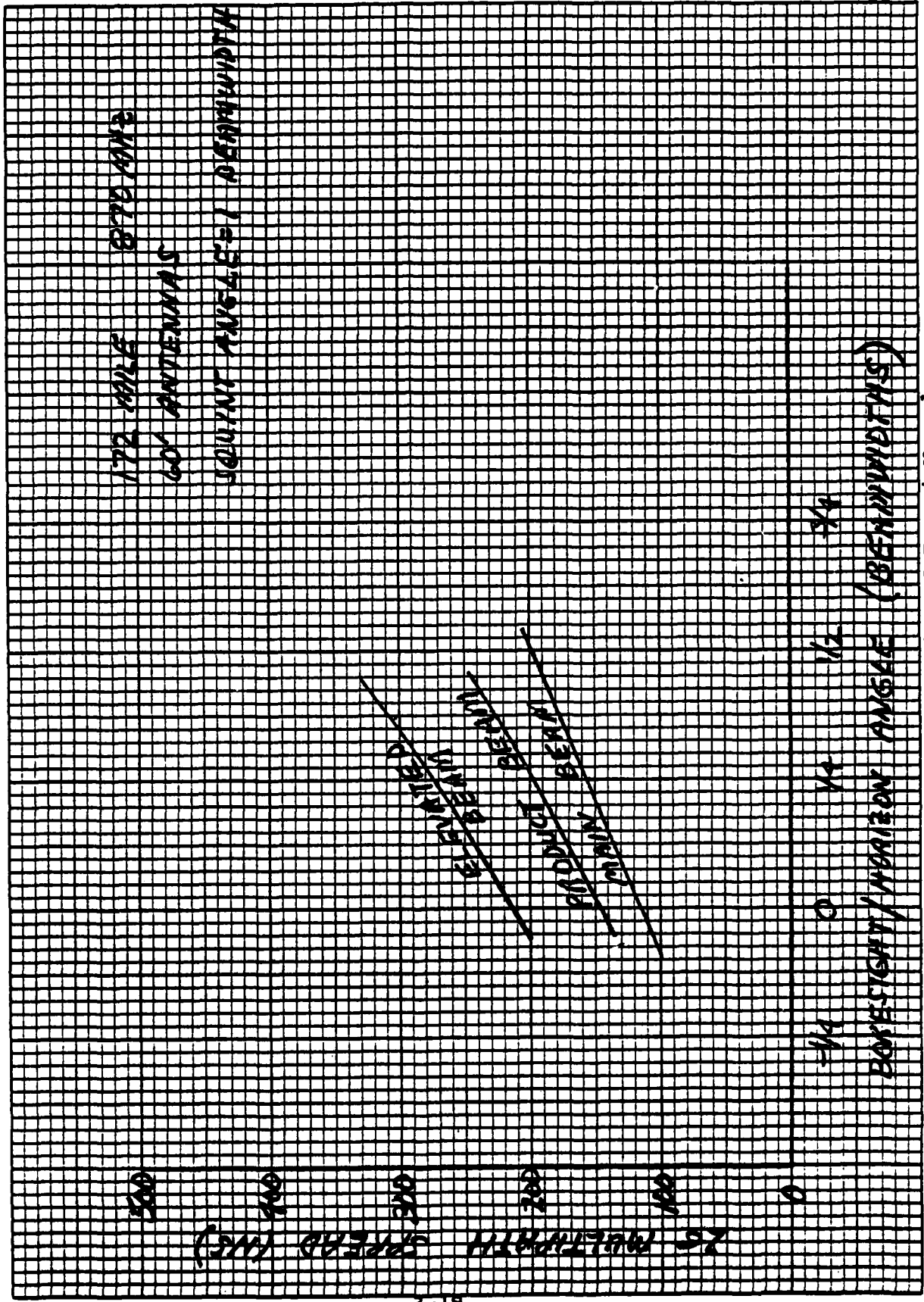
Fig. 3.9 Multipath Characteristics, RADC Test Link

Fig. 3.10 Multipath Characteristics, S.Tepesi-Yamanlar
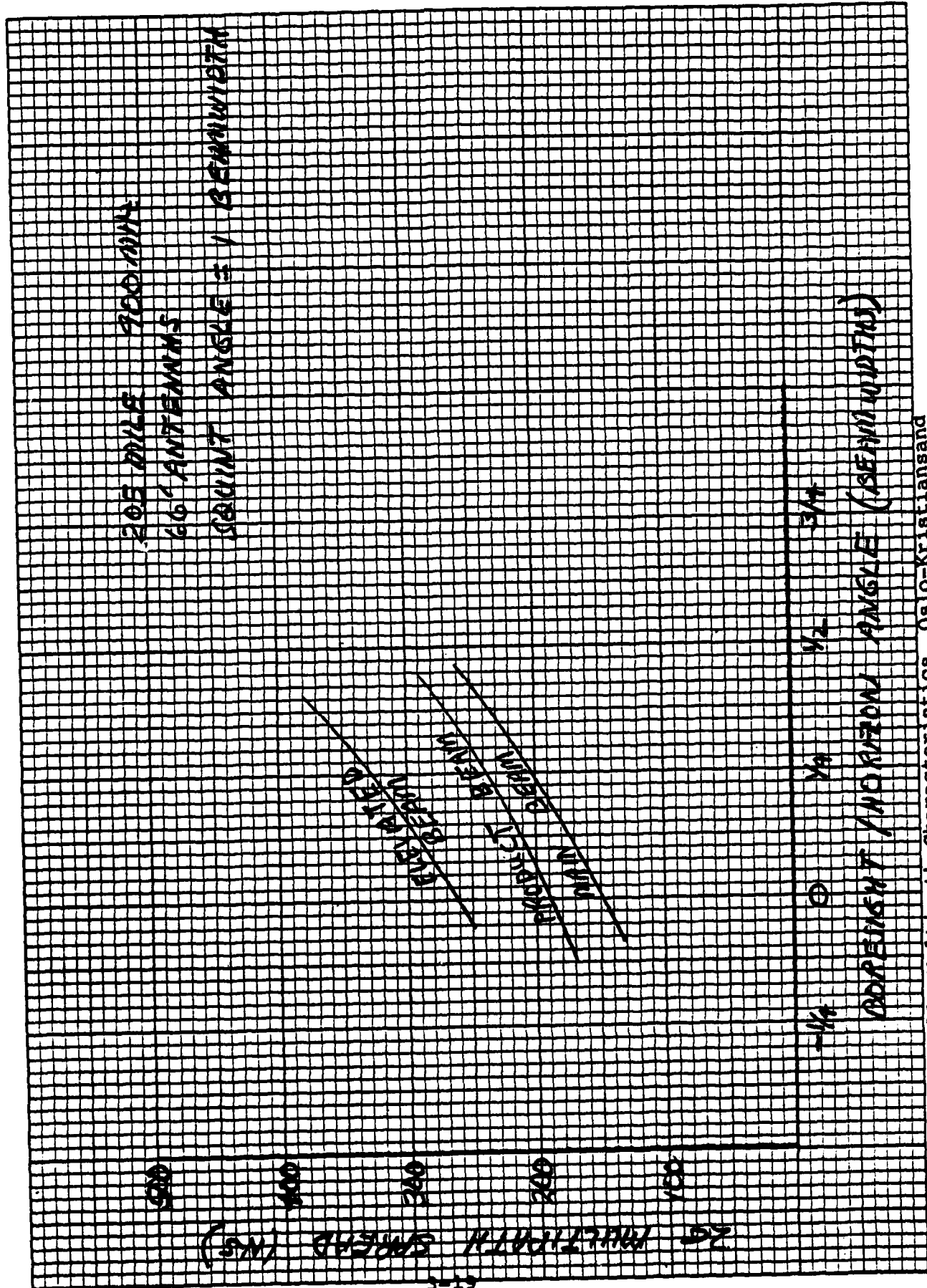
Fig. 3.11 Multipath Characteristics, Oslo-Kristiansand

systems there is considerably more multipath and a steeper slope
with pointing angle. Optimum performance of a digital VAD sys-
tem at these frequencies may result from pointing angles some-
what less than 1/4 beamwidth.

In summary the optimum VAD ststem utilizes a squint angle
of approximately 1 beamwidth with a boresight/horizon angle ap-
proximately equal to 1/2 beamwidth for C-band digital systems
and somewhat less than 1/4 beamwidth for L-band systems. In
all cases, however, the optimum configuration results in less
received signal power in the elevated beam. The use of pointing
angles with equal beampowers,which has been suggested [3.4],is
suboptimum because too much power is blocked in the main beam
by the foreground.

3.2 Long Term Variability

Tropospheric scatter systems are subject to two fading
phenomena — short term multipath fading and long term power
fading. The short term fading of the instantaneous received
power within periods of time ranging from less than a second to many
minutes results from random fluctuations in the relative phasing
between component waves arriving at the receiver over slightly
different propagation paths. The long term power fading results
from slow changes in average atmospheric refraction, in the
intensity of refractive index turbulence, and in the degree
of atmopsheric stratification. The power fading is characterized
by hourly or diurnal variations. The evaluation of troposcatter
system performance is accomplished in part by determining the
hourly median path loss where the median is computed to include
the short term multipath fading and in turn considering the
median path loss as a random variable subject to a power fading

3-20

distribution. The median path loss calculation utilizes fixed values of the mean and variance of the refractive index and an assumption on the degree of atmospheric stratification. In Section 2 we have presented a prediction method for the computation of median path loss. This method has the following important characteristics:

- The average atmospheric refraction is fixed by utilizing an effective earth's radius of 4/3 the actual radius to account for the mean refractive index.

- The intensity of refractive index turbulance is fixed by the refractive index variance which is chosen to correspond to dry winter afternoons.* This period of time generally experiences the poorest propagation conditions.

- The atmospheric structure is derived from turbulent scattering theory which leads to a refractive index spectrum slope of n=11/3. This structure is more applicable for higher frequency (> 1 GHz) troposcatter systems than the stratified layer assumption used in the NBS prediction method.

- The aperture-to-medium coupling loss is included as an integral part of the path loss calculations.

For this method the power fading of the median path loss is determined by variations in the effective earth radius factor K, variations in the refractive index variance σ_n^2, and changes in the atmospheric structure leading to other values of the refractive index spectrum slope n. Given probability density functions on the parameters K, σ_n^2, and n, the computation of the median path loss long term distribution would be

_____

* This time period is referred to as Time Block 2 (TB2) in the NBS prediction method.

straightforward. Unfortunately there is little empirical data available to derive such densities. Some experimental evidence and analysis [3.5] indicate that the refractive index variance σ_n^2 is the dominating factor in producing significant variations in the median path loss. Development of experimental data on σ_n^2 over long periods of time for different geographical areas would provide a basis for predicting long term variability of troposcatter systems. At the present time the only method of predicting this variability is to use path loss data taken from existing systems and integrated into the NBS variability model [3.6]. Much of the empirical path loss data has been taken from systems with operating carrier frequencies below 1 GHz. The performance prediction for new troposcatter systems operating in the 4 to 5 GHz frequency region may be subject to large errors as a result. However, in the absence of empirical data on either σ_n^2 or median path loss at these new frequencies, an extrapolation of the NBS variability model is the only realistic engineering choice. In the next subsection we briefly review this model and describe the specific parameters integrated into the SIGNATRON prediction computer program for computation of long term variability. In the subsequent subsection the special issues which must be addressed in the evaluation of the long term variability of an angle diversity system are considered.

3.2.1 NBS Long Term Variability Model

Considerable experimental evidence suggests that the long term distribution of the hourly median path loss is normally distributed in dB. If we denote L(p) as the hourly median path loss in dB, which is not exceeded p% of the time, the normal distribution is defined as follows:

3-22

$$\frac{p}{100} = \text{prob} \left\{ \text{ median path loss } \leq L(p) \right\}$$

$$\frac{1}{\sigma_L \sqrt{2\pi}} \int_{-\infty}^{L(p)} \exp \left[\left(\xi - L(50) \right)^2 / 2\sigma_L^2 \right] d\xi \ . \qquad (3.1)$$

where $L(50)$ is the median path loss computed using the method of Section 2 and σ_L is the long term standard deviation. The NBS Long Term Variability Model [3.6] uses empirical data to determine $L(10)$ and $L(90)$ from which normal probability graph paper can be used to plot $L(p)$ at other values of p. This calculation includes the effect of prediction uncertainty through a parameter called service probability. The service probability is the probability that a new system will meet the long term performance predictions.

A parameter called effective distance, d_e, has been found to be superior to other parameters such as path length, angular distance, and distance between actual or theoretical horizons, in predicting the long term variability. The effective distance is defined in terms of d_{s_1} which is the distance for equal diffraction and scatter path loss and d_{s_0} which is the smooth earth distance between radio horizons. These parameters are computed from the following relations

$$d_{s_1} = 65 (100/f)^{1/3} \text{ km} \qquad (3.2)$$

$$d_{s_0} = d - 3 \sqrt{2 h_{t_e}} - 3 \sqrt{2 h_{r_e}} \qquad (3.3)$$

where the effective antenna heights h_{t_e} and h_{r_e} are expressed in meters, the path length d is in kilometers, and the radio

frequency f is in MHz. The effective distance is defined in the NBS model as

$$
d_e = \begin{cases} 130/ \left[1+(d_{s_1} - d_{s_0}) /d\right] \text{ km,} & d_{s_0} \le d_{s_1} \\[2mm] 130 + d_{s_0} - d_{s_1} \text{ km,} & d_{s_0} \ge d_{s_1} \end{cases} \tag{3.4}
$$

A variability function $Y(p)$ which depends on the effective distance and can be corrected for frequency and climate effects is used to determine $L(10)$ and $L(90)$ from the relation

$$
L(p) = L(50) - Y(p) \tag{3.5}
$$

The variability function is defined by

$$
Y(p) = Y_0(p, d_e) \, g(p, f)
$$

where $g(p, f)$ represents an average of many effects that are frequency sensitive. The NBS variability model provides empirical curves and an analytic function representation for $Y_0(p, d_e)$. In addition, the model uses a parameter $V(50, d_e)$ to adjust the long term reference median path loss computed by the NBS method to the median loss $L(50)$ in (3.5). For dry winter afternoons this adjustment is 0 dB.

The analytic function representation for $Y_0(p, d_e)$ is given for dry winter afternoons (Time Block 2) as

$$
\left. \begin{array}{c} Y_0(10, d_e) \\[4mm] -Y_0(90, d_e) \end{array} \right\} = \left[c_1 \, d_e^{n_1} - f_2(d_e) \right] \exp\!\left(-c_3 d_e^{n_3} \right) + f_2(d_e)
$$

$$
\tag{3.6}
$$

3-24

where

$$f_2(d_e) = f_\infty \left[1 - (1 - f_m/f_\infty) \exp(-c_2 d_e^{n_2}) \right] \qquad (3.7)$$

and the constants have values (d_e in kilometers)

	$Y_o(10, d_e)$	$-Y_o(90, d_e)$
c_1	1.04×10^{-5}	1.05×10^{-5}
c_2	4.28×10^{-8}	7.00×10^{-13}
c_3	3.51×10^{-8}	7.64×10^{-8}
n_1	2.71	2.59
n_2	2.91	4.80
n_3	3.41	3.68
f_m	9.15	7.05
f_∞	2.8	2.8

For frequencies greater than 400 MHz, the curves for $g(p,f)$, winter afternoons, provided in the NBS model can be well approximated by

$$g(10, f) = g(90, f) = \begin{cases} 1 - 0.6 \, \text{LOG} \, (.0005 \, f) & 400 < f < 2000 \\ 1.0 & 2000 < f. \end{cases}$$

$$(3.8)$$

For a normal distribution, other points on the loss distribution are calculated from

$$Y(0.01) = 3.33Y(10) \qquad Y(99.99) = 2.90Y(90)$$
$$Y(0.1) = 2.73Y(10) \qquad Y(99.9) = 2.41Y(90)$$
$$Y(1.0) = 2.00Y(10) \qquad Y(99) = 1.82Y(90).$$

These calculations and the loss distribution resulting from (3.5) provide the long term variability of the median path loss

for a continental temperate climate during winter afternoons. The NBS variability model provides numerous curves and other variability functions to accommodate other portions of the season and other climatic areas.

The path loss distribution (3.5) corresponds to a service probability of 50%, i.e., 50% of the systems built would exceed the performance predictions. Conservative engineering practice would recommend the selection of a service probability of 95%. For this choice the loss distribution must be adjusted by the prediction error according to the NBS formula

$$L_{0.95}(p) = L(p) + 1.65 / \overline{12.73 + 0.12Y^2(p)}. \tag{3.9}$$

The variability predictions used in this study utilize the NBS long term variability model with a service probability of 95%. The median path loss $L(50)$ is computed using the method of Section 2, which corresponds to the loss for turbulent scattering conditions during dry winter afternoons in a temperate continental climate. The formulas 3.1 through 3.9 are then used to derive the loss distribution. The mean E_b/N_o distribution for evaluation long term variations in digital system performance is determined from the path loss distribution by the formula

$$\frac{\bar{E}_b}{N_o}(p) = P_T + G_T + G_R - L_{.95}(p) - \lceil 10 \text{ LOG } (R_b) + NF - 174 \rceil + 1.6$$

$$\tag{3.10}$$

where

$\quad P_T \qquad = \text{transmit power in dBm}$

$\quad G_T \qquad = \text{transmit antenna gain in dB}$

$\quad G_R \qquad = \text{receiver antenna gain in dB}$

$L_{.95}(p)$ = path loss not exceeding p% of the time for unit gain antennas[*] and a service probability of 0.95

R_b = data rate in b/s

NF = receiver noise figure in dB

-174dBm = received noise power in 1 Hz bandwidth

1.6 dB = factor relating median to mean for a complex Gaussian scatter channel.

3.2.2 Long Term Variability in an Angle Diversity System

In space and frequency diversity systems, the common scattering volume is virtually the same for each diversity and hence the long term median path loss varies the same for each diversity. In angle diversity system, however, the common volumes are separated and the long term variability is not identical for the angle diversity beams. The effect of this decorrelation of the diversity power fading may improve the system availability because a power fade in the main beam diversity is not always accompanied by a power fade in the squnited diversity beam. Physically one can imagine this situation in a vertical angle diversity system where the inhomogeneous structure of the atmosphere results in say a larger refractive index variance or superior atmospheric stratification at heights corresponding to the elevated beam than at heights defined by the main-beam common volume. Since the common volumes in a vertical angle diversity system are separated by approximately one beamwidth Ω at a distance d/2 from the link terminals, this decorrelation results from atmospheric variations over distances on the order of Ωd/2. For typical troposcatter applications this distance is on the order of one or more miles at a height above the

---

[*] Aperture to medium coupling loss of the actual diameter antennas is included in this parameter.

3-27

earth's surface also on the order of a few miles. Experimental evidence verifying the long term power fading decorrelation in angle diversity systems has been reported on by Monsen [3.7] and Troitskiy [3.8]. Data from these angle diversity experiments will be used to establish the availability improvement from power fading decorrelation.

The long term median path loss can be described by a multi-variated normal distribution when each path loss is given in dB. We consider a dual vertical angle diversity system with or without additional frequency or space diversity. Let x_i represent the median path loss in dB for diversity i and number of diversities such that the main beam diversities are odd and the elevated beam diversities are even, e.g., for a 2S/2F/2A system we have

x_1, x_3 mainbeam space diversity channels

x_5, x_7 mainbeam frequency diversity channels

x_2, x_4 elevated beam space diversity channels

x_6, x_8 elevated beam frequency diversity channels.

Because of the power fading correlation in space and frequency diversity, one has

$$x_1 = x_3 = x_5 = x_7$$

$$x_2 = x_4 = x_6 = x_8$$

and x_1 and x_2 are described by the joint normal density function

$$f(x_1, x_2) = \frac{1}{2\pi\sigma |R|^{\frac{1}{2}}} e^{-\underline{x}'R\underline{x} / 2\sigma^2} \qquad (3.11)$$

where

$$\underline{x} = \begin{bmatrix} x_1 - m_1 \\ x_2 - m_2 \end{bmatrix}$$

$$R = \begin{bmatrix} 1 & a\rho \\ a\rho & a^2 \end{bmatrix} .$$

3-28

m_1 = mean value of median path loss for diversity 1

m_2 = mean value of median path loss for diversity 2

σ = mainbeam path loss standard deviation

$a\sigma$ = elevated beam path loss standard deviation

ρ = power fading correlation coefficient.

The NBS variability model discussed in the last subsection provides a method for determining the path loss standard deviation σ. Since $\rho=0$ and $a=1$ for space and frequency diversity systems, determination of σ completely specifies the long term variability for these systems. In angle diversity systems the parameters ρ and a will also influence the long term variability of the effective received signal power.

In order to assess the effect of decorrelated power fading and an increase in the elevated beam standard deviation, we use the mean diversity path loss in dB as a system measure of performance. This measure corresponds to the geometric mean of the diversity signal-to-noise ratios which asymptotically for large signal-to-noise ratio governs the short term performance of both analog and digital systems. Thus we define the mean diversity path loss

$$x = \frac{1}{2} (x_1 + x_2) \tag{3.12}$$

and a system availability function as $x(p)$, where $x(p)$ is the mean diversity path loss not exceeded p% of the time, viz.,

3-29

$$\frac{p}{100} = \text{prob} \left\{ \text{mean diversity path loss} \leq x(p) \right\} .$$

Since the sum of two normal random variables is also normal, we have

$$\frac{p}{100} = \frac{1}{\sigma_x / \sqrt{2\pi}} \int_{-\infty}^{x(p)} \exp\left[(\xi - \bar{x})^2 / 2\sigma^2 \right] d\xi \qquad (3.13)$$

where the long term mean and variance are equal to

$$\bar{x} = \frac{1}{2} \; (\bar{x}_1 + \bar{x}_2)$$

$$\sigma_x^2 = \overline{(x - \bar{x})^2} = \frac{1}{4} \overline{\left[(x_1 - m_1) + (x_2 - m_2) \right]^2}$$

$$= \frac{\sigma^2}{4} \; (1 + 2\rho a + a^2) .$$

The percent availability for the angle diversity system is

$$p = 100 \left[1 - Q \left\{ \frac{x(p) - (m_1 + m_2)/2}{\frac{1}{2}\sigma \; \sqrt{1 + 2\rho a + a^2}} \right\} \right] \qquad (3.14)$$

where $Q(\cdot)$ is the normal distribution function

$$Q(u) = \frac{1}{\sqrt{2\pi}} \int_u^\infty e^{-v^2/2} \; dv . \qquad (3.15)$$

Equation (3.14) for angle diversity should be contrasted with the result for space or frequency diversity when $\rho = 0$, $a = 1$, viz.,

$$p = 100 \left[1-Q \left(\frac{x(\rho) - \hat{m}_1}{\sigma} \right) \right]. \qquad (3.16)$$

Note that m_1 for the angle diversity system is not necessarily equal to $\hat{m}_1$ for the space or frequency diversity systems. As an example, when angle diversity is used in place of frequency diversity, the additional power amplifier required for frequency diversity results in a 3 dB improvement for angle diversity, i.e., $m_1 = \hat{m}_1 + 3$.

In (3.14) one can see that the effect of the power fading correlation coefficient is to improve system availability with decreasing values of the coefficient but, on the other hand, an increase $(a > 1)$ in the elevated beam path loss standard deviation decreases the system availability. In order to evaluate the result of these competing effects, we examine some previous angle diversity experimental data.

Long term variability data was taken on the Bell Laboratories experimental angle diversity link reported on by Monsen [3.7]. The important characteristics of this link were

- triple vertical angle diversity
- 2.17 GHz operating frequency
- 179 statute mile path
- 28' transmit antenna, 50' steerable receive antenna
- 1 Kw transmit power
- 1.6 beamwidth separation between beams.

Measurements of hourly median signals once or twice a week over a period from September 1970 through February 1971 provided

a set of 43 independent hourly median samples. The long term received power[*] means, standard deviations, and correlation co-efficient for the lowest two vertical beams have been computed and are given in the following table as a function of antenna pointing angle relative to the horizon.

Now let us compare the availability of a space/frequency diversity system with space/angle diversity system. We select an antenna pointing angle of 0.5 beamwidths as both the results of Section 3.1 and the data in Table 3.3 suggest that performance will be maximized. For a space/frequency diversity system

$$2S/2F \text{ diversity: } m_1 = m_2 = -86.7 \text{ dBm}$$

$$a = 1 \quad \rho = 0$$

$$p = 100 \left[1 - Q\left(\frac{x + 86.7}{6.1} \right) \right]$$

For the 2S/2A diversity system, the second power amplifier used to derive the other frequency in the 2S/2F system can be tuned to the same frequency with a resulting increase in received power of 3 dB. Thus for the space/angle diversity system

$$2S/2A \text{ Diversity} = m_1 = -83.7 \text{ dBm}$$

$$m_2 = -90.0 \text{ dBm}$$

$$\sigma = 6.1$$

$$a = 7.2/6.1 = 1.18$$

$$\rho = 0.743$$

and from Eq. (3.14)

$$p = 100 \left[1 - Q\left(\frac{x + 86.85}{1.0186 \times 6.1} \right) \right] .$$

---

[*] Received power and path loss are used interchangeably here since they are related by an additive constant.

Table 3.3

Long Term Variability Data, BTL Link

Antenna Angle to Horizon Beamwidths	$\bar{x}_1$ dBm	$\bar{x}_2$ dBm	σ dB	$a\sigma$ dB	ρ
1.50	-89.1	-98.8	6.8	7.2	0.875
1.16	-87.4	-97.4	6.5	7.5	0.846
0.83	-86.4	-95.4	6.3	7.4	0.828
0.50	-86.7	-93.0	6.1	7.2	0.743
0.16	-89.3	-91.3	6.7	7.3	0.711
-0.16	-93.8	-89.7	6.8	6.8	0.735
-0.50	-99.9	-87.8	6.2	6.9	0.907
-0.83	-105.0	-87.2	5.8	7.0	0.922

The angle diversity system has slightly decreased availability because its mean diversity received power is 0.15 dB less and because the effective standard deviation is increased by a factor of 1.018. Thus in some cases the squint loss and increased standard deviation of the elevated beam path loss overcome the availability improvement due to the 3 dB power amplifier gain and the power fading decorrelation. For this experimental system, however, the squint loss was considerably larger than would be designed for an operational system.

When the squint loss is equal to 6 dB there is exact cancellation of the 3 dB power amplifier gain with the mean diversity loss associated with squinted dual angle diverssty system. For operational systems the net gain due to these two factors will normally be positive since the antenna beams can be placed closer together than the 1.6 beamwidth separation in the BTL experimental system. The net gain due to the power fading correlation coefficient and elevated beam standard deviation is more difficult to assess because of the rather limited empirical data. The BTL data suggests that the two effects tend to cancel each other out. Troitskiy [3.8] has presented data on three links which show a smaller power fading correlation coefficient than found from the BTL data. Table 3.4 summarizes Troitskiy's experimental results. The power fading correlation coefficient was measured between envelope powers in watts rather than dBm and is designated $\tilde{\rho}$. Ir the Appendix we show that $\tilde{\rho}$ is overbounded by ρ but the bound is tight and to a good approximation $\tilde{\rho} \doteq \rho$.

It is surprising that the results in Table 3.4 show a smaller power fading correlation coefficient when these links have the

3-34

beams closer together in the sky than the beams were in the BTL experimental link. Also it is unfortunate that Troitskiy did not report on data from which the elevated beam standard deviation can be calculated. A major goal of the AAC field test program will be to obtain estimates of both the power fading correlation coefficient and the elevated beam standard deviation.

This data will be used to help resolve what, if any, availability improvement can be attributed to long term decorrelation of angle diversity beams.

Table 3.4

Experimental Results, Ref. Troitskiy [3.8]

Path Length Miles	Freq. GHz	Beam-width mr	Angle Between Beams mr	Scatter Angle mr	Hours of Data	$\tilde{\rho}$
188	1.0	12.5	11.6	35	500	0.50
174	4.35	12.5	8.7	33	240	0.56
267	4.35	5.8	6.9	50	100–150	0.679

SECTION 3

REFERENCES

[3.1] D.T. Gjessing and K.S. McCormick, "On the Prediction of the Characteristic Parameters of Long-Distance Tropospheric Communication Links", *IEEE Trans. on Communications*, Vol. 22, No. 9, p. 1325, Sept. 1974.

[3.2] P.Monsen, S.Parl, J.N.Pierce, "*Adaptive Antenna Control*", Interim Technical Report, ECOM Contract DAAB07-76-C-8085, December 22, 1976.

[3.3] A. Sherwood , and L. Suyemoto, "*Multipath Measurements Over Troposcatter Paths*", Mitre Corporation, Report MTP-170, April 1976.

[3.4] M.W.Gough, G.C.Rider, "Angle Diversity In Troposcatter Communications", *Proc. IEE*, Vol. 122, No.7, July 1975, pp.713-719.

[3.5] E.E. Gossard, "Refractive Index Variance and its Height Distribution in Different Air Masses", *Radio Sci.*, Vol.12, No.1, 1977, pp.89-105.

[3.6] P.L.Rice, et.al., "Transmission Loss Predictions for Tropospheric Communications Circuits", *NBS Tech. Note 101*, Vols. I and II, US Dept. of Commerce, National Bureau of Standards, May 7, 1965.

[3.7] P.Monsen, "Performance of an Experimental Angle Diversity Troposcatter System," *IEEE Trans. on Comm.*, Vol. COM-20, No.2, April 1972, pp. 242-247.

[3.8] V.N.Troitskiy, "Efficiency of Angle-Diversity Reception in Long-Distance Tropospheric Propagation," *Telecommun. & Radio Eng.*, 1972, 27, pp.17-23.

SECTION 4

DIGITAL SYSTEM PERFORMANCE

The bit error rate performance of a digital data system
operating over an angle diversity troposcatter link is dependent
on the received power at each feedhorn, the correlation between
diversity channels, and the multipath characteristics of the
composite diversity system. As one of the end products of this
study, we will develop the mathematical formalism to predict (1)
the average bit error rate as a function of the hourly median
received power for the main beam diversity channel and (2) the
long term probability that the average bit error rate is exceeded.
The formalism will be converted into computer programs for con-
venient calculation of these results for specific angle diversity
proposed applications.

The first goal is concerned with evaluating the short term
(less than a minute) fading characteristics of the troposcatter
channel. The second goal deals with the availability of the
digital troposcatter system as a result of hourly and daily varia-
tions in path parameters. The path loss and multipath prediction
model developed under this program provides the basis for the
calculation of the short term path parameters while the results
from 3.2 and the NBS long term variability data will be used to
assess the availability question.

Computation of bit error rate statistics implies a choice
of digital modulation format and receiver processing technique.
We have selected QPSK for the modulation format and a generalized
adaptive decision-feedback equalizer (DFE) for the processor.
QPSK is the present choice of the two developed troposcatter modems,
MD-918 and the DAR-4, because of its bandwidth efficiency, nearly

constant envelope characteristic, and optimal detection capability. The DFE has been shown in extensive field testing of the MD-918 modem to provide excellent performance over an extremely wide range of channel conditions such as might be anticipated in an angle diversity application. The MD-918 DFE modem is also the modem to be used in the AAC field tests.

The general problem of computing the short term bit error rate (BER) distriubution for a fading multipath channel is a difficult if not impossible task. One can determine the BER disstribution for a flat fading channel with diversity order D in a straightforward manner [4.1] but the introduction of implicit diversity due to multipath precludes a closed form transformation of variables. The short term mean BER for a space or frequency diversity system can be determined following the procedure developed in [4.2] with a resulting expression in the form of a determinant. The BER distribution can be estimated by finding the mean BER and then defining an equivalent, non integer, flat fading diversity system by matching the mean BER's in the region of interest. The effective order of diversity D_e for the equivalent flat fading system could then be used to derive the short term BER statistics. The effective diversity order would reflect the correlation loss between diversity channels, the squint loss of elevated beams, implicit diversity due to multipath, and the intersymbol interference penalty which limits the usable implicit diversity. Thus, the computation of mean bit error rate is a logical first step in the evaluation of system performance. In the subsection to follow, the analysis developed in [4.2] is extended to include correlated explicit diversity channel systems such as angle diversity.

4.1 Mean Bit Error Rate Derivation

4.1.1 Communication System Definition

The communication system model under consideration is shown in Fig. 4.1. Complex notation is used to represent in-phase and quadrature components and explicit modulation/demodulation operations are not shown. The data to be transmitted (s_k) are selected from the set $(\pm 1 \pm j)$ for a quaternary phase-shift-keying system. The transmitted waveform is

$$s(t) = \sum_{k=-\infty}^{\infty} s_k f(t-kT) \tag{4.1}$$

where T is the interval between successive symbol transmission, i.e., symbol interval. The data rate for this QPSK system is 2/T bits/second. The transmitter impulse response f(t) is defined as a unit energy real function.

The fading multipath channel can be represented by an ensemble of zero-mean random functions with complex Gaussian statistics. Individual diversity channels in an angle diversity system will exhibit correlation between each other which can be completely described by the second moment of the channel impulse response $h_i(t)$,

$$\overline{h_i(t) \ h_j^*(\tau)} = \delta(t-\tau) \ \overline{E}_b \ A_{ij} p_{ij}(t), \quad i, \ j = 1, 2, \ldots D, \tag{4.2}$$

where $\delta(t)$ is the impulse function, $\overline{E}_b$ is the mean received energy per bit for the main beam diversity channel, A_{ij} represents a relative received power difference between the diversity channels, and $p_{ij}(t)$ is a unit area function equal to the mean squared envelope of the impulse response. It represents the average cross power response at each delay value to impulse function excitation and will be referred to as the cross multipath profile. Twice the RMS width of the profile is the cross multipath spread, $2\sigma_{ij}$. For convenience the main beam diversity channel is designated as channel 1 which requires $A_{11} = 1$. In a typical angle diversity
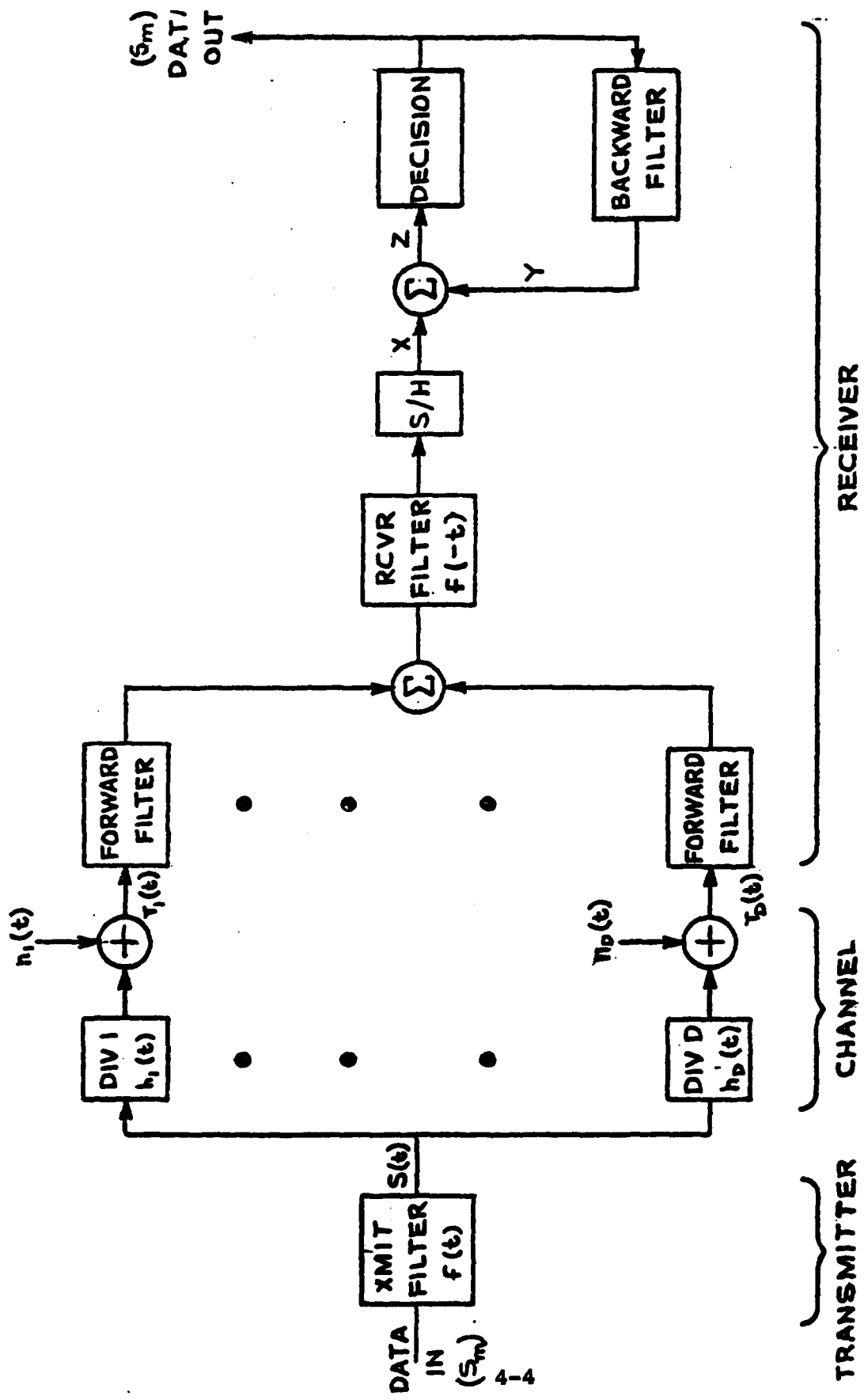
Fig. 4.1 Communication System Model

application utilizing dual vertical feedhorns on each antenna with odd numbers designating main beam diversities and even numbers designating elevated beam diversities, the characterization has the special form

$$A_{ii} = 1 \quad , \quad p_{ii}(t) = p_i(t); \quad i \text{ odd} \tag{4.3.1}$$

$$A_{ii} \leq 1 \quad , \quad p_{ii}(t) = p_2(t); \quad i \text{ even} \tag{4.3.2}$$

$$A_{i,i+1} \leq 1 \quad , \quad p_{i,i+1} = p_{12}(t); \quad i \text{ odd} \tag{4.3.3}$$

$$p_{ij}(t) = 0 \ , \ i \neq j \text{ and } i \text{ (odd)} \neq j-1 \tag{4.3.4}$$

Conditions (4.3.1) (4.3.4) state that all main beam diversities have equal statistics and are independent of each other. Conditions (4.3.2) and (4.3.4) state that all elevated beams have equal statistics and are independent of each other. Finally, conditions (4.3.3) and (4.3.4) state that the cross multipath profile is the same for each feedhorn pair but that the correlation between feedhorn ports on different antennas is zero. Note that the elevated beam in a vertical angle diversity system generally has less received power because of its larger scattering angle. The results from Section 3.1 contend that in a duplex angle diversity system it is not advantageous to point the antennas down to equalize the received powers in the two feedhorns.

The definition of $\bar{E}_b$ as the received energy per bit for the main beam diversity, $A_{11} = 1$, follows from the fact that one received bit is represented by the pulse

$$\pm 1 \int_{-\infty}^{\infty} f(t-u) \, h_1(u) \, du$$

which has energy

$$\int_{-\infty}^{\infty} dt \left| \int_{-\infty}^{\infty} f(t-u) h_1(u) du \right|^2 = A_{11} \int_{-\infty}^{\infty} dt \int_{-\infty}^{\infty} f^2(t-u) \, \bar{E}_b p_1(u) \, du$$

$$= \bar{E}_b \int_{-\infty}^{\infty} p_1(u) \, du = \bar{E}_b$$

The ensemble representation is used here because the analysis to follow assumes a slowly varying multipath channel which the equalizer can track. Hence the mean BER performance is determined by computing the channel ensemble average of the bit error probability for the Decision-Feedback Equalizer (DFE). An overbar is used to denote channel ensemble averages. Brackets $\langle \rangle$ will be used to denote average over noise or source statistics for a particular channel realization. For the white Gaussian noise channels the additive noise terms $n_i(t)$ are zero mean and have second moments

$$\langle n_i(t) \, n_j^*(\tau) \rangle = N_o \, \delta_{ij} \, \delta(t-\tau), \quad i, \, j=1,2,\ldots D,$$

where N_o is the noise spectral density in watts/Hz.

Each forward filter in a realizable DFE consists of a finite length tapped delay line filter with tap spacing of τ_s seconds. If there are K_2 "late" taps and K_1 "early taps", the tapped delay line filter impulse response is

$$w_i(t) = \sum_{k=-K_1}^{K_2} w_{ik}^* \, \delta(t-k\tau_s) \qquad (4.4)$$

where the tap gain value is chosen with a complex conjugate for notational convenience later. The receiver filter has impulse response $f(-t)$ which matches the transmit pulse waveform. For this choice, in the absence of multipath, and after time synchronization, the optimum tap weights for the main beam diversity forward filter reduce to one tap on and the rest off. The output of the receiver filter is sampled at the symbol rate $1/T$ to produce the sample X_m. The backward filter correction sample is summed with the sampled receiver filter output X_m to produce the detection variable z_m at the mth symbol epoch. The backward filter weights previous decision $\hat{s}_{m-i}$ by the complex weight b_i to form the sample output

$$Y_m = \sum_{i=1}^{B} b_i \hat{s}_{m-1} \qquad\qquad (4.5)$$

at the decision time for the s_m symbol. The decision on s_m is denoted as $\hat{s}_m$. The decision process takes the form

$$z_m = x_m + Y_m$$

$$\hat{s}_m = sgn\ (Re(z_m)) + jsgn\ (Im(z_m))$$

where sgn is the signum function.

The parameters of the DFE are the number of forward filter taps K, the forward filter tap spacing, τ_s and the number of backward filter taps, B. The optimum DFE requires $K = \infty = B$ and $\tau_s = 1/W$ where W is the two-sided bandwidth. A practical choice of parameters for troposcatter channels was determined from computer simulation of a fading channel equalizer application to be $K = 3 = B$ and $\tau_s = T/2$.

4.1.2 DFE Performance Analysis

Previous methods of determining average bit error rate (ABER) performance of practical equalizer structures have been restricted to Monte Carlo simulations [4.3, 4.4] using an ensemble of multipath channels. An analytic approach for calculating the ABER is complicated by the presence of an intersymbol interference term in the signal-to-noise ratio (SNR) expression for a particular channel realization. Because of this term, an average over the channel ensemble is a formidable task. On the other hand, omission of the intersymbol interference term leads to a mean BER which for a fixed SNR monotonically decreases with increasing multipath spread. For any practical equalizer for a fixed SNR the mean BER will initially decrease for increasing multipath spread but then increase as

the multipath exceeds the equalizer's capability to mitigate the intersymbol interference. Elimination of the intersymbol term provides a convenient lower bound which both shows the intersymbol interference penalty and is an accurate performance estimate for small multipath spreads. However, the lower bound is too loose for performance calculation when the rms multipath spread is on the order of the forward filter width. The analytic procedure to be developed allows accurate calculation of the lower bound for no intersymbol interference and by an approximation of the intersymbol interference effect provides a good performance estimate for the large multipath case.

For notational simplicity the analysis consideres a nondiversity channel and extends the final results for higher order diversity systems including angle diversity. The received signal has the form

$$r(t) = \sum_{m=-\infty}^{\infty} s_m \int_{-\infty}^{\infty} h(u) \ f(t-mT-u) \ du + n(t) \tag{4.6}$$

We define the combined transmitter and receiver response as

$$g(t) = \int_{-\infty}^{\infty} f(t+u) \ f(u) \ du$$

and its convolution with the channel as

$$\sqrt{\overline{E_b}} \, q(t) = \int_{-\infty}^{\infty} g(t-u) \ h(u) \ du. \tag{4.7}$$

For a sampling time t_o, the detection variable z has the form

$$z = \sum_{k=-K_1}^{K_2} w_k^* \left[\sum_{m=-\infty}^{\infty} s_m \sqrt{\overline{E_b}} \, q(t_o - mT - k\tau_s) + v(t_o - k\tau_s) \right],$$

where the $K = K_1 + K_2 + 1$ forward filter taps are apportioned between K_2 "past" taps and K_1 "future" taps and one center tap . The noise variate

$$v(t_o) = \int n(t_o - u) \ f(u) \ du$$

is zero-mean Gaussian with second moment

4-8

$$\langle v(t_o-k\tau) \; v^*(t_o-\ell\tau) \rangle = N_o \; g(k\tau-\ell\tau).$$

There exists an obvious representation in a $K=K_1+K_2+1$ dimensional column vector form, viz.,

$$z = \underline{w}' \left(\sqrt{\bar{E}_b} \; \sum_{m=-\infty}^{\infty} s_m \; \underline{q}_m + \underline{v} \right) \tag{4.8}$$

where the accent mark refers to complex conjugate transpose. The vector $\underline{w}$ represents the forward filter complex tap gains, $\underline{q}_m$ represents the sampled continuous filter response for the mth transmitted symbol, and $\underline{v}$ is a zero-mean Gaussian noise vector process with positive definite covariance matrix $N_o G_o$ with element values $N_o g(k\tau-\ell\tau)$.

For QPSK, every other bit decision is made on the real part of z and there is quadrature symmetry and thus the real noise power affecting that decision is

$$\delta_o^2 = \langle \text{Re}(\underline{w}'\underline{v})^2 \rangle = \frac{N_o}{2} \underline{w}'G_o\underline{w} \tag{4.9}$$

If one assumes $s_m=0$, $m \neq 0$, there is no intersymbol interference and the analysis for the mean BER leads to an SNR expression for a particular channel realization which is a quadratic form of the type $\underline{q}_o' \; G_o^{-1} \; \underline{q}_o$ where $\underline{q}_o$ is a complex Gaussian vector with statistics determined by the channel and G_o is a positive definite matrix. After a diagonalization procedure the average of the bit error probability function of the SNR can be computed for both coherent and differentially coherent detection. This calculation leads to the lower bound expression. When the intersymbol interference is present an effective signal-to-noise ratio can be defined which leads to a quadratic form but both the vector and the matrix have random components. A method of averaging over a function of this quadratic form is not apparent. One course worth considering is to approximate the intersymbol interference effect

in a manner which will modify the G_o matrix but keep its deterministic nature. This can be accomplished if the following two approximations are made..

(1) Assume the interference symbols s_m, $m \neq 0$, are Gaussian distributed rather than complex binary.

(2) Approximate the matrix contribution to G_o due to intersymbol interference by its mean.

This approach assumes that the intersymbol interference after equalization in a fading multipath channel can be well approximated by an equivalent non-fading additive Gaussian noise term. Since most of the bit errors are a result of fades in the desired signal, gross approximation in the interference characteristics do not significantly alter the mean BER.

One can reasonably assume that the backward filter cancels the interference contribution due to past symbols, i.e., symbols which arrive before the symbol currently being decided on. If we arbitrarily take the symbol selected for decision as s_o, the remaining interference is classified as future and is given by

$$\sqrt{\overline{E}_b} \sum_{m=1}^{M} s_i \, \underline{w}' \underline{q}_i = \underline{w}' \underline{v}_1 \, . \tag{4.10}$$

The sum can be truncated after a few terms as the dot product will disappear for large i due to the finite duration of the pulse function $q(t)$. The first approximation is to take s_i as a zero mean complex Gaussian with mean magnitude squared value γ^2. This quantity should be less than two as approximating a unit magnitude binary variable by a unit variance Gaussian variable will certainly lead to pessimistic performance results due to the tails of the Gaussian distribution. A choice of $\gamma^2 = 1/2$ was found to provide excellent agreement between calculated and measured values.

Equation (4.8) can be rewritten as

$$z = \underline{w}' \left(\underline{q}_o \sqrt{\overline{E}_b} \, s_o + \underline{v} + \underline{v}_1 \right) \tag{4.11}$$

4-10

and since the additive noise contribution from $\underline{v}$ is independent
of the source digit contribution from $\underline{v}_1$, the effective noise
power for the decision on the real part of z is

$$\delta^2 = \left\langle \left[\text{Re}\left(w'(v + v_1) \right) \right]^2 \right\rangle$$

$$\delta^2 = \frac{N_o}{2} \underline{w}' \, G_o \underline{w} + \frac{1}{2} \underline{w}' \, \langle \underline{v}_1 \underline{v}_1' \rangle \, \underline{w} = \frac{N_o}{2} \underline{w}' \, G \underline{w} \qquad (4.12)$$

Performing the indicated averaging with respect to the source
digits, one finds from the definition of $\underline{v}_1$ in (4.10) the covariance
matrix

$$\langle \underline{v}_1 \underline{v}_1' \rangle = \overline{E}_b \, \gamma^2 \sum_{m=1}^{M} \underline{q}_i \, \underline{q}_i' \, . \qquad (4.13)$$

The signal-to-noise ratio (SNR) affecting the decision on the real
part of z is then

$$\rho \equiv \frac{\overline{E}_b}{2\delta^2} \left[\text{Re}\left(\underline{w}' \underline{q}_o \right) \right]^2 \qquad (4.14)$$

which we seek to maximize as a function of the forward filter
weight vector, $\underline{w}$. Consider the generalized dot product defined
on the positive definite matrix G, i.e.,

$$(\underline{u}, \, \underline{v}) \equiv \underline{u}' G \underline{v}. \qquad (4.15)$$

Equation (4.14) can be written as

$$\rho = \frac{\overline{E}_b}{N_o} \frac{[\text{Re}(\underline{w}, G^{-1} \underline{q}_o)]^2}{(\underline{w}, \underline{w})'} \qquad (4.16)$$

and by a generalization of the Schwartz Inequality we obtain

$$\rho \leq \frac{\overline{E}_b}{N_o} \frac{|(w, G^{-1} \underline{q}_o)|^2}{(\underline{w}, \underline{w})} \leq \frac{\overline{E}_b}{N_o} (G^{-1} \underline{q}_o, G^{-1} \underline{q}_o) \qquad (4.17)$$

with equality if and only if

$$\underline{w}_{opt} = G^{-1} \underline{q}_o \qquad (4.18)$$

Note (4.18) results in a pure real term in (4.16) to satisfy the Re (·) requirement.

The maximum SNR is then

$$\rho_{max} = \frac{\overline{E}_b}{N_o} \underline{q}_o' \, G^{-1} \underline{q}_o \qquad (4.19)$$

As a check on the normalization, if $\sigma = 0$ and $t_o = 0$ we have from Eq. (4.7)

$$q(-k\tau) = g(-k\tau) = G_{ok} \qquad (4.20)$$

and then

$$\rho_{max} = \frac{\overline{E}_b}{N_o} g(0) = \frac{\overline{E}_b}{N_o} \qquad (4.21)$$

as is expected in the absence of multipath.

We will now establish that the mean square error function

$$\langle \epsilon^2 \rangle = \frac{1}{2} \langle |z - ds|^2 \rangle \qquad (4.22)$$

which is minimized by the decision-feedback equalizer leads to the same set of forward filter weights as maximization of the SNR in (4.16) for the appropriate choice of scale factor d. After squaring and averaging, equation (4.22) becomes

$$\langle \epsilon^2 \rangle = \overline{E}_b \underline{w}' \underline{q}_o \underline{q}_o' \underline{w} - 2\sqrt{\overline{E}_b} \, d \, \text{Re}\left(\underline{w}' \underline{q}_o\right) + \frac{1}{2}N_o \, \underline{w}' \, G\underline{w} + d^2$$

$$= |\sqrt{\overline{E}_b} \, \underline{w}' \underline{q}_o - d|^2 + N_o \, \underline{w}' \, G\underline{w}. \qquad (4.23)$$

Minimization of (4.23) is equivalent to the LaGrange multiplier problem

$$\min_{\underline{w}} \left[\underline{w}' G\underline{w} - 2\beta \, \underline{w}' \, \underline{q}_o \right] \qquad (4.24)$$

which has solution

$$\underline{w} = \beta \, G^{-1} \underline{q}_o. \qquad (4.25)$$

Since Eq.(4.18) and (4.25) are the same except for an unimportant
scale factor, we have established that the maximum signal-to-noise
ratio for a minimum mean-square error DFE and a particular channel
realization is the quadratic form given by Eq.(4.19). The matrix
G is defined from (4.12) and (4.13) as

$$G = G_o + \frac{\overline{E_b}}{N_o} \gamma^2 \sum_{m=1}^{M} \underline{q_i} \underline{q_i}' \qquad (4.26)$$

where G_o is a function of the transmitter impulse response and is
a deterministic matrix. The second term in (26) is a random matrix
with statistics determined by the channel ensemble. Using G in
this form for calculation of the mean BER requires an average over a
function of a quadratic form which has both random vectors and
random matrix. The second approximation used to compute this
average is to replace the random interference term by its mean,
i.e.

$$G \doteq G_o + \frac{\overline{E_b}}{N_o} \gamma^2 \sum_{m=1}^{M} \overline{\underline{q_i} \underline{q_i}'} \qquad (4.27)$$

The matrix G is now a deterministic function of the transmitter and
receiver filter characteristics and the channel statistics. The
vector $\underline{q_o}$ is a random vector associated with the fading channel
ensemble. The average bit error rate can now be computed by taking
the average over the channel ensemble. The bit error probability
for QPSK for any member of the channel ensemble is from (4.11) and (4.19)

$$P_c = \tfrac{1}{2} \, \text{pr} \, \{\xi > 1\} + \tfrac{1}{2} \, \text{pr} \, \{\xi < -1\} \qquad (4.28)$$

where ξ is a zero-mean Gaussian random variable with standard devi-
ation equal to $\sqrt{1/2\rho_{max}}$. The bit error probability is

$$P_c = (2\pi)^{-\frac{1}{2}} \int_{2\rho_{max}}^{\infty} \exp\,(-u^2/2) \; du = \frac{1}{2} \, \text{erfc} \, \sqrt{\rho_{max}} \qquad (4.29)$$

The subscript c denotes that the detection process was coherent, i.e. the receiver knows the transmitted carrier phase. Differential detection of phase-shift-keyed signals yields a bit error probability [4.5]

$$p_d = \tfrac{1}{2} e^{-\rho_{max}} \tag{4.30}$$

The tap gains of an adaptive MMSE equalizer remove the phase and frequency difference between the transmitter and receiver carrier clocks to an ambiguity of 180° for binary transmission and 90° for quaternary transmission. This ambiguity is eliminated by differentially encoding the transmitted data. The performance of coherently detected and differentially encoded data signals for a fixed ρ_{max} is approximately double the error rate given by (4.29). When practical degradations are included in the analysis the performance is closer to the differential detection expression (4.30). Thus the ensemble average of p_c is of interest as a fading channel performance bound and the ensemble average of p_d is of interest as an estimate of realizable modem performance.

Let $y(x)$ be the probability density function for ρ_{max} and $Y(S)$ its Laplace transform. We want to calculate the ensemble averages

$$\overline{p}_c = \int_0^\infty \tfrac{1}{2} \, \text{erfc} \, \sqrt{x} \; y(x) \, dx \tag{4.31}$$

$$\overline{p}_d = \int_0^\infty \tfrac{1}{2} e^{-x} \, y(x) \, dx = \tfrac{1}{2} Y(1) \tag{4.32}$$

The Laplace transform $Y(s)$ is easily obtained after a diagonalization of the quadratic form in Eq. (4.19).

$$x = \frac{\overline{E}_b}{N_o} \, \underline{q}'_o \, G^{-1} \, \underline{q}_o = \frac{\overline{E}_b}{N_o} \, \underline{\alpha}' \, \underline{\alpha} \tag{4.33}$$

where $\underline{\alpha}$ is a zero-mean complex Gaussian vector with a diagonal covariance matrix $\Gamma_{ij} = \lambda_i \delta_{ij}$. The diagonalization resulted from the transformation

4-14

$$\underline{\alpha} = MG^{-\frac{1}{2}} \underline{q}_0 \tag{4.34}$$

and M is the normalized orthogonal matrix for the matrix

$$G^{-\frac{1}{2}} \overline{\underline{q}_0 \underline{q}'}_0 G^{-\frac{1}{2}}, \text{ i.e.} \tag{4.35}$$

$$G^{-\frac{1}{2}} \overline{\underline{q}_0 \underline{q}'}_0 G^{-\frac{1}{2}} M = M\Gamma \tag{4.36}$$

$$M'M = I. \tag{4.37}$$

Thus the eigenvalues λ_i are also the eigenvalues of the symmetric matrix $G^{-\frac{1}{2}} \overline{\underline{q}_0 \underline{q}'}_0 G^{-\frac{1}{2}}$ and the unsymmetric matrix $G^{-1} \overline{\underline{q}_0 \underline{q}'}_0$. Since the components of $\underline{\alpha}$ are uncorrelated Gaussian, the probability density for ρ_{max} is the convolution of exponential densities which yields a Laplace transform in product form.

$$Y(s) = \prod_{k=-K_1}^{K_2} \left(1 + \frac{\bar{E}_b}{N_0} \lambda_k s\right)^{-1} \tag{4.38}$$

The mean BER for DPSK is

$$\bar{p}_d = \tfrac{1}{2} Y(1) = \tfrac{1}{2} \prod_{k=-K_1}^{K_2} \left(1 + \frac{\bar{E}_b}{N_0} \lambda_k\right)^{-1}. \tag{4.39}$$

For coherent detection it is necessary to find the coefficients A_{ik} in a partial fraction expansion of $Y(s)$, i.e.,

$$Y(s) = \sum_{k=-K_1}^{K_2} A_k \left(1 + \frac{\bar{E}_b}{N_0} \lambda_k s\right)^{-1}.$$

A recursive method for finding the coefficients and the resulting error probability for coherent detection is detailed in [4.4] where the mean BER for the infinite length optimum single pulse receiver was determined. We will concentrate on the DPSK expression (4.39)

because the DPSK bit error probability curve for the Gaussian
noise non fading channel closely matches the BER for the MD-918
modem, i.e., the implementation loss and differential encoding
loss in the CPSK detection system is approximately equal to the
loss incurred in ideal DPSK relative to ideal CPSK. Figure 4.2
illustrates this result. Since in a fading channel application
most of the bit errors will occur during periods of low SNR, the
correspondence between ideal DPSK and the measured DFE modem
should be closest at low SNR.

For a DPSK system or for the use of the DPSK expression to
approximate the Gaussian noise non fading performance of a practi-
cal modem, calculation of the average bit error probability does
not require the determination of the eigenvalues. Note that (4.39)
has the determinant form

$$\bar{P}_d = \frac{1}{2}(dt|I + \frac{\bar{E_b}}{N_O} G^{-1}C|)^{-1} \tag{4.40}$$

where the covariance matrix C is a function of the transmitter
filter multipath profile, and the sampling time t_o.

$$C_{k\ell} = C_{k\ell}(t_o) = q(t_o - k\tau_s q^*(t_o - \ell\tau_s) = \int_{-\infty}^{\infty} g(t_o - k\tau_s - u)g(t_o - \ell\tau_s - u)p(u)du. \tag{4.41}$$

The matrix G as defined in (4.27) has the form

$$G_{k\ell} = g(k\tau_s - \ell\tau_s) + \frac{\bar{E_b}}{N_O} \gamma^2 \sum_{m=1}^{M} C_{k\ell}(t_o - mT). \tag{4.42}$$

The matrices (4.47) and (4.48) and the signal-to-noise ratio com-
pletely determine the mean BER. The extension to a diversity con-
figuration with a forward filter associated with each diversity
input and arbitrary correlation between diversity channels involves
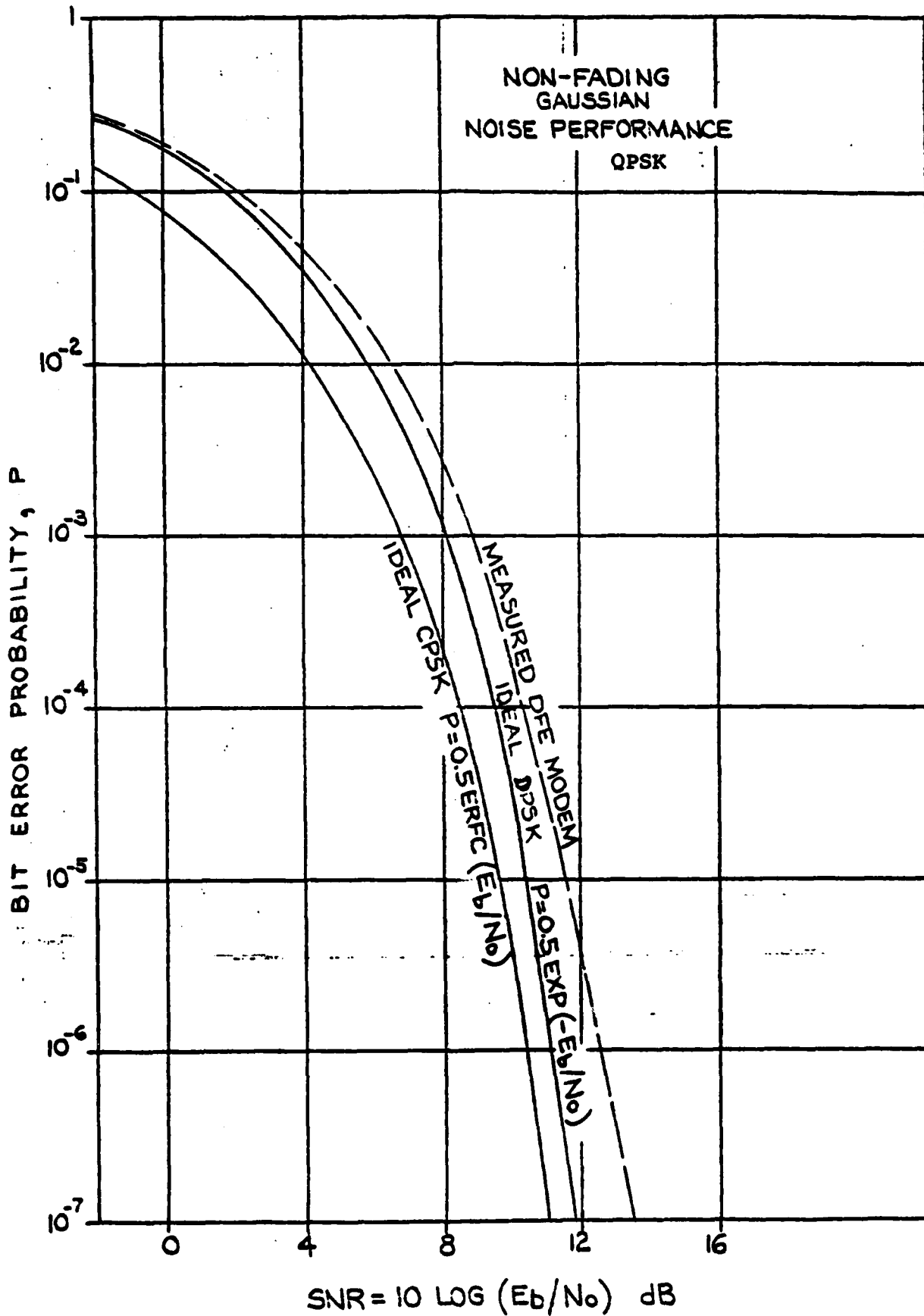a straightforward generalization of the matrices C and G. Let

4-16

Fig. 4.2   Non Fading Performance

4-17

$$\hat{C} = \begin{bmatrix} C^{(11)} & C^{(12)} & \cdots & C^{(1D)} \\ C^{(21)} & C^{(22)} & \cdots & C^{2D)} \\ \cdot & & & \\ \cdot & & & \\ \cdot & & & \\ C^{(D1)} & C^{(D2)} & \cdots & C^{(DD)} \end{bmatrix}, \qquad \hat{G} = \begin{bmatrix} G^{(11)} & G^{(12)} & \cdots & G^{(1D)} \\ G^{(21)} & G^{(22)} & \cdots & G^{(2D)} \\ \cdot & & & \\ \cdot & & & \\ \cdot & & & \\ G^{(D1)} & G^{(D2)} & \cdots & G^{(DD)} \end{bmatrix}$$

where

$$C_{k\ell}^{(ij)} = q_i(t_o - k\tau_s) q_j^*(t_o - \ell\tau_s) = \int_{-\infty}^{\infty} g(t_o - k\tau_s - u) g(t_o - \ell\tau_s - u) p_{ij}(u) du \tag{4.43}$$

$$-k_1 \leq k, \ell \leq K_2$$

$$1 \leq i, j \leq D$$

and

$$G_{k\ell}^{(ij)} = g(k\tau_s - \ell\tau_s) + \frac{\bar{E}_b}{N_o} \gamma^2 \sum_{m=1}^{M} C_{k\ell}^{(ij)}(t_o - mT) \tag{4.44}$$

The average BER has the same form as 4.40

$$\bar{P}_d = \frac{1}{2}\left(\det\left|I + \frac{\bar{E}_b}{N_o} \hat{G}^{-1} \hat{C}\right|\right)^{-1} \tag{4.45}$$

but the matrix rank has been increased from the number of forward filter weights K to DK where D is the number of diversity channels. Fortunately for the usual angle diversity application the matrix rank can be reduced to 2K. Under the conditions specified in 4.3 for a dual vertical angle diversity system in conjunction with space and/or frequency diversity, the matrices $\hat{C}$ and $\hat{G}$ reduce to

4-18

$$\hat{C} = \begin{bmatrix} C^{(11)} & C^{(12)} \\ C^{(12)} & C^{(22)} \end{bmatrix} \quad \hat{G} = \begin{bmatrix} G^{(11)} & G^{(12)} \\ G^{(12)} & G^{(22)} \end{bmatrix} \tag{4.46}$$

and the mean BER is

$$\overline{P_d} = \frac{1}{2} \left(\det\left| I + \frac{\overline{E_b}}{N_o} \hat{G}^{-1} \hat{C} \right| \right)^{-D/2} \tag{4.47}$$

where D/2 is the number of main beam diversity channels.

Equation (4.47) with definitions (4.43) and (4.44) for the matrices; $i_j = 1, 2$; is the basic equation used in this program to compute mean BER for angle diversity performance of digital systems.

4.2 Performance Prediction Results

The method of computing the average bit error probability for a troposcatter equalizer has been applied to the three tropo-scatter system examples. The path parameters for these systems have been given in Table 3.1 of Section 3. The troposcatter equalizer chosen for the analysis is the MD-918 modem developed by Sylvania/SIGNATRON for U.S.Army ECOM under the Megabit Digital Troposcatter Subsystem [4.3]. The modem uses differentially en-coded 4 PSK modulation and a four channel adaptive decision-feedback equalizer [4.4] for reception. There are three taps per forward filter diversity channel with tap spacing equal to one-half a 4 PSK symbol interval. The backward filter uses three taps in its transversal filter realization with tap spacing equal to the symbol interval.

Before the error probability can be computed, squint loss must be calculated and the 2σ multipath spread must be determined

for the main beam, elevated beam, and cross beam (or product) multipath profiles. These values have been computed in Section 3 and were presented in Figs. 3.2 - 3.4 and 3.8 - 3.10. The selected values for the error probability computation are given in Table 4.1

Table 4.1

2σ Multipath Spread

System	Boresight/ Horizon Angle	Squint Loss	Main Beam	Elev. Beam	Product Beam
	Beamwidth	dB	nsec	nsec	nsec
RADC	1/2	1.9	132.	164.	130.
S.Tepesi/ Yamanlar	1/4	5.4	155.	273.	200.
Oslo/ Kristiansand	1/4	4.3	201.	329.	240.

The data rate chosen for the calculation was 6.3 Mb/s as it corresponds to typical user requirements for strategic digital troposcatter. With a 4 PSK modulation format, the bit symbol interval T is then 317 nanoseconds. The $2\sigma_o/T$ values for the main beam diversity are 0.42, 0.49, and 0.63 for the RADC, S.Tepesi, and the Oslo path, respectively.

The results of the error probability computation are plotted as a function of the mean diversity $\bar{E}_b/N_o$ for no diversity reception (1 power amplifier). For an angle diversity application, the squint loss and the availability of a redundant power amplifier must be considered in any system comparison with conventional systems. Since the 2S/2F configuration requires two power amplifiers, any comparison with angle diversity should be on the same basis and it also follows that a 2S/2A system would require a second power amplifier for failure and maintenance

redundancy reasons. For these practical considerations the 2S/
2A system utilizes two power amplifiers tuned to the same fre-
quency. Thus, in effect, the transmit power per diversity of a
2S/2A system is 3 dB more than in analogous 2S/2F system. This
factor is not considered in the presentation of error probability
vs. $\bar{E}_b/N_o$ since $\bar{E}_b$ represents received bit energy. The 3 dB
advantage of the 2S/2A system over the 2S/2F system is included
in a later comparison of average bit error probability vs. time
availability. For a 2S/2A configuration the squint loss, S_L in
dB, is included in the mean diversity $\bar{E}_b/N_o$ as follows;

Mean Diversity $\overline{E_b}/N_o$ = No Diversity $\overline{E_b}/N_o$ - $S_L/2$,

which accounts for all of the elevated beams having a loss of
S_L dB relative to the main beam.

The use of mean diversity $\bar{E}_b/N_o$ allows an evaluation
of the effects of diversity correlation and implicit diversity
in the comparison between frequency and angle diversity. The
correlation between diversity branches reduces the effectiveness
of angle diversity but for small to moderate multipath condi-
tions, the increased multipath spread of the elevated beams
produces more implicit diversity in the angle diversity system.
Thus, the predicted results shown in Figs. 4.3 - 4.5 show
slightly better performance for the 2S/2A system when $2\sigma_o/T$ for
the mainbeam diversity is greater than 0.49 (Figs.4.4,4.5) but
slightly better performance for the 2S/2F system when the cor-
relation effect is dominant at smaller multipath spreads (Fig.
4.3). For larger multipath spread/symbol length ratios, it can
be expected that the 2S/2F system will again outperform the
2S/2A system because the multipath spread in the elevated beam

Fig. 4.3 Digital System Performance, RADC Test Link

4-22

Fig. 4.4 Digital System Performance, S.Tepesi-Yamanlar

4-23

MODEL DATE

PREDICTED MD-918
MODEM PERFORMANCE
6.3 Mb/s
$2\tau_o/T = 0.63$
SQUINT LOSS = 4.3 dB
205 MILE L-BAND PATH

2S/2F
2S/2A
2S/2F/2A
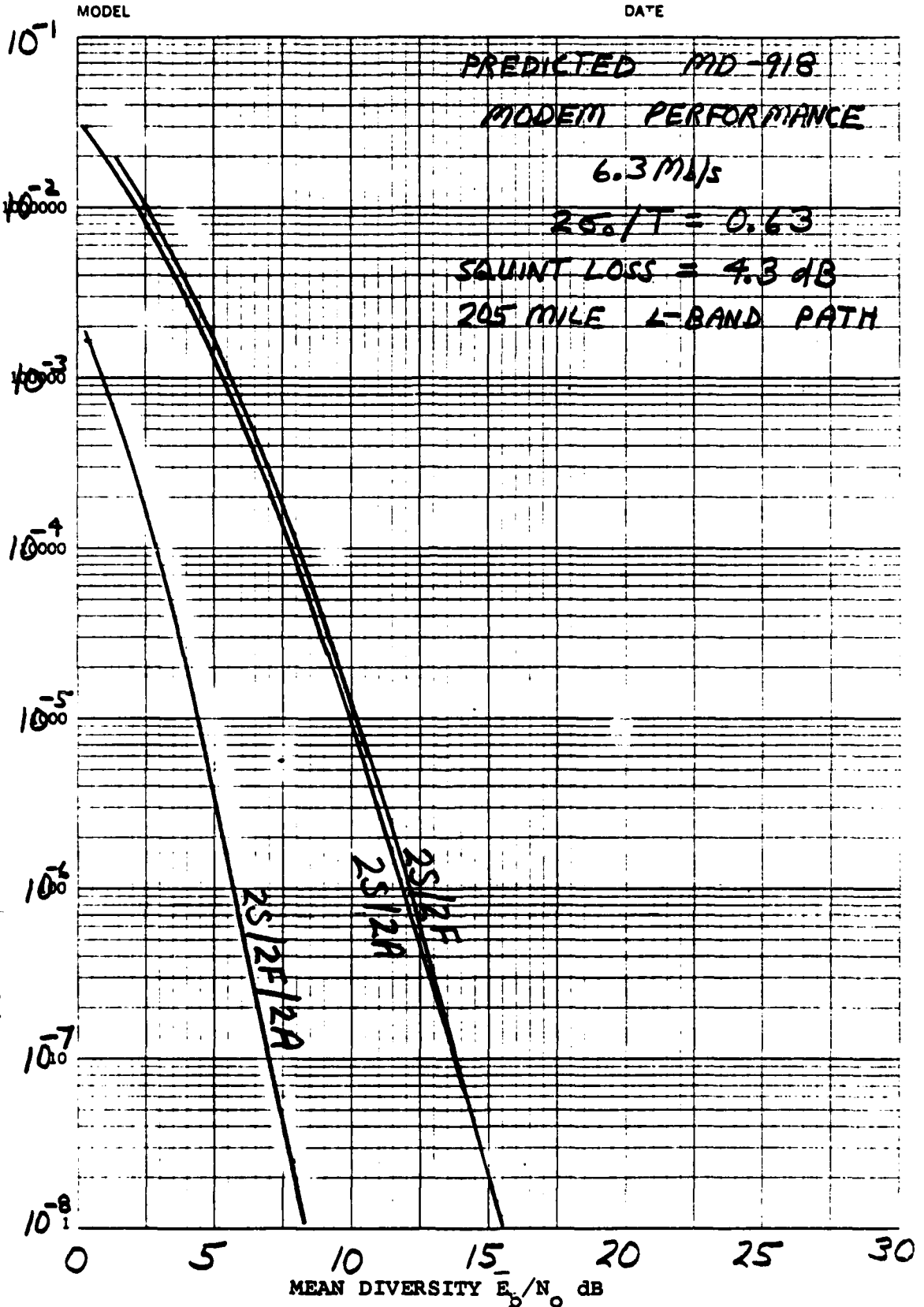
MEAN DIVERSITY E_b/N_o dB
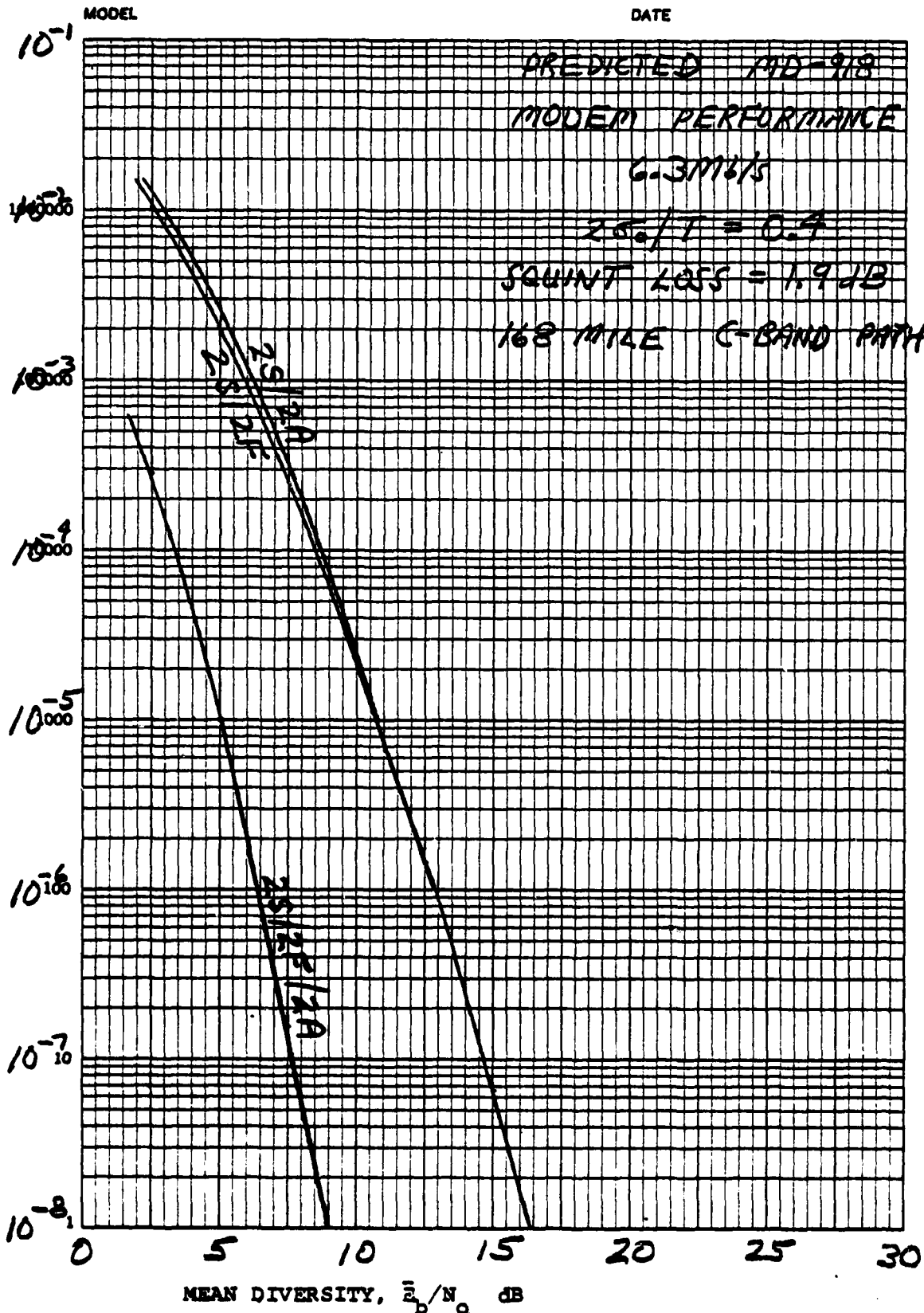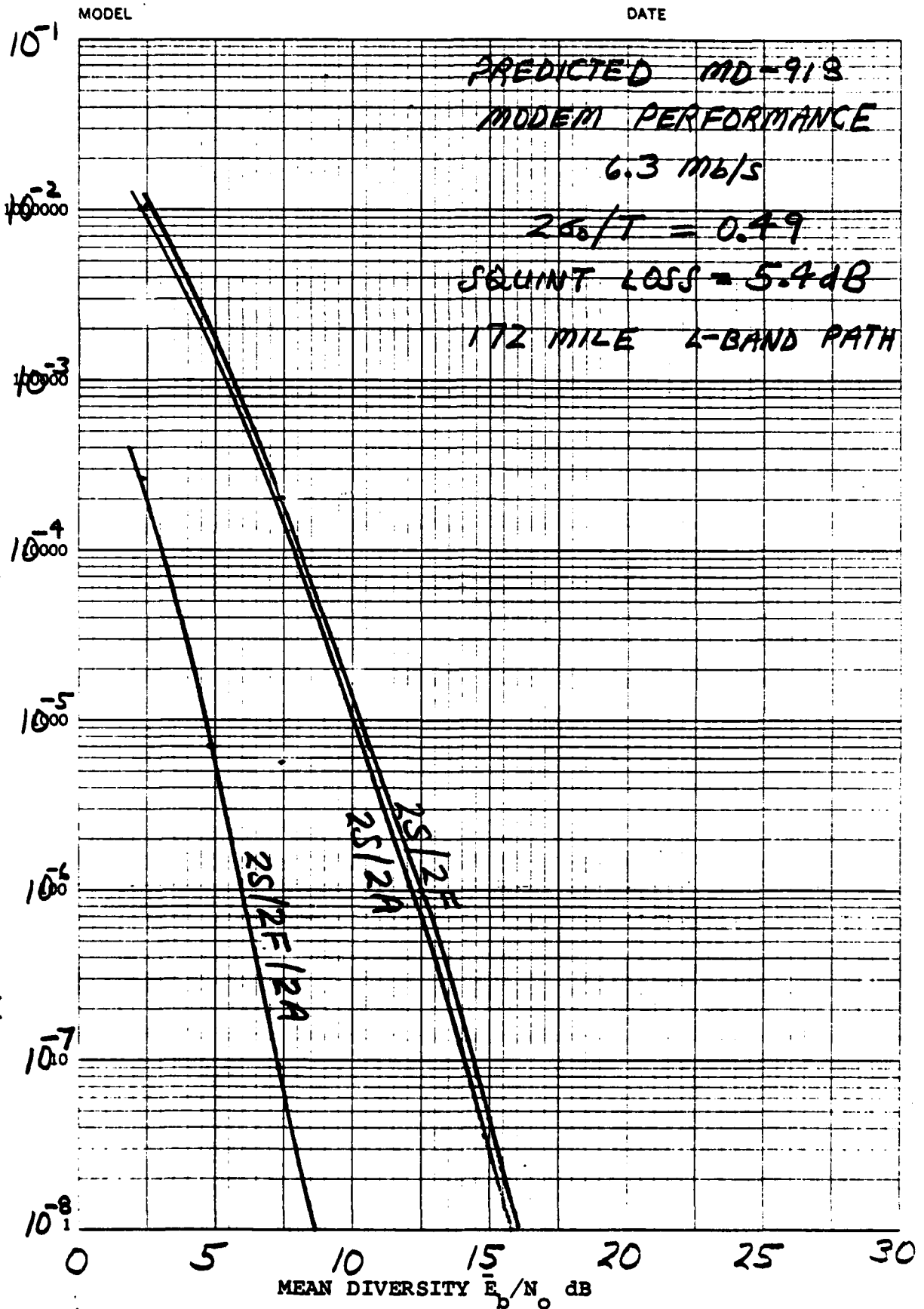
Fig. 4.5   Digital System Performance, Oslo- Kristiansand

4-24

will exceed the design capability of the modem equalizer. This result is shown in Fig. 4.6 where predicted performance for a 12.6 Mb/s system operating on the 172 mile L-band path is shown. It should be pointed out, however, that an expanded, i.e., more taps, DFE could be used to compensate for this effect with the result of better angle diversity performance than frequency diversity performance for these multipath ranges.

It should be emphasized again that the performance comparisons gleaned from Figs.4.3 - 4.6 are based on an equal received bit energy constraint. This comparison is useful in determining the relative effects of diversity correlation and implicit diversity. It can be very misleading if this constraint is used for system comparisons. A realistic method of comparing system performance is to compare the average bit error probability as a function of time availability for each system, i.e., what fraction of the time for a given system will the average bit error probability be larger than a certain value. To accomplish this comparison we first determine the distribution of the median path loss using the common volume integration model of Section 2 and the NBS time availability analysis reviewed in Section 3. The common volume integration model includes the effect of aperture to medium coupling loss and provides a path loss parameter normalized to unit gain antennas. To convert median path loss into $\bar{E}_b/N_o$ in dB, the relationship is

$$\bar{E}_b/N_o = P_T + G_T + G_R - L - NF - 10LOG(R_b) + 174 + 1.6$$

where

P_T = transmit power in dBm
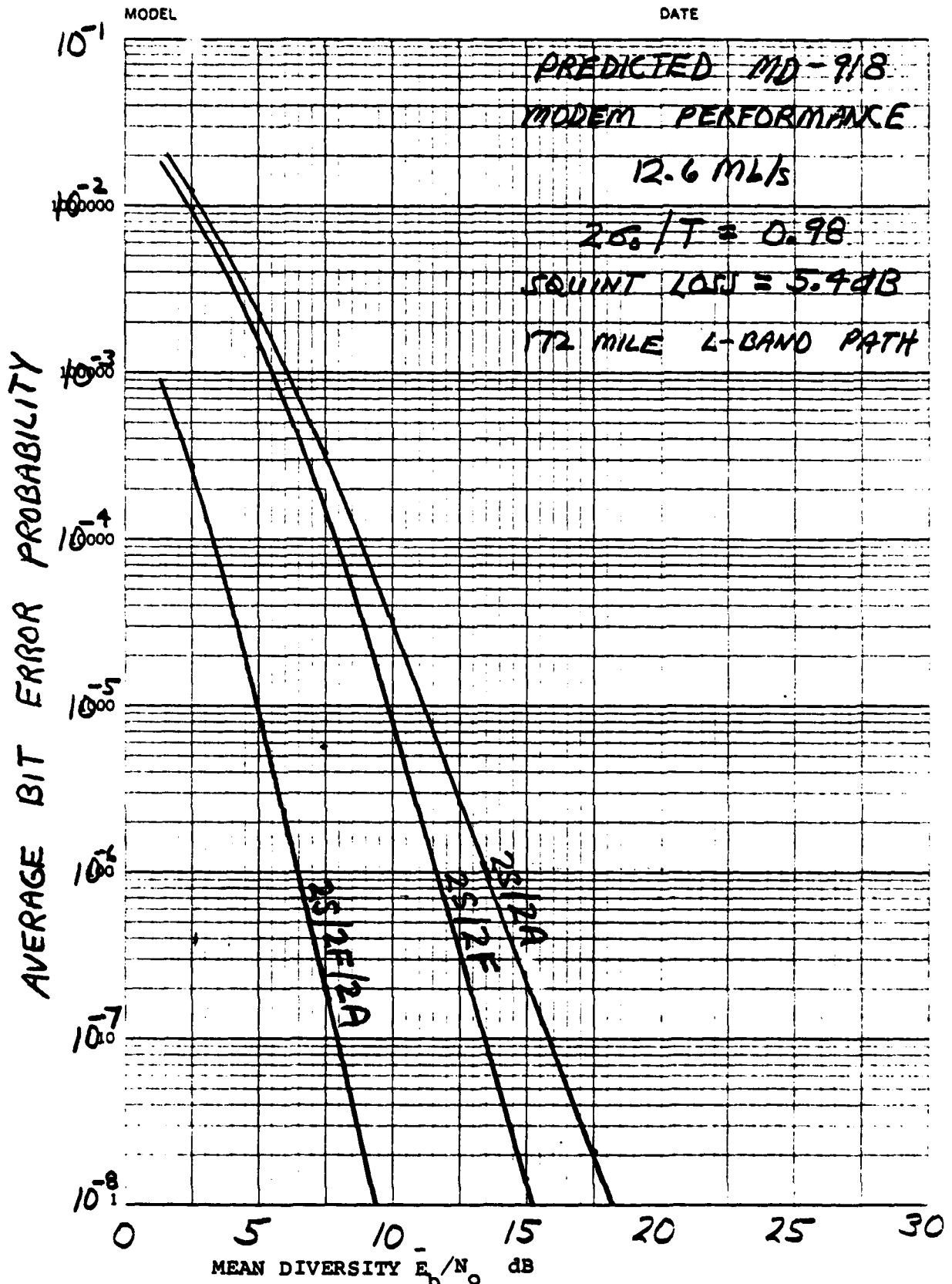
$G_{T/R}$ = antenna gain of transmitter receiver in dB

Fig. 4.6   12.6 Mb/s Performance, S.Tepesi-Yamanlar

4-26

L = total path loss including coupling loss effects

NF = noise figure

R_b = data rate in b/s

174 = noise power in 1 Hz bandwidth in dBm

1.6 = dB amount that the mean exceeds the median for a Rayleigh fading channel.

The antenna gain formula for troposcatter reflectors of diameter D is

$$G = 10 \text{ LOG}\left(\pi^2 D^2 \epsilon / \lambda^2\right)$$

where $0 < \epsilon < 1$ is the antenna efficiency with typical value on the order of 0.57.

In the calculation of median path loss the refractive index variance dependence is based on Fried's [4.5] results at optical wavelengths. Also a service probability of 0.95 has been selected as a conservative measure. We have not collected sufficient empirical data to establish the absolute accuracy of the prediction model. However, the model is very useful for comparisons of different systems on a particular link. During the next study phase, effort is planned to determine the absolute accuracy of the median path loss prediction over a wide range of troposcatter system types. For the RADC test link where empirical data is available, the winter median path losses for the two space diversity antenna receivers were measured [4.6] to be 258 and 260 dB. Our predicted value for this link for winter conditions is 258 dB which is excellent agreement. The path loss test report [4.7] for the link acceptance of the Oslo-Kristiansand link in the summer of 1962 shows a median path loss of 217 dB. Because considerably stronger signals are experienced in the

summer, this result also compares favorably with our winter
prediction of 231 dB for this link. No empirical data were
available on the S.Tepesi-Yamanlar DCS link.

The total path loss (or $\bar{E}_b/N_o$) distributions for the three
example systems are given in Figs. 4.7 - 4.9. The average bit
error probability curves from Figs. 4.3 - 4.5 are used with the
$\bar{E}_b/N_o$ distribution to determine the error rate availability.
Note that the ordinates of Figs. 4.7 - 4.9 represent the no
diversity received bit energy with a single power amplifier
whereas the abscissas of Figs. 4.3 - 4.5 are expressed as the
average over the diversity branches of the received bit energy.
The relationships between these values are given by the follow-
ing·for the different system configurations:

$$\bar{E}_b/N_o (1PA) = AVG\ \bar{E}_b/N_o \qquad\qquad 2S/2F$$

$$\bar{E}_b/N_o (1PA) = S_L/2 - 3 + AVG\ \bar{E}_b/N_o \qquad 2S/2A$$

$$\bar{E}_b/N_o (1PA) = S_L/2 + AVG\ \bar{E}_b/N_o \qquad 2S/2F/2A$$

The 3 dB for 2S/2A accounts for the use of the additional
power amplifier at the same frequency in this configuration.
The quantity S_L is the squint loss of the elevated beam relative
to the main beam. Since in many examples the 2S/2F and 2S/2A
performance are approximately equal on an AVE $\bar{E}_b/N_o$ basis, the
system gain of 2S/2A over 2S/2F is equal to $3 - S_L/2$ which is
usually positive and yields the system improvements shown in
Figs. 4.7-4.9. Note that the performance improvement afforded
by 2S/2F/2A over 2S/2A is not all that large because the added
diversity is reduced by the need to utilize the second power
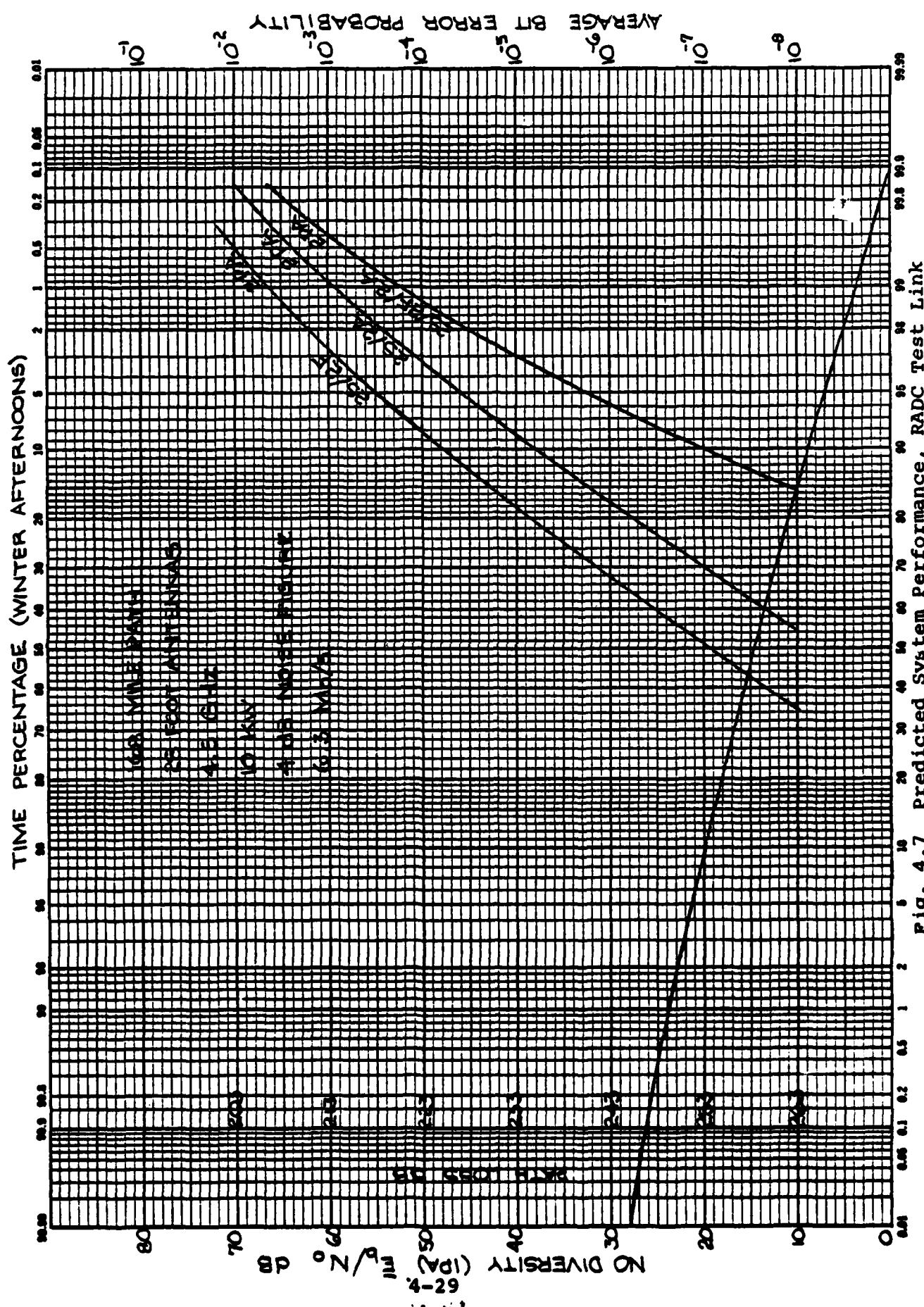amplifier at the diversity frequency resulting in a 3 dB system
loss.

4-28

Fig. 4.7 Predicted System Performance, RADC Test Link
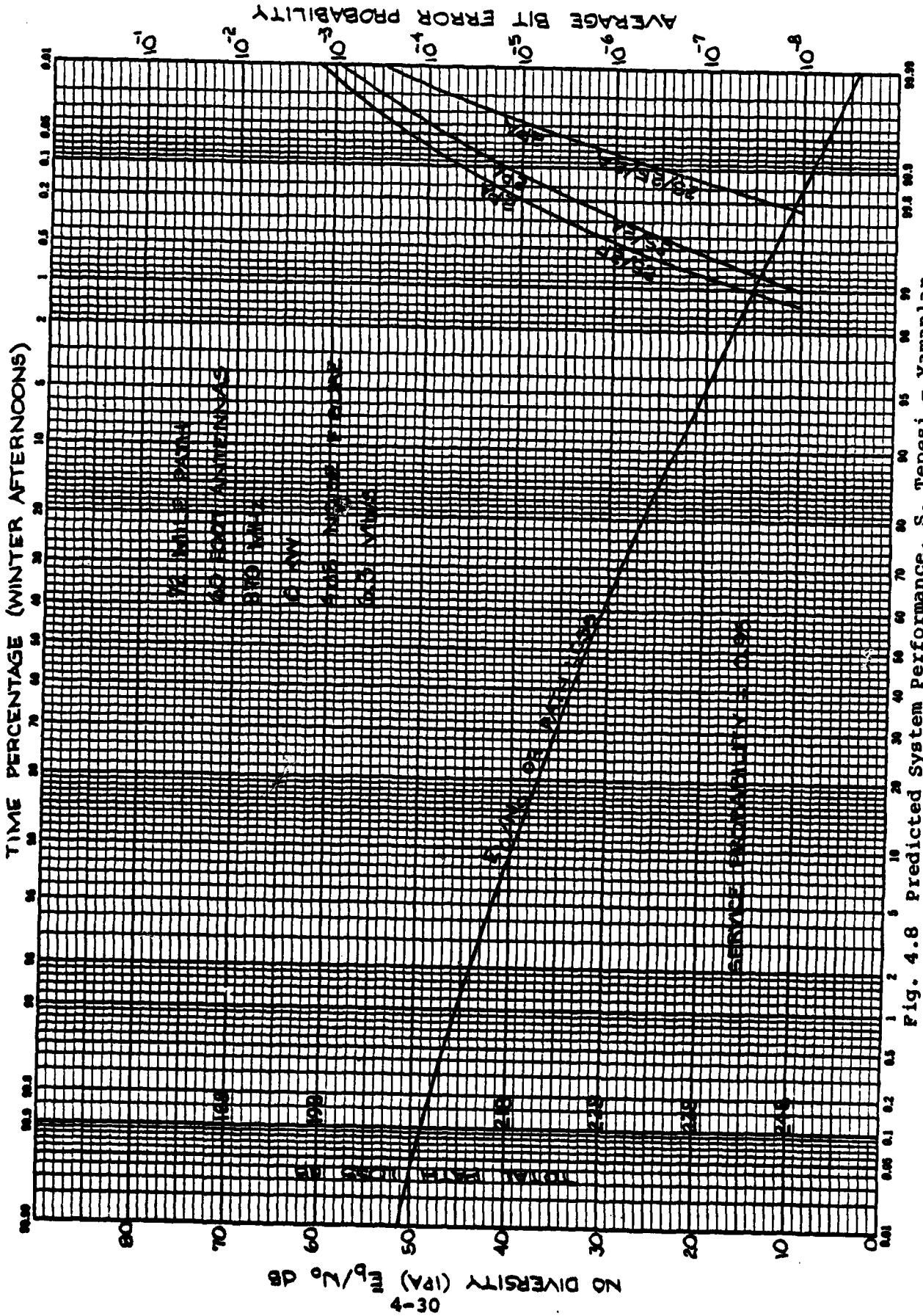
4-29

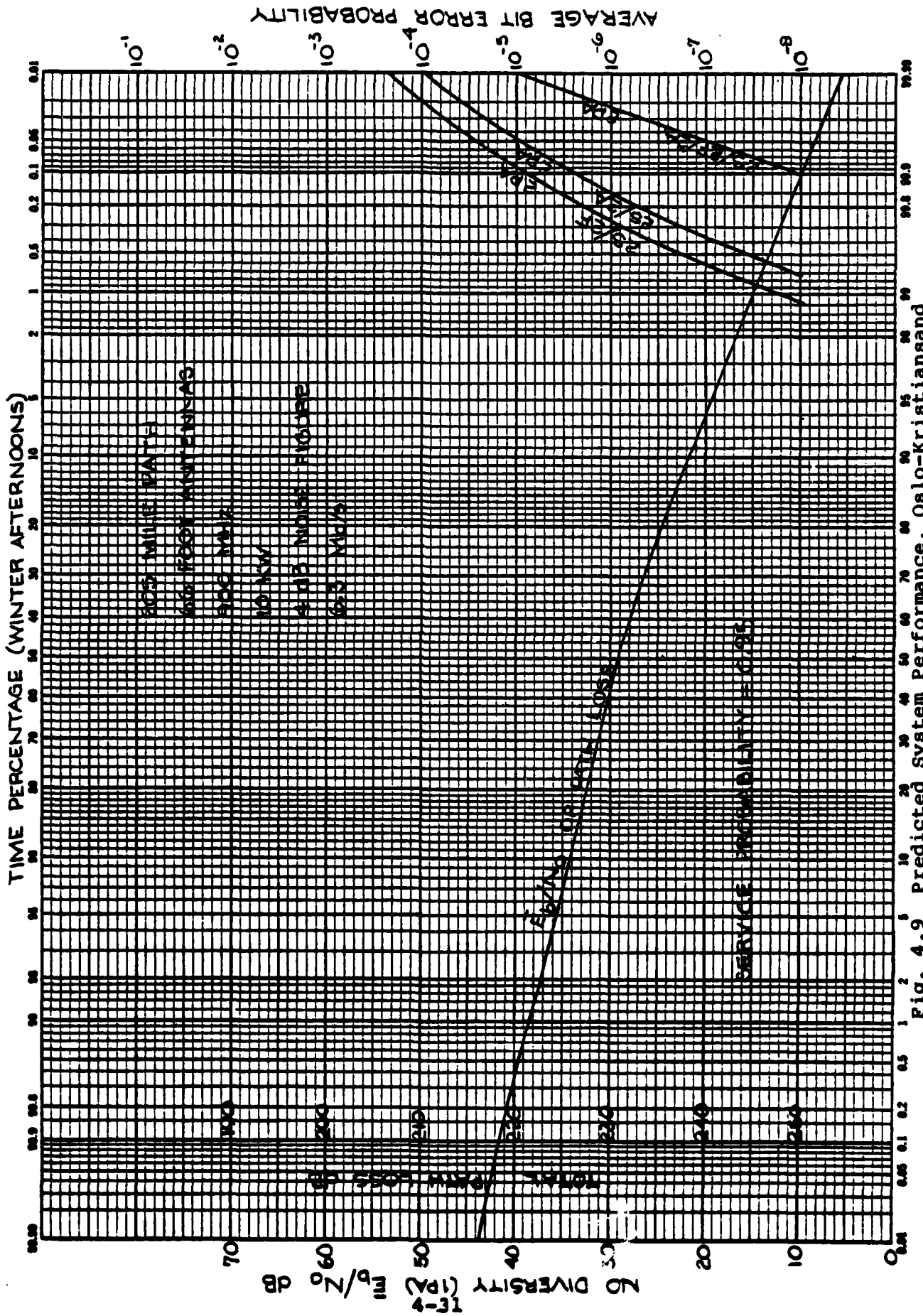Fig. 4.8 Predicted System Performance, S. Tepesi - Yamanlar

Fig. 4.9 Predicted System Performance, Oslo-Kristiansand

4-31

4.3 Frequency Conversion of L-band Systems

Most DCS troposcatter systems have operating carrier frequencies below 1 GHz. In certain situations, the availability of frequencies within the host country might make it attractive to convert a troposcatter link to an S-band or C-band carrier frequency. At these higher frequencies the path loss, aperture to medium coupling loss, and antenna gains are larger. For the turbulent scattering model the scatter angle dependence of the scatter power varies as $\theta^{-11/3}$ which results in a path loss dependence (not including coupling loss) with frequency of $f^{5/3}$. This dependence should be contrasted with the NBS model which is based on a layer theory with a path loss dependence of f^3. The turbulent scatter theory is viewed as more accurate for shorter wavelength systems and for worse time-of-the year, i.e., winter, predictions. The antenna gain varies as f^2 and when both transmitting are receiving antennas are taken into account the total antenna gain improvement is f^4. Thus in the absence of coupling loss, higher frequencies of operation would result in an improvement of $f^{7/3}$. The coupling loss results from a shrinkage of the usable common volume and thus is a function of the beamwidth and the scatter power dependence $\theta^{-11/3}$. For very narrow beamwidth, $\Omega \ll \theta_o$, where θ_o is the smallest scattering angle visible from both terminals, the scatter power dependence is not important and the coupling loss is solely a function of the beamwidth. For this asymptotic small beamwidth case, the coupling loss is proportional to the common volume shrinkage which varies as Ω^{-3} where Ω is the (assumed equal) transmit and receive antenna beamwidths. The resulting asymptotic coupling loss varies as f^3 since Ω is inversely proportional to f. Thus, in the limit

$\Omega \ll \theta$, the link SNR varies as

$$\text{Asymptotic}\atop{\Omega \ll \theta_o} \qquad \text{Link SNR} \propto f^{-5/3 + 4 - 3} = f^{-2/3} \ .$$

However, for L-band systems, the asymptotic limit is not approached and one might realistically expect the link SNR to improve with frequency. Moreover, one must consider the distribution of total path loss (total path loss includes coupling loss effects) at the different frequencies of interest. In many examples the NBS model for long term variability predicts smaller variation in path loss for higher frequency systems. This smaller variation would result in a better system availability at higher frequency.

A quantitative evaluation of the above results from computation of total path loss for the 2 example L-band systems after hypothetical conversion to S and C band. The results are given in Table 4.2. For convenience, $\bar{E}_b/N_o$ at a 6.3 Mb/s rate is used to define the link SNR. We see that for both examples conversion to S-band provides considerable improvement which is even larger at the higher availabilities. Conversion from S-band to C-band provides about the same performance as the asymptotic limit is still not achieved.

Although these results are very encouraging for applications where frequency conversion are being considered, there are two factors which the cautious engineer should consider. First, insufficient empirical data has been collected and analyzed to validate the turbulent scatter model and the resulting $f^{-5/3}$ dependence of path loss over the frequency range of

Table 4.2

E_b/N_o Frequency Dependence
6.3 Mb/s, Service Prob. = 0.95

Avail-ability	172 Mile, f_c = 0.87 GHz 60' Ant., 10 KW			205 Mile, f_c = 0.9 GHz 66' Ant., 10 KW		
	f_c E_b/N_o	$3f_c$ E_b/N_o	$5f_c$ E_b/N_o	f_c E_b/N_o	$3f_c$ E_b/N_o	$5f_c$ E_b/N_o
90%	23.5	27.9	27.3	22.5	24.5	24.1
99%	15.5	21.5	20.9	15.5	19.1	18.7
99.9%	9.1	16.6	16.0	10.4	15.0	14.6
99.99%	4.6	12.4	11.8	6.2	11.5	11.1

interest. Second, the NBS long term variability model is based upon empirical data taken primarily on systems operating below 1 GHz.

SECTION 4

REFERENCES

[4.1]   J.L.Osterkolz and D.R.Smith, "The Effects of Digital
        Tropo Error Statistics on Asymchronous Digital System
        Design", NTC Conf. Rec., Vol.2, New Orleans,Dec.1975,
        pp. 28-25 to 28-31.

[4.2]   P.Monsen,"Theoretical and Measured Performance of a
        DFE Modem on a Fading Multipath Channel", IEEE Trans.
        on Communications, Vol. COM-25, No. 10, October 1977,
        pp. 1144 - 1153.

[4.3]   C.J.Grzenda, D.R.Kern, and P.Monsen, "Megabit Digital
        Troposcatter Subsystem," NTC Conference Record, New
        Orleans, December 1975, pp. 28-15 to 28-19.

[4.4]   P.Monsen,"High Speed Digital Communication Receiver,
        U.S. Patent No. 3,879,664, April 22, 1975.

[4.5]   D.L.Fried, "Optical Heterodyne Detection of an Atmo-
        sphereically Distorted Wavefront", Proc. IEEE, Vol.55,
        No.1, 1967, pp.57-67.

[4.6]   A. Sherwood, and L Suyemoto, "Multipath Measurements
        Over Troposcatter Paths", Mitre Corporation, Report
        MTP-170, April 1976.

[4.7]   S.Bruscantini,Path Loss Test Report,Oslo-Kristiansand,
        NATO Memo.for File, 26 October 1962.

APPENDIX

POWER FADING CORRELATION COEFFICIENT

The power fading correlation coefficient can be measured from the received powers at watts or in dBm. In this Appendix we derive the relationship between these coefficients. It is shown for a special case that the watt measure of the correlation coefficient is overbounded by the dBm measure and for a practical example the coefficients are shown to be close in value.

The density function for the hourly median path loss (or received power) in dB (or dBm) is given by

$$f(x_1 x_2) = \frac{1}{2\pi\sigma|R|^{\frac{1}{2}}} \ e^{-\underline{x}' R^{-1} \underline{x}/2\sigma^2} \tag{A.1}$$

where

$$\underline{x} = \begin{bmatrix} x_1 - m_1 \\ s_2 - m_2 \end{bmatrix}$$

$$R = \begin{bmatrix} 1 & a\rho \\ a\rho & a^2 \end{bmatrix}$$

m_1 = mean value of hourly median path loss (dBm) for mainbeam

m_2 = mean value of hourly median path loss (dBm) for elevated beam

σ = standard deviation of mainbeam path loss

$a\sigma$ = standard deviation of elevated beam path loss

ρ = power fading correlation coefficient.

The correlation coefficient is defined as

$$\rho = \frac{\overline{x_1 x_2} - \overline{x}_1 \overline{x}_2}{\left(\overline{x_1^2} - \overline{x}_1^2\right)^{\frac{1}{2}} \left(\overline{x_2^2} - \overline{x_2^2}\right)^{\frac{1}{2}}} = \left(\overline{x_1 x_2} - m_1 m_2\right) \Big/ a\sigma^2$$

(A.2)

The path loss in watts is

$$y_i = 10^{x_i/20} = e^{0.115\,x_i} = e^{\alpha x_i}, \quad \alpha = 0.115, \quad i = 1, 2$$

and its correlation coefficient is

$$\tilde{\rho} = \frac{\overline{y_1 y_2} - \overline{y}_1 \overline{y}_2}{\left(\overline{y_1^2} - \overline{y}_1^2\right)^{\frac{1}{2}} \left(\overline{y_2^2} - \overline{y}_2^2\right)^{\frac{1}{2}}} = \left(\overline{y_1 y_2} - \overline{y}_1 \overline{y}_2\right) \Big/ \sigma_1 \sigma_2$$

(A.3)

The mean and variance for y_1 is found by direct integration

$$\overline{y}_1 = \frac{1}{\sigma\sqrt{2\pi}} \int_{-\infty}^{\infty} e^{\alpha x - (x - m_1)^2/2\sigma^2} \, dx = e^{\alpha m_1 + \frac{1}{2}\alpha^2\sigma^2}$$

$$\overline{y_1^2} = \frac{1}{\sigma\sqrt{2\pi}} \int_{-\infty}^{\infty} e^{2\alpha x - (x - m_1)^2/2\sigma^2} \, dx = e^{2\alpha m_1 + 2\alpha^2\sigma^2}$$

$$\sigma_1^2 = \overline{y_1^2} - \overline{y}_1^2 = e^{2\alpha m_1 + \alpha^2\sigma^2} \left(e^{2\alpha^2\sigma^2} - 1 \right)$$

The results for y_2 follow immediately by substituting $a\sigma$ for σ in the above expressions.

$$\overline{y_2} = e^{\alpha m_2 + \frac{1}{2}\alpha^2 a^2 \sigma^2}$$

$$\overline{y_2^2} = e^{2\alpha m_2 + 2\alpha^2 a^2 \sigma^2}$$

$$\sigma_2 + \overline{y_2^2} - \overline{y_2}^2 = e^{2\alpha m_2 + \alpha^2 a^2 \sigma^2}\left(e^{\alpha^2 a^2 \sigma^2} - 1\right)$$

To find $\overline{y_1 y_2}$, we find it convenient to perform an orthogonal transformation on $\underline{x}$ to produce an independent joint normal process. Let Q be the orthogonal matrix which diagonalizes R, i.e.,

$$QRQ' = \Gamma \; , \; \Gamma_{ij} = \lambda_i \, \delta_{ij}, \; i, \; j = 1, \; 2$$

where

$$Q = \begin{bmatrix} \underline{e}_1 \\ \underline{e}_2 \end{bmatrix}$$

and $\underline{e}_1$ and $\underline{e}_2$ are the eigenvectors of R,

$$R\underline{e}_i = \lambda_i \underline{e}i \; .$$

The transformation is

$$\underline{u} = Q\underline{x}, \; \underline{x} = Q'\underline{u} \tag{A.4}$$

and the density function of $\underline{u}$ is

$$f(\underline{u}) = \frac{1}{2\pi\sigma|R|^{\frac{1}{2}}} \ e^{-\underline{u}'T^{-1}\underline{u}/2\sigma^2} \tag{A.5}$$

which shows the independent nature of u_1 and u_2. Now

$$\overline{Y_1Y_2} = e^{\overline{\alpha(x_1 + x_2)}} = \overline{e^{\underline{b}'\underline{x} + \underline{b}'\underline{m}}}$$

where

$$\underline{b} = \begin{bmatrix} \alpha \\ \alpha \end{bmatrix}$$

$$\underline{m} \quad \begin{bmatrix} m_1 \\ m_2 \end{bmatrix}$$

Since $\underline{x} = Q'\underline{u}$, we have

$$\overline{Y_1Y_2} = e^{+\underline{b}'\underline{m}} \ \overline{e^{\underline{b}'Q'\underline{u}}} = e^{\underline{b}'\underline{m}} \ \overline{e^{\underline{c}'\underline{u}}} = e^{\underline{b}'\underline{m}} \ \overline{e^{c_1u_1}} \ \overline{e^{c_2u_2}}$$

where we have used the independence of u_1 and u_2 and where

$$\underline{c} = \begin{bmatrix} c_1 \\ c_2 \end{bmatrix} = Q\underline{b} \ .$$

We have already evaluated terms of the form $\overline{e^{\alpha x}}$ to find

$$\overline{e^{c_iu_i}} = e^{c_i\lambda_i/2} \ .$$

The power fading correlation coefficient is thus

$$\tilde{\rho} = \frac{e^{+\alpha(m_1+m_2)}\left[e^{-(c_1\lambda_1+c_2\lambda_2)/2} - e^{\frac{1}{2}\alpha^2\sigma^2(1+a^2)}\right]}{e^{\alpha(m_1+m_2)}\sqrt{e^{\alpha^2\sigma^2}\left(e^{\alpha^2\sigma^2}-1\right)e^{\alpha^2a^2\sigma^2}\left(e^{\alpha^2a^2\sigma^2}-1\right)}}$$

$$\tilde{\rho} = \frac{e^{-c(c_1\lambda_1+c_2\lambda_2)/2} - e^{-\frac{1}{2}\alpha^2\sigma^2(1+2^2)}}{e^{\alpha^2\sigma^2(1+a^2)/2}\sqrt{\left(e^{\alpha^2\sigma^2}-1\right)\left(e^{\alpha^2a^2\sigma^2}-1\right)}} \qquad (A.6)$$

For the special case of equal variances, a=1, (A.6) reduces to a much simpler form. The eigenvalues and eigenvector for R when a=1 are

$$\lambda_1 = \sigma^2(1-\rho)$$

$$\lambda_2 = \sigma^2(1+\rho)$$

$$\underline{e}_1 = \frac{1}{\sqrt{2}}\begin{bmatrix} 1 \\ -1 \end{bmatrix}$$

$$\underline{e}_2 = \frac{1}{\sqrt{2}}\begin{bmatrix} 1 \\ 1 \end{bmatrix}$$

with the result

$$\tilde{\rho} = \frac{e^{\alpha^2\sigma^2\rho}-1}{e^{\alpha^2\sigma^2}-1} \qquad (A.7)$$

A-5

One can show that $\tilde{\rho} \leq \rho$ by using the inequality

$$1-x \leq e^{-x}, \quad x \geq 0.$$

Let $\rho = 1-\epsilon$, $\epsilon > 0$, and (A.7) becomes

$$\tilde{\rho} = \frac{e^{\alpha^2 \sigma^2} e^{-\alpha^2 \sigma^2 \epsilon} - 1}{e^{\alpha^2 \sigma^2} - 1} \leq \frac{e^{\alpha^2 \sigma^2}\left(1 - \alpha^2 \sigma^2 \epsilon\right) - 1}{e^{\alpha^2 \sigma^2} - 1}$$

$$\leq 1 - \frac{\alpha^2 \sigma^2 \epsilon\, e^{\alpha^2 \sigma^2}}{e^{\alpha^2 \sigma^2} - 1}$$

$$\tilde{\rho} \leq 1 - \frac{\alpha^2 \sigma^2 \epsilon \left(1 + \alpha^2 \sigma^2 + \frac{\alpha^4 \sigma^4}{2} + \ldots\right)}{\alpha^2 \sigma^2 + \frac{\alpha^4 \sigma^4}{2} + \frac{\alpha^6 \sigma^6}{6} + \ldots}$$

$$\tilde{\rho} \leq 1 - \frac{\epsilon \left(1 + \alpha^2 \sigma^2 + \frac{\alpha^4 \sigma^4}{2} + \ldots\right)}{1 + \frac{\alpha^2 \sigma^2}{2} + \frac{\alpha^4 \sigma^4}{6} + \ldots} \leq 1 - \epsilon.$$

Numerical examples show that to a good approximation $\tilde{\rho} \doteq \rho$ for the above special case and when $a \neq 1$. For example, for the BTL data we have

$$\rho = 0.74$$
$$\sigma = 6.1$$
$$a = 1.18$$

and the calculated result is $\tilde{\rho} = 0.68$.

Distribution List, Second Interim Technical Report.
Adaptive Antenna Control System

No. Copies	Contract Code	Address
3	W15P8E	Commander US Army Communications R&D Command Center for Communications Systems ATTN: DRDCO-COM-RM-3 Fort Monmouth, NJ 07703
2	CCM-RD	Commander US Army Communications System Agency ATTN: CCM-RD-T Fort Monmouth, NJ 07703
2	DCEC- Code R220	Director Defense Communications Engineering Center ATTN: Code R220 1860 Wiehle Avenue Reston, Virginia 22099
1	CC-OPS-SM	Commander US Army Communications Command ATTN: CC-OPS-SM Fort Huachuca, AZ 85613
12		Defense Documentation Center ATTN: DDC-TCA Cameron Station (Bldg 5) Alexandria, Virginia 22314